

OXYGEN ISOTOPE FRACTIONATION BETWEEN HYDROXYAPATITE (HAP)-
BOUND CARBONATE AND WATER AT LOW TEMPERATURES

OXYGEN ISOTOPE FRACTIONATIO BETWEEN HYDROXYAPATITE (HAP)-
BOUND CARBONATE AND WATER AT LOW TEMPERATURES

By KESIA IE, B.Sc.

A Thesis submitted to the School of Graduate Studies in Partial Fulfillment of the
Requirements for the Degree Master of Science

McMaster University

© Copyright by Kesia Ie, August 2016

MASTER OF SCIENCE (2016)

McMaster University

Earth and Environmental Science- Geochemistry

Hamilton, Ontario

TITLE: Oxygen isotope fractionation between Hydroxyapatite (HAP)-bound carbonate and water at low temperatures

AUTHOR: Kesia Ie, B. Sc (Honours) (McMaster University)

SUPERVISOR: Dr. Sang-Tae Kim

NUMBER OF PAGES: x, 139

Preliminaries Abstract

Calcium phosphates are important compounds as they exist in natural aqueous systems such as rivers, lakes, ocean, and soil. These calcium phosphates are widely used to provide information on paleotemperatures as well as many anthropological features, such as paleodiets. One of the most ubiquitous forms of calcium phosphate is hydroxyapatite ($\text{Ca}_{10}(\text{PO}_4)_6(\text{OH})_2$) which is a major component of hard tissue such as bones, fossils, and tooth enamel. The oxygen isotope systematics in the hydroxyapatite associated with carbonate-water system will provide further information to allow for the reconstruction of terrestrial and marine environments. For example, Fricke et al. (1998) used oxygen isotope analysis of the carbonate components of hydroxyapatite in tooth enamel of mammals to investigate changes in terrestrial climate. Therefore, the purpose of this research study was to examine the oxygen isotope systematics in inorganic carbonate-bearing hydroxyapatite and water at low temperatures.

This Master's thesis followed and modified the methods described in Lécuyer et al. (2010) in an attempt to synthesize hydroxyapatite crystals and carbonate-bearing hydroxyapatite. The crystals synthesized were characterized in terms of several conditions (i.e., influence of mixing rate and maturations, pH, and concentrations of NaHCO_3). Methods to produce hydroxyapatite were developed and analyzed using X-Ray diffraction analysis. The results demonstrated a strong dependence of pH in the hydroxyapatite solutions. Moreover, the effect of concentrations of NaHCO_3 was deemed to be essential in order to obtain the desired amount of structural carbonates in the hydroxyapatite crystals.

Furthermore, this research evaluated the temperature dependence of oxygen isotopic fractionation between HAP-bound carbonate and water at 10, 25, and 40 °C. Our study is the first to assess the two mixing-rates experiments with different maturations (7 and 14 days) on the oxygen isotope effects and fractionation behaviour between HAP-bound carbonate and water. Both maturation time and the effect of initial concentration of NaHCO_3 were found to be the most important in determining the equilibrium conditions in our experiments.

ACKNOWLEDGEMENTS

First of all, I would like to express the deepest appreciation to my supervisor, Dr. Sang-Tae Kim, for giving me the opportunity to work under his supervision as well as enough patience to support me throughout these 2 years. I am extremely grateful and indebted to him for his expert, sincere, valuable guidance, and his encouragement to pursue graduate studies.

I would also like to thank Martin Knyf and Mohammed El Shenawy for their amazing support, sense of humor, for always willing to help preparing to normalizing my samples, and help me to understand geochemistry. I am grateful to MRSI crew (past and present), especially Nick Randazzo and Chris Spencer for your assistance throughout this entire project and giving me meaningful input. I could not have done this without you guys! I would also like to thank Hillary MacDougall, Jillian Wyman, and Febryan Yudha for their peer review feedback. I would also like to thank Salome Santos-Blaguski, Alex Paulin, Cassandra Lo, and everyone at the SGES main office for their assistance to fellow graduate students and myself.

Thank you to the SGES who has enhanced my education from undergraduate to graduate career. Also, I am thankful for the funding provided to me by McMaster University and through the Donors of the American Chemical Society- Petroleum Research Fund (ACS-PRF), Natural Science and Engineering Research Council (NSERC) Grant, Ontario Ministry of Research and Innovation – Ontario Research Fund (MRI-ORF), Canada Foundation for Innovation – Leaders Opportunity Fund (CFI- LOF) which supported Dr. Sang-Tae Kim. Additionally, thanks to my committee members, Dr. Greg Slater and Dr. Henry Schwarz, for their research guidance.

Lastly, I would like to thank Febryan Yudha for always believing in me when I didn't, to do better and think positive everyday. To my family: Papi, Mami, Kayla, Kevina, and my dog (baci) for your prayers, unceasing support, and of course home cooked meals. You guys always inspire me to become a better person I can be, and providing the greatest motivation and encouragement in life. I love you all!

TABLE OF CONTENTS

PRELIMINARIES

ABSTRACT.....	iii
ACKNOWLEDGEMENTS.....	iv
LIST OF TABLES.....	vii
LIST OF FIGURES.....	viii

Chapter 1: Introduction to phosphate minerals in stable isotope geochemistry

1.0 introduction.....	1
1.1 Oxygen isotope fractionation between biogenic phosphate (bioapatite) and water..	2
1.2 Oxygen isotope effects in the dissolved inorganic phosphate (DIP) and water system.....	8
1.3 Oxygen isotope fractionation between HAP-bound carbonate and water.....	14
1.4 Thesis structure.....	17
References.....	19

Chapter 2: Synthesis of carbonate-bearing hydroxyapatite at 25 °C

Abstract.....	27
2.1 Introduction.....	28
2.2 Experimental methods.....	32
2.2.1 Inorganic precipitation of carbonate-bearing hydroxyapatite.....	32
2.2.2 pH measurements.....	33
2.2.3 X-ray diffraction.....	34
2.2.4 Quantification of structural carbonate (CO ₃ ²⁻) in HAP.....	35
2.3 Results and discussion.....	35
2.3.1 Lécuyer et al. (2010) vs. this study.....	36
2.3.2 Effect of pH on carbonate-bearing HAP.....	37
2.3.3 Effect of mixing rate on carbonate-bearing HAP.....	41
2.3.4 Effect of NaHCO ₃ concentration on carbonate phase in HAP.....	44
2.3.5 Effect of NaHCO ₃ concentration on carbonate-bearing HAP.....	45
2.4 Conclusions.....	47
References.....	50
Tables.....	55
Figures.....	60

Chapter 3: Oxygen isotope fractionation between hydroxyapatite (HAP) and water at low temperatures

Abstract.....	72
3.1 Introduction.....	73
3.2 Experimental methods.....	77
3.2.1 Overall experimental stages.....	77
3.2.2 Solution preparation.....	78

3.2.2.1 Instantaneous mixing experiments.....	78
3.2.2.2 Time-series experiments.....	79
3.2.2.3 Slow mixing experiments.....	79
3.2.3 pH calibration.....	80
3.2.4 Oxygen isotope analysis of HAP-bound carbonate ($\delta^{18}\text{O}_{\text{HAPBC}}$).....	81
3.2.5 Oxygen isotope analysis of water ($\delta^{18}\text{O}_{\text{H}_2\text{O}}$).....	81
3.2.6 Oxygen isotopic analysis of phosphate ($\delta^{18}\text{O}_{\text{PO}_4}$).....	82
3.3 Results.....	83
3.3.1 Mineralogy of the precipitates based on XRD analyses.....	84
3.3.2. Oxygen isotope compositions of hydroxyapatite-bound carbonate ($\delta^{18}\text{O}_{\text{HAPBC}}$).....	86
3.3.3 Oxygen isotope compositions of waters ($\delta^{18}\text{O}_{\text{H}_2\text{O}}$).....	87
3.3.4 Oxygen isotope fractionation between carbonate-bearing HAP and water ($1000\ln\alpha_{\text{HAPBC-H}_2\text{O}}$).....	87
3.3.4.1 Pure HAP-bound carbonate.....	87
3.3.4.2 Non-pure HAP-bound carbonate (mixture of OCP and HAP).....	89
3.3.5 Oxygen isotope fractionation between HAP and water.....	89
3.4 Discussion.....	90
3.4.1 Oxygen isotope fractionation between carbonate-bearing HAP and water ($1000\ln\alpha_{\text{HAPBC-H}_2\text{O}}$).....	91
3.4.1.1 Effect of mixing rates and maturations on oxygen isotope fractionation between HAP-bound carbonate and water.....	92
3.4.1.2 Effect of NaHCO_3 concentrations on oxygen isotope fractionation between HAP-bound carbonate and water.....	95
3.4.2 Oxygen isotope fractionation between HAP and water ($1000\ln\alpha_{\text{HAP-H}_2\text{O}}$).....	98
3.5 Conclusions.....	100
References.....	103
Tables.....	108
Figures.....	119

Chapter 4: Conclusions and research contributions

4.1 Research summary.....	132
4.2 Candidate’s contributions to collaborative research.....	135
4.2.1 Synthesis of hydroxyapatite-bound carbonate at 25 °C.....	135
4.2.2. Oxygen isotope fractionation between HAP-bound carbonate and water at low temperatures.....	136
4.3 Future investigation in stable isotope geochemistry.....	136
References.....	139

LIST OF TABLES

Chapter 1

Table 1.1 Summary of oxygen isotope fractionations between phosphate and water

Table 1.2 Method analysis for oxygen isotope fractionation between phosphate and water.

Chapter 2

Table 2.1 Different phases of calcium phosphates, in order from the most soluble to the least soluble

Table 2.2 Solution chemistry of all instantaneous-rate mixing experiments at 25 °C

Table 2.3 Solution chemistry of all slow-rate mixing experiments at 25 °C

Table 2.4 Comparison of experimental conditions employed by Lécuyer et al. (2010) and this study

Table 2.5 Initial and final pH and mineralogy based on XRD results from this study for synthesizing HAP crystals.

Table 2.6 Various calcium phosphate phases and their corresponding synthesis conditions

Chapter 3

Table 3.1. Different phases of calcium phosphates in order from the most soluble to the least soluble compounds

Table 3.2. Comparisons between two methods that was developed by Lécuyer et al. (2010) and this study for synthesizing hydroxyapatite crystals

Table 3.3. Final pH and mineralogy based on XRD results

Table 3.4. Oxygen isotope compositions of hydroxyapatite-bound carbonate and water that were inorganically precipitated under the instantaneous mixing at 10, 25, and 40 °C

Table 3.5. Oxygen isotope compositions of hydroxyapatite-bound carbonate and water that were inorganically precipitated from time-series experiments at 25 °C

Table 3.6. Oxygen isotope compositions of hydroxyapatite-bound carbonate and water that were inorganically precipitated under the slow mixing experiment at 25 °C

Table 3.7 Solution chemistry of all of instantaneous-rate mixing experiments

Table 3.8. Solution chemistry of all of instantaneous-rate mixing rate for the time-series experiments

Table 3.9. Solution chemistry of all slow-rate mixing experiments at 25 °C

Table 3.10. Oxygen isotope data and oxygen isotope fractionation factors between HAP and water at 10, 25, and 40 °C

LIST OF FIGURES

Chapter 1

Figure 1.1 Oxygen isotope fractionation between biogenic PO_4 and water

Figure 1.2 Speciation of phosphate as a function of pH and temperature

Figure 1.3 Oxygen isotope fractionation equation between biogenic phosphates and water vs. DIP and water

Figure 1.4 Oxygen isotope fractionation equation between biogenic phosphates and water vs. DIP and water

Figure 1.5 Oxygen isotope fractionation equation between inorganic HAP-bound carbonate and water compared to the inorganic calcite and water and the biogenic phosphate and water

Chapter 2

Figure 2.1 Schematic illustration for the instantaneous-rate mixing experiment used in this study to synthesize HAP-bound carbonate at 25°C

Figure 2.2 Schematic illustration for the slow-rate mixing experiment employed in this study to synthesize HAP-bound carbonate at 25 °C

Figure 2.3 The calibration of mass-44 peak area based on different weights of laboratory standard Carrara marble

Figure 2.4 XRD results from the instantaneous-rate mixing experiments at 25 °C. Different maturation periods, initial concentrations of NaHCO_3 , and low final pH values induced mixtures of OCP, brushite, and HAP

Figure 2.5 XRD results from the instantaneous mixing rates at 25 °C from different maturation periods, initial concentrations of NaHCO_3 , and high final pH that demonstrated pure brushite (MRSI-Bagg-20) and pure HAP crystals

Figure 2.6 XRD results from all of the slow mixing experiments that demonstrated mixtures of OCP and HAP crystal

Figure 2.7 XRD results that demonstrated pure OCP (left) and pure HAP (right), both under slow mixing rates of 2.08 mL/hr (2 days) and 7 days of maturation of the mixed solutions

Figure 2.8 Reference standard XRD peaks of HAP phase (top), OCP phase (middle), and brushite phase (bottom)

Figure 2.9 Dried samples of the instantaneous mixing rate (left) and slow mixing rate (right)

Figure 2.10 Mixtures of HAP and OCP under microscope from the instantaneous precipitation rate experiments: MRSI-Ie-8 (left) and MRSI-Ie-12 (right)

Figure 2.11 Mixtures of HAP and OCP under microscope from slow mixing rate experiments: MRSI-Ie-34SP (left) and MRSI-Ie-35SP (right)

Figure 2.12 All of the pure HAP crystals under microscope from the instantaneous mixing rate experiments: TOP: MRSI-Bagg-23, BOTTOM: MRSI-Ie-1TS (left) and MRSI-Ie-17B (right)

Figure 2.13 Pure brushite crystals from the instantaneous mixing rate experiment: MRSI-Bagg-20 (left) and pure OCP crystals from the slow mixing rate experiment: MRSI-Ie-28SP (right)

Chapter 3

Figure 3.1. Schematic illustration demonstrating the instantaneous mixing method used in this study to synthesize HAP and HAP-bound carbonate at 10, 25, and 40 °C

Figure 3.2. Schematic illustration demonstrating the time-series experiments used in this study to synthesize HAP and HAP-bound carbonate at 25 °C

Figure 3.3. Schematic illustration demonstrating the slow mixing method used in this study to synthesize HAP and HAP-bound carbonate at 25 °C

Figure 3.4. The calibration of mass 44 peaks area based on different weights of Carrara laboratory standards

Figure 3.5. XRD results from the instantaneous mixing experiments that demonstrated pure HAP

Figure 3.6. XRD results that demonstrated of pure OCP (left) and pure HAP (right) under slow mixing rate of 2.08 mL/hr (2 days)

Figure 3.7. XRD results from slow mixing rate of 0.594 mL/hr (7 days) that demonstrated mixtures of OCP and HAP crystal

Figure 3.8. Pure HAP crystals from the instantaneous mixing rate experiments

Figure 3.9. All of the heterogeneous HAP crystals under microscope from time-series fast precipitation experiments: MRSI-Ie-1FP (left) and MRSI-Ie-8FP (right)

Figure 3.10. Mixtures of HAP and OCP under microscope: MRSI-Ie-34SP (left) and MRSI-Ie-35SP (right)

Figure 3.11. Pure OCP crystals from slow mixing rate experiment (MRSI-Ie-28SP)

Figure 3.12. Oxygen isotope fractionation between inorganic carbonate-bearing HAP and water from the instantaneous mixing rate method compared to the inorganic calcite and water, carbonic acid system and water, and inorganic carbonate-bearing HAP and water

Figure 3.13. Oxygen isotope fractionation between non-pure inorganic carbonate-bearing HAP and water from the slow mixing rate method maturations at 25 °C

Figure 3.14. Oxygen isotope fractionation between non-pure inorganic HAP-bound carbonate and water from the slow mixing rate method maturations at 25 °C vs. pure inorganic HAP-bound carbonate and water from the instantaneous mixing rate method

Figure 3.15. Oxygen isotope fractionation between inorganic HAP and water compared to the dissolved inorganic phosphate and water

Figure 3.16. Oxygen isotope fractionation between inorganic HAP and water trends with yield HAP (%) based on XRD analysis

Figure 3.17. Oxygen isotope fractionation between HAP-bound carbonate and water trends with temperature as a function of initial concentrations of NaHCO₃ in the PC solutions

Figure 3.18. A schematic illustration of the effect of initial concentrations of NaHCO₃ in the HAP-bound carbonate and water system at low temperatures

Figure 3.19. Oxygen isotope fractionation between HAP-bound carbonate and water under slow mixing rates experiments at 25 °C

Figure 3.20. Oxygen isotope fractionation equation between HAP and water compared to the oxygen isotope fractionation between biogenic phosphate and water

CHAPTER 1:

Introduction to phosphate minerals in stable isotope geochemistry

1.0 Introduction to phosphate minerals in stable isotope geochemistry

Phosphorus (P) occur mainly as a tetrahedral PO_4^{3-} chemical group and salts of the tribasic phosphoric acid (H_3PO_4) (Elliot, 1994). Phosphates, especially apatites ($\text{Ca}_5(\text{PO}_4)_3(\text{F}, \text{OH}, \text{Cl})$), are a critical nutrient for biological processes which exist in natural aqueous systems (e.g., rivers, lakes, ocean, and soil/groundwater), minerals, as well as organic matter. The minerals of apatite, such as fluorapatite, chlorapatite, and hydroxyapatite, are the most abundant of naturally occurring calcium phosphates on Earth and are commonly found in igneous rocks, metamorphic rocks, bones, tooth enamel, fossils, and many pathological calcifications (Elliot, 1994; Kohn et al., 2002). These calcium phosphate minerals have been utilized in various scientific fields, such as biology, anthropology, medicine, and chemistry. In particular, phosphate minerals have been used in geology over the last two decades by analyzing its oxygen isotope composition.

In the early interest, Tudge (1960) discovered the possibility of measuring the oxygen isotope composition of biogenic apatites (bioapatite). Since then, the oxygen isotope composition of phosphates has been well documented and further developed in the reconstruction of Earth's surface environment between fresh and marine waters from which the phosphate precipitated (Longinelli and Nuti, 1973a,b; Kolodny et al., 1983; Lécuyer et al., 1996; Lécuyer et al., 1999; Kohn and Cerling, 2002; Blake et al., 2010). Therefore, a number of oxygen isotope fractionation equations between various bioapatites (e.g., invertebrates shells, fish bones/teeth) and water have been proposed to reconstruct paleoclimate variations in both marine and terrestrial environments

(Longinelli and Nuti, 1973a; 1973b; Kolodny et al., 1983; Lécuyer et al., 1996; Puceat et al., 2010). Longinelli and Nuti (1973a) first proposed the temperature relationship between the oxygen isotope compositions of phosphate ($\delta^{18}\text{O}_{\text{PO}_4}$) and that of parent water ($\delta^{18}\text{O}_{\text{H}_2\text{O}}$) who reported the following equation:

$$T (^{\circ}\text{C}) = 111.4 - 4.3 (\delta^{18}\text{O}_{\text{PO}_4} - \delta^{18}\text{O}_{\text{H}_2\text{O}}) \quad (1)$$

This equation (1) is later confirmed by Kolodny et al. (1983) whose demonstrated the temperature dependence on the oxygen isotope fractionation between bioapatite (fish bones and teeth) and water.

The stable isotope compositions of biogenic materials, such as bone and teeth enamel, record a combination of environmental parameters and biological processes. Geochemists often use stable isotopes of hydrogen, carbon, nitrogen, and oxygen that are preserved in biogenic materials, such as fossil, bones, and teeth enamel, to reconstruct past environmental changes and the behaviour on the biology of the specie(s) from which the bioapatite formed (Kohn and Cerling, 2002). In general, bioapatite paleothermometry is more useful in isotope analysis for biogenic materials than biogenic carbonate. This is because of their nearly great preservation after the organism's death, resistant in post-depositional exchange, as well as their great sensitivity during the formation of temperature to the aqueous environment (Kolodny et al., 1983; Kohn and Cerling, 2002). For instance, bioapatites from teeth and bones have helped to elucidate the wide distributions of biogenic materials to investigate the oxygen isotope of dinosaur thermoregulation (Fricke and Rogers, 2000; Straight et al., 2009; Eagle et al., 2011), mammalian biology/physiology (Amiot et al., 2007; Eagle et al., 2010), and the oxygen

isotope evidence from using bones and teeth enamel of extinct terrestrial/marine vertebrates to examine paleoclimates (Iacumin et al., 1996; Dettman et al., 2001; Kohn et al., 2003).

1.1 Oxygen isotope fractionation between biogenic phosphate (bioapatite) and water

Bioapatite is represented by the chemical formula $\text{Ca}_5(\text{PO}_4, \text{CO}_3, \text{F})_3(\text{OH}, \text{F}, \text{Cl}, \text{CO}_3)$ and contains oxygen atoms in its structure as carbonates (CO_3^{2-}), phosphate (PO_4), and hydroxide (OH). The oxygen isotope composition of bioapatite can be a powerful paleoenvironmental proxy (e.g., temperature of ancient oceans) because bioapatites typically form in isotopic equilibrium with the body of water due to their strong P-O bonds in apatite (Vennemann et al., 2002; Joachimski et al., 2006; Trotter et al., 2008). At low temperatures, the strong P-O bonds in apatite are highly resistant to alteration processes, whereas at increasing temperature the isotopic exchange with water is much more rapid which may lead to isotopic disequilibrium (Lécuyer et al. 1999; O'Neil et al., 2003). The oxygen isotope compositions of marine fossil carbonates ($\delta^{18}\text{O}_{\text{carb}}$) are useful for the reconstruction of sea-surface temperatures (Zachos et al., 1994; Trotter et al., 2008). Nevertheless, marine fossil calcium carbonates are more prone to diagenetic alteration because calcium carbonates show higher solubilities in water (Blake et al., 1997; Puceat et al., 2003; Trotter et al., 2008; Puceat et al., 2010). As a result, oxygen isotope studies of bioapatites have greater resistance to diagenetic alteration because of mineralized phosphatic tissues (e.g., tooth enamel) and better preservation of organisms after death than calcium carbonates.

Table 1.1 Summary of oxygen isotope fractionations between phosphate and water.

Name	Temperature (°C)	Phosphate		Sample origins	Oxygen isotope	
		Type	Source		Process	Effect
Biogenic phosphate and water from (Longinelli and Nuti, 1973a)	3-27	Biogenic phosphate from invertebrate shells -Carbonate dominant	Marine water and freshwater (1 sample)	Natural samples and analyzed using BiPO ₄ -Solid phase	Biotic	Equilibrium
Biogenic phosphate and water from (Longinelli and Nuti, 1973b)	3-25	Biogenic phosphate from fish teeth and bones -Phosphate dominant	Marine water	Natural samples and analyzed using BiPO ₄ -Solid phase	Biotic	Equilibrium
Phosphate of biogenic apatite and water (Kolodny et al., 1983)	3-23	Biogenic apatite from fish bone apatite	Freshwater	Natural samples with precipitation of BiPO ₄ -Solid phase	Biotic	Equilibrium
Phosphate and water (Lécuyer et al., 1996)	12-28	Biogenic apatite from living lingulids -Phosphate dominant	Marine water	Natural samples with precipitation of Ag ₃ PO ₄ -Solid phase	Biotic	Equilibrium
Dissolved inorganic phosphate and water (Blake et al., 1997)	15-35	Flourapatite (microbial apatite) -Carbonate dominant	Orthophosphate as K ₂ HPO ₄ catalyzed by the enzyme PPase* from freshwater and soil slurries	Synthetic laboratory experiments with precipitation of Ag ₃ PO ₄ -Aqueous phase	Biotic	Equilibrium
Dissolved inorganic phosphate and water (Lécuyer et al., 1999)	50-135	Orthophosphate -Phosphate dominant	Orthophosphate as K ₂ HPO ₄	Synthetic laboratory experiments with precipitation of Ag ₃ PO ₄ -Aqueous phase	Abiotic	Kinetic
Phosphate and water (O'Neil et al., 2003)	70-180	Orthophosphate -Phosphate dominant	K ₂ HPO ₄ and H ₂ PO ₄	Synthetic laboratory experiments with precipitation of Ag ₃ PO ₄ -Aqueous phase	Abiotic	Equilibrium
Biogenic apatite and water (Puceat et al., 2010)	8-28	Biogenic apatite from fish tooth enamel	Marine water	Natural samples with controlled laboratory experiments and precipitation of Ag ₃ PO ₄ -Solid phase	Biotic	Equilibrium
Dissolved phosphate and water (Chang and Blake, 2015)	3-37	Orthophosphate	Orthophosphate catalyzed by the enzyme PPase from eukaryotic source	Synthetic laboratory experiment -Aqueous phase	Biotic	Equilibrium

*PPase = Enzyme inorganic pyrophosphatase

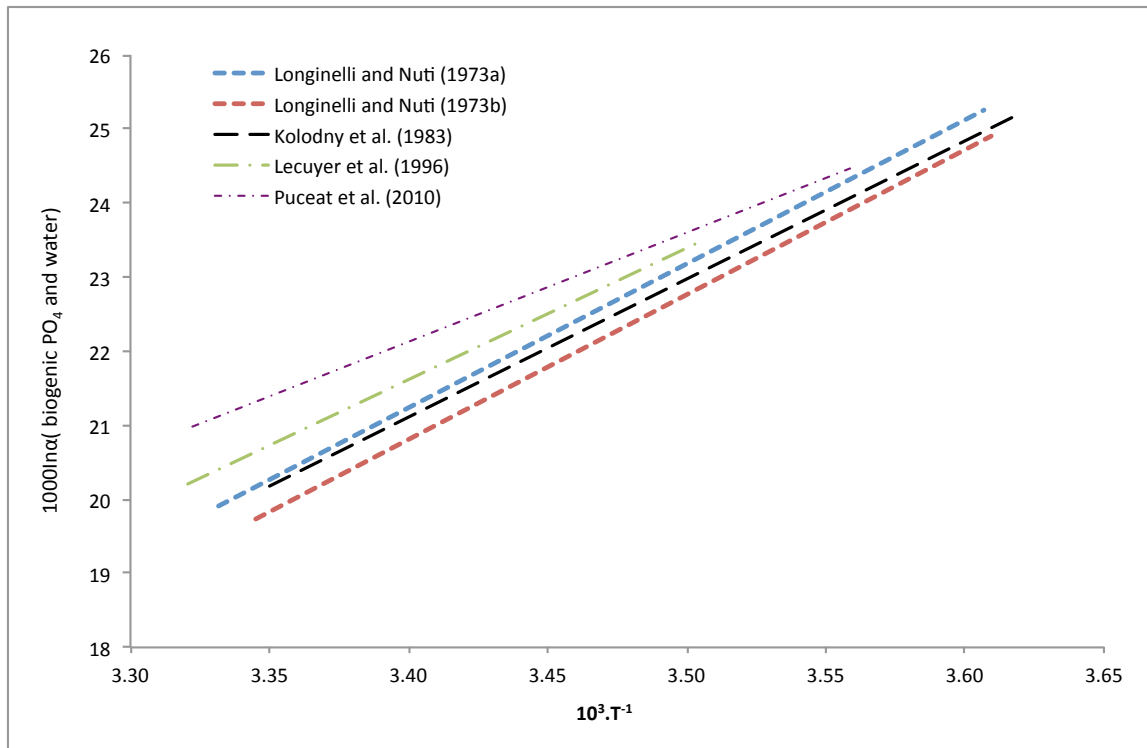


Figure 1.1 Oxygen isotope fractionation between biogenic PO₄ and water (Longinelli and Nuti, 1973a, 1973b; Kolodny et al., 1983; Lécuyer et al., 1996; Puceat et al., 2010).

The temperature dependence of the oxygen isotope fractionation between bioapatite and water has been examined by several researchers and they have reported similar results (Fig. 1.1) (Longinelli and Nuti, 1973a, 1973b; Kolodny et al., 1983; Lécuyer et al., 1996). However, Puceat et al. (2010) found that there are some discrepancies on the oxygen isotope ratios of bioapatites and water caused by different analytical techniques used in the oxygen isotope analysis of phosphates (Table 1.2). The differences in analytical methods, in particular among different standard calibrations, have significant implications for the reconstruction of paleotemperature. As a result, Puceat et al. (2010) established a new oxygen isotope fractionation relationship between phosphate and water on fish raised in aquariums at a controlled temperature. The new

phosphate and water fractionation equation revealed a nearly similar slope as the empirical fractionation equations that were produced by Longinelli and Nuti (1973a, 1973b) and Kolodny et al. (1983), but an offset of about + 2.2 ‰ (Fig. 1.1) (Puceat et al., 2010; Zheng, 2015). According to Zheng (2015), kinetic effect may introduce either in the laboratory or nature that causes these large offsets in the oxygen isotope fractionation during the precipitation of phosphate (Blake et al., 2005; Zheng, 2015).

Table 1.2 Method analysis for oxygen isotope fractionation between phosphate and water.

Name	Chemical purification	Gas extraction	pH	Analytical measurement	Standards	
					Name	$\delta^{18}\text{O}$
Biogenic phosphate and water from (Longinelli and Nuti, 1973a)	BiPO ₄ (Tudge, 1960)	BrF ₃	N/A	N/A	N/A	N/A
Biogenic phosphate and water from (Longinelli and Nuti, 1973b)	BiPO ₄ (Tudge, 1960)	BrF ₃	N/A	N/A	N/A	N/A
Phosphate of biogenic apatite and water (Kolodny et al., 1983)	BiPO ₄ (Tudge, 1960)	BrF ₅	7.5-8.5	Mass spec	NBL-1	20.9
Phosphate and water (Lécuyer et al., 1996)	Ag ₃ PO ₄ (Crowson et al., 1991)	BrF ₅	7.5-8.5	VG SIRA 10 mass spec	NBS120c	21.7
Dissolved inorganic phosphate and water (Blake et al., 1997)	Ag ₃ PO ₄ (O'Neil et al., 1994)	Graphite	7.0	CF-IRMS	N/A	N/A
Dissolved inorganic phosphate and water (Lécuyer et al., 1999)	Ag ₃ PO ₄ (O'Neil et al., 1994)	Graphite	N/A	VG Prism mass spec	NBS120C	21.75
Phosphate and water (O'Neil et al., 2003)	Ag ₃ PO ₄ (Crowson et al., 1991)	BrF ₅	1.8-9.2	N/A	N/A	N/A
Biogenic apatite and water (Puceat et al., 2010)	Ag ₃ PO ₄ (Joachimski et al., 2009)	Graphite	N/A	TC/EA with Finnigan Delta ^{plus} XP	NBS 120c	22.6
Dissolved phosphate and water (Chang and Blake, 2015)	MAP* and Ag ₃ PO ₄	Graphite	7.4	TC/EA with Finnigan Delta ^{plus} XP and CF-IRMS	YR-1a and Yr-3.2	21.8

N/A= Not specified

1.2 Oxygen isotope effects in the dissolved inorganic phosphate (DIP) and water system

The different factors (i.e., temperatures, absence/presence of microbial/enzymatic processes, and pH) are important in the effect of exchange rates and equilibrium oxygen isotope fractionation between DIP and water systems (Blake et al., 1997; Lécuyer et al., 1999; Chang and Blake, 2015). It has been known for years that in phosphate, the covalent P-O bonds are strong (Blake et al., 1997; Lécuyer et al., 1999; O’Neil et al., 2003). Essentially, the strong bonds cause the rate of oxygen isotope exchange between both DIP and water, and bioapatite and water are exceptionally slow at low temperatures, particularly in the absence of enzymatic catalysis (Tudge, 1960; Blake et al., 1997; Chang and Blake, 2015). The temperature coefficients of the phosphate and water, and carbonate and water oxygen fractionations are insensitive to temperature change and thus cannot be used for paleotemperature determinations (Longinelli, 1966; O’Neil et al., 2003). However, a major advantage of the phosphate isotope paleothermometer is that isotopic exchange between DIP and water is very rapid in biochemical enzyme-catalyzed reactions, especially at low temperatures (Zheng, 1996; Blake et al., 1997; Chang and Blake, 2015). For example, Blake et al. (1997) and Liang and Blake (2009) were able to synthesize carbonate fluorapatite (francolite) in laboratory experiments, which involved microbial mediation of mineralization process at low temperatures between 5 to 35 °C. Another research thesis by Blake (1997) aimed the first laboratory controlled calibration of oxygen isotope fractionation between DIP and water to catalyze the exchange reaction between 6 to 22 °C using the enzyme inorganic pyrophosphatase (PPase) (Blake, 1997).

These DIP and water experiments emphasized that the presence of microbial/enzymatic processes at low temperatures show a rapid exchange of oxygen isotopes between DIP and water (Blake, 1997; Blake et al., 1997; Blake et al., 2005; Liang and Blake; 2009).

Conversely, at high temperatures, the rates of exchange between DIP and water increase rapidly even with the absence of microbial/enzymatic processes. This rapid exchange rate between DIP and water have been demonstrated by Lécuyer et al. (1999) and O'Neil et al. (2003) at high temperatures above 75 °C. Lécuyer et al. (1999) studied the oxygen isotope exchange between DIP and water from 50 °C to 135 °C using the protocol of Ag_3PO_4 graphite method that was proposed by O'Neil et al. (1994) (Table 1.2). The article stated the first experimental results for the kinetic and equilibrium DIP and water vs. bioapatite and water fractionation factor as a function of temperature (Lécuyer et al., 1999). It was found that the experiments demonstrated isotope exchange only above 75 °C and a complete isotope exchange at their highest run temperature (135 °C), whereas, at 50 °C, the precipitation experiments showed no isotopic exchange with water (Lécuyer et al., 1999). This demonstration supported the effect of slow exchange rates at low temperatures that has been discovered over the years in the absence of microbial enzyme (Tudge, 1960; Blake et al., 1997). Furthermore, O'Neil et al. (2003) proposed the effects of phosphate speciations on both rates of isotopic exchange and oxygen isotope equilibrium fractionation factors between DIP and water over the temperature range 70-180 °C. The pH range of O'Neil et al. (2003) experiments, between 1-3 (low pH) and 7-9 (high pH), was designed to span a range of equilibrium distribution of phosphate species (Fig. 1.2). At relatively low pH (H_3PO_4 and H_2PO_4^-), O'Neil et al.

(2003) discovered that the exchange rate is much more rapid especially at higher temperature. On the other hand, phosphate species like KHPO_4^- is more dominant at relatively high pH (O'Neil et al., 2003). Thus, the main purpose of O'Neil et al. (2003) research study was to test the proposal of Lécuyer et al. (1999) study which concluded that bioapatite forms in nature “with a large disequilibrium isotope effect” as stated by Lécuyer et al. (1999) (O'Neil et al., 2003). According to Lécuyer et al. (1999), the large disequilibrium isotope effect is caused by the enrichment of about 8‰ in the experimental results between DIP and water extrapolation line in Lécuyer et al. (1999)'s study, and bioapatite and water at 20 °C (Fig. 1.3) (Lécuyer et al., 1999). However, O'Neil et al. (2003) stated that “most biogenic phosphate forms in approximate oxygen isotope equilibrium with the ambient water or body fluids of the organisms” and that at low temperatures the isotope fractionations could possibly be even larger than Lécuyer et al. (1999)'s extrapolation line (O'Neil et al. 2003; Zheng, 2015).

Due to strong covalent P-O bonds in phosphate, O'Neil et al. (2003) were unable to demonstrate experiments below 70 °C because the exchange rate was extremely slow (~2.5 years) among different aqueous phosphate species in their experiments. As shown in Fig. 1.3, all of the oxygen isotope fractionation between bioapatites and water are closer to O'Neil et al. (2003) low pH extrapolation fractionation line. However, since O'Neil et al. (2003) did not determine experiments at low temperatures, the extrapolation fractionation could not demonstrate as a 'true' oxygen fractionation equilibrium line. This is because a combination of three different aqueous phosphate species were found (H_3PO_4 , H_2PO_4^- , and $\text{H}_2\text{P}_2\text{O}_7^{2-}$) at relatively low pH, and at lower temperatures should

have larger fractionation and further from the oxygen isotopic fractionation between biogenic phosphates and water (O'Neil et al., 2003). In other words, undissociated H_3PO_4 will have a higher $\delta^{18}\text{O}$ than the dissociated ionic species that develop as pH increases and temperature increases (O'Neil et al., 2003).

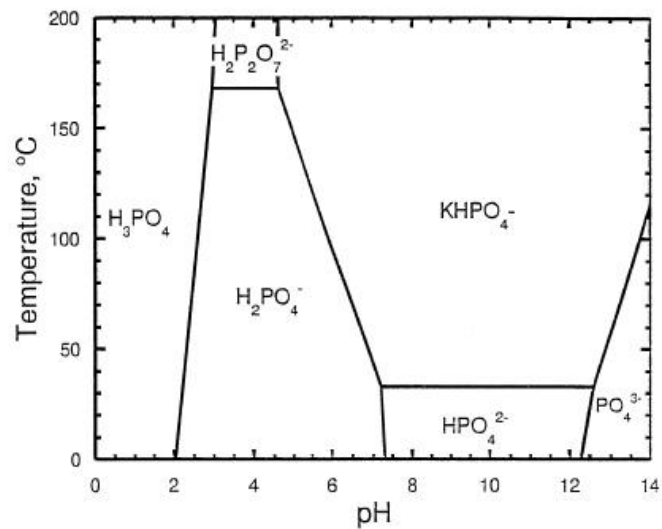


Figure 1.2 Speciation of phosphate as a function of pH and temperature. Retrieved from O'Neil et al. (2003).

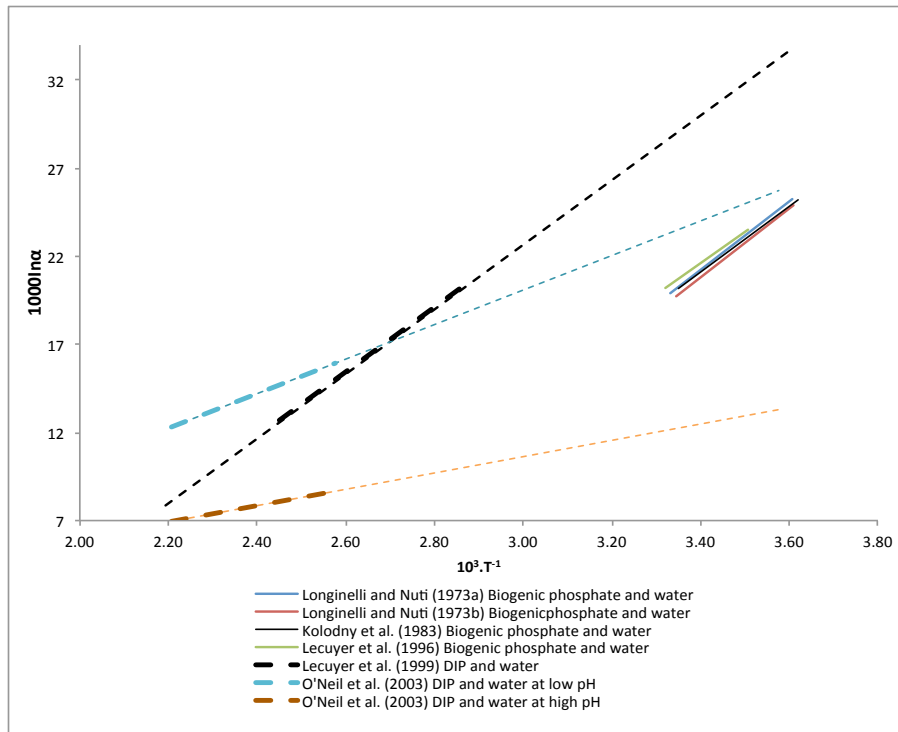


Figure 1.3 Oxygen isotope fractionation equation between biogenic phosphates and water (Longinelli and Nuti, 1973a, 1973b; Kolodny et al., 1983; Lécuyer et al., 1996) vs. DIP and water (Lécuyer et al., 1999; O’Neil et al., 2003).

A recent study by Chang and Blake (2015) presented a new equation of oxygen isotopic fractionation between DIP and water, catalyzed by the enzyme PPase, from expanded range of 3-37 °C (Table 1.1). In order to detect the influence of ambient water oxygen on DIP values, the authors used three different waters (-13, -6 and +14‰) in the experimental solutions with pH adjusted to 7.4 (Chang and Blake, 2015). The research study followed the principal of the partial exchanged method that was conducted by Northrop and Clayton (1966). Likewise, this partial exchange technique has been used extensively in many phosphate and water studies (i.e., Lécuyer et al., 1999; O’Neil et al., 2003). Water with three different oxygen isotopic compositions are usually used in DIP

and water systems in order to detect oxygen isotope exchange (with or without microbial enzyme) and to confirm attainment of equilibrium between DIP and water (Lécuyer et al., 1999; O’Neil et al., 2003; Chang and Blake, 2015). The two-direction approach and partial exchange technique are mostly used in phosphate and water studies because the phosphate system is poorly understood than the carbonate and water system, and obscured by factors due to the relatively poor precision of isotopic measurements especially for small apatite sample analysis (Lécuyer, 2004). From this technique, Chang and Blake (2015) determined a linear regression and a negative relationship ($1000\ln\alpha_{\text{PO}_4\text{-water}}$ increasing with decreasing temperatures) in both series of experiments (Fig. 1.4). The values of oxygen isotope fractionation between DIP and water in the two isotopically lighter waters (-13‰ and -6‰) reached a steady state and represented thermodynamic equilibrium values (Chang and Blake, 2015). These results are consistent with previous results (Blake et al., 1997; Liang and Blake, 2009) that this rapid equilibrium was attained due to the extensive exchange of oxygen between DIP and water catalyzed by reversible hydrolysis of PPase.

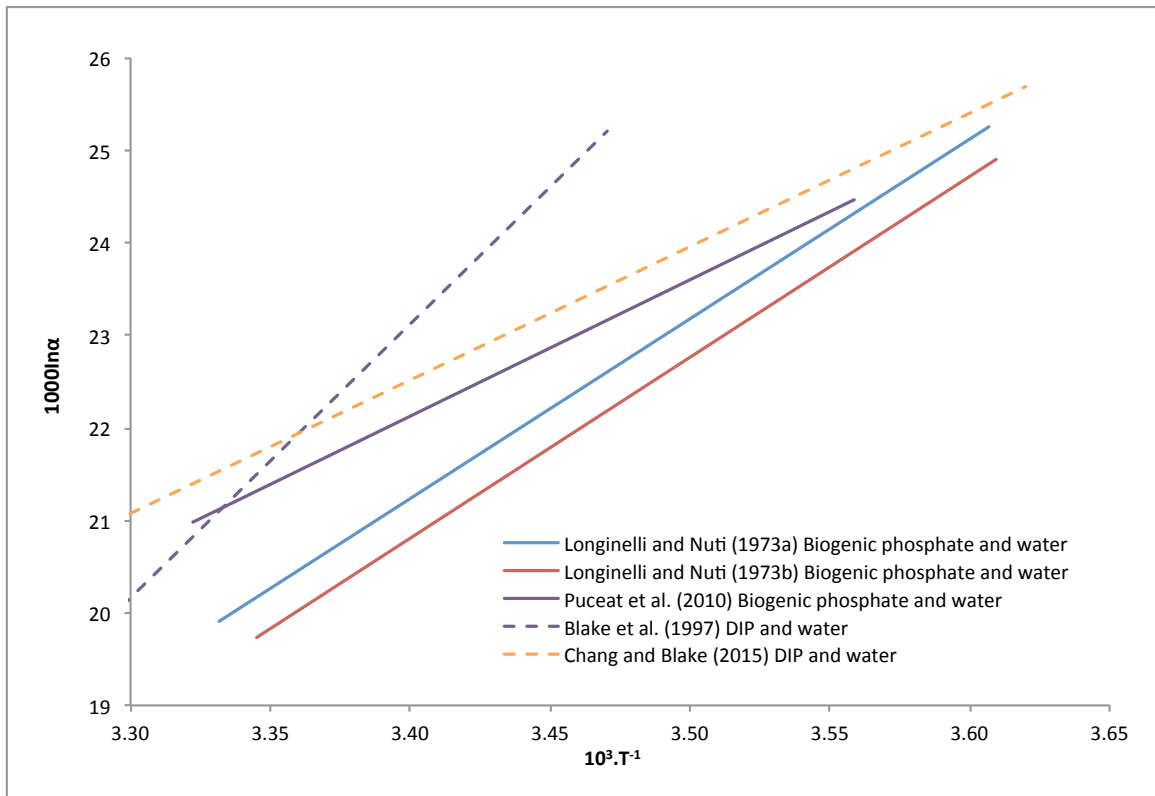


Figure 1.4 Oxygen isotope fractionation equation between biogenic phosphate and water (Longinelli and Nuti, 1973a, 1973b; Puceat et al., 2010), and DIP and water (Blake et al., 1997; Chang and Blake, 2015).

1.3 Oxygen isotope fractionation between HAP-bound carbonate and water

Since the pioneering studies of Longinelli and Nuti (1973a, b) and Kolodny et al. (1983), several studies on oxygen isotope fractionation between phosphate and water have been performed to quantify marine paleotemperature (Lécuyer et al., 1996; Puceat et al., 2003; Trotter et al., 2008; Puceat et al., 2010; Chang and Blake, 2015). As mentioned in section 1.1, bioapatite contains oxygen in structural carbonate (CO_3^{2-}). As suggested by Bryant et al. (1996) and Iacumin et al. (1996), the climatic signal can be determined through the variations of this structural CO_3^{2-} by dissolving structural CO_3^{2-} in apatite into

H₃PO₄. While, a plethora of studies have determined the oxygen isotope systematics between the phosphate in apatite and water, few research has been conducted on the oxygen isotope systematics between carbonate-bearing HAP and water. Therefore, Lécuyer et al. (2010) was the first to investigate the oxygen isotope fractionation between the structural CO₃²⁻ of inorganically precipitated hydroxyapatite (HAP) and water in the temperature range of 10-37 °C (Table 1.1). This study demonstrated that there is temperature dependence of the oxygen isotope fractionation between HAP-bound carbonate and water (Lécuyer et al., 2010). Lécuyer et al. (2010) observed that oxygen isotope fractionation factors between HAP-bound carbonate and water decrease from 32.46-32.80 ‰ at 10 °C to 24.50-25.24 ‰ at 37 °C. However, this fractionation relationship has a different slope compared to the carbonate and water system by Kim and O'Neil (1997) (Fig. 1.5). Thus, due to a steeper slope found between the oxygen isotope fractionation between inorganic carbonate-bearing HAP and water, Lécuyer et al. (2010) concluded that the oxygen isotope equilibrium could not be demonstrated with increasing temperature (Lécuyer et al., 2010). Moreover, Lécuyer et al. (2010) observed that the oxygen isotope fractionation between HAP-bound carbonate and water demonstrated a large isotopic difference up to approximately - 3.5‰ decreasing temperatures compared to the bioapatites and water that was proposed by Kolodny et al. (1983) (Fig. 1.5). From these observations, Lécuyer et al. (2010) found that this discrepancy is caused by the analytical methods employed either from Lécuyer et al. (2010) or Kolodny et al. (1983) (Lécuyer et al., 2010). As discussed in section 1.1, the difference in the analytical techniques used between each laboratories can create an offset

to the empirically determined oxygen isotopic fractionations (Puceat et al., 2010; Chang and Blake., 2015).

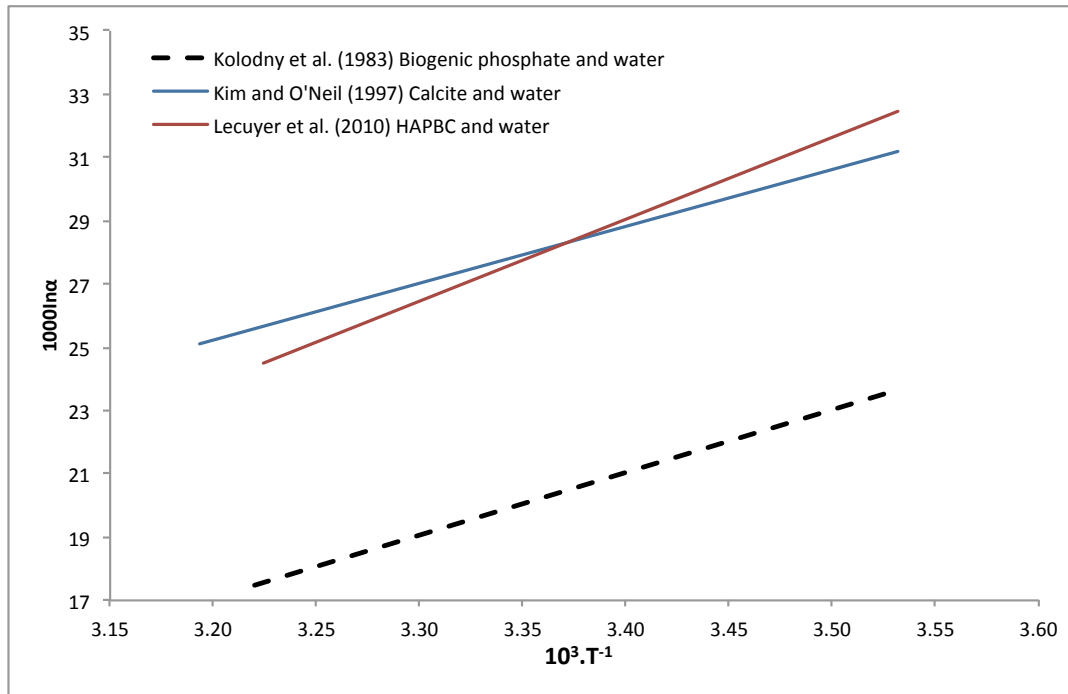


Figure 1.5 Oxygen isotope fractionation equation between inorganic HAP-bound carbonate and water compared to the inorganic calcite and water equation (Kim and O'Neil, 1997) and the biogenic phosphate and water equation (Kolodny et al., 1983).

Furthermore, inorganic carbonate-bearing HAP tends to have lower amount of structural CO_3^{2-} than most bioapatites (Lécuyer et al., 2010). Koch et al. (1997) and Zazzo et al. (2004) reported sufficient amount of structural CO_3^{2-} amounts of approximately 3.4 to 4.0 wt% for the untreated tooth enamel from bioapatite samples, whereas the study by Lécuyer et al. (2010) only contained 0.05-0.23 wt% amounts of structural CO_3^{2-} from their inorganic HAP. Lécuyer et al. (2010) explained that these differences of the amount of structural CO_3^{2-} between bioapatites and inorganic HAP are

caused by the lack of organic matrix which lead to a higher degree of crystallization of inorganic carbonate-bearing HAP.

The oxygen isotope fractionation between HAP-bound carbonate and water that was conducted by Lécuyer et al. (2010), was then subsequently used in recent studies by Eagle et al. (2010, 2011) and Suarez and Passey (2014). These studies used the advent of the carbonate clumped isotope paleothermometer which allows temperature information to be retrieved from carbonates as diverse as corals, foraminifera, soil carbonates and bioapatite (Ghost et al., 2006; Eagle et al., 2010; 2011; Suarez and Passey, 2014; Spencer and Kim, 2015). Specifically, Eagle et al. (2011) used the oxygen isotope fractionation between HAP-bound carbonate-water by Lécuyer et al. (2010) in order to calculate the $\delta^{18}\text{O}$ value of parent water from which the bioapatite from fossilized teeth of large Jurassic sauropods formed. This is due to the fact that there was no other existing fractionation equation for inorganic carbonate in apatite at low temperatures other than Lécuyer et al. (2010) experimental study.

1.4 Thesis structure

Chapter 1 provides an overview of phosphate minerals and their applications in stable isotope geochemistry. It also discusses previous studies on the oxygen isotope fractionation between phosphate and water, DIP and water, as well as phosphate-bound carbonate and water.

Chapters 2 and 3 are presented as a research paper format. Chapter 2 acts as an important stepping stone in the refinement of the synthesis method for carbonate-bearing

HAP that was first described by Lécuyer et al. (2010). Various physicochemical conditions, such as solution pH, initial solution concentrations of NaHCO_3 , mineral precipitation rate, and formation temperature were tested in order to obtain pure HAP crystals and thus to better determine the oxygen isotope fractionation between HAP-bound carbonate and water. Chapter 3 explores the temperature dependence of oxygen isotope fractionation between phosphate and water, as well as HAP-bound carbonate and water between 10 and 40 °C. Additionally, this chapter evaluates the effects of mineral precipitation rates and three distinct initial concentrations of NaHCO_3 on the oxygen isotope compositions of the HAP crystals. These parameters are crucial for the attainment of the oxygen isotope equilibrium in the HAP-bound carbonate and water system, and the phosphate and water system.

Chapter 4 contains the conclusions of this thesis. This chapter summarizes the research completed, includes the candidate's contributions to the research, identifies the applications associated with the research findings, and outlines future areas of investigation.

References

- Amiot, R., Lécuyer, C., Escarguel, G., Billon-Bruyat., J-P., Buffetaut, E., Langlois, C., Martin, S., Martineau, F. and Mazin J-M. (2007) Oxygen isotope fractionation between crocodilian phosphate and water. *Palaogeography, Paleoclimatology, Palaeoecology* **243**, 412-420.
- Ayliffe, L. K., Lister, A. M. and Chivas, A. R. (1992) The preservation of glacial-interglacial climatic signatures in the oxygen isotopes of elephant skeletal phosphate. *Palaogeology Paleoclimatology Palaeoecology* **99**, 179-191.
- Balter V. and Lécuyer C. (2004) Determination of Sr and Ba partition coefficients between apatite and water from 5 °C to 60 °C: A potential new thermometer for aquatic paleoenvironments. *Geochimica et Cosmochimica Acta* **68**, 423-432.
- Bassett, D., MacLeod, L., Miller, J. and Ethington, R. (2007) Oxygen isotopic composition of biogenic phosphate and the temperature of early ordovician seawater. *Palaios* **22**, 98-103.
- Blake, R. E., O'Neil, J. R. and Garcia, G. A. (1997) Oxygen isotope systematics of biologically mediated reactions of phosphate: Microbial degradation of organophosphorus compounds. *Geochemica et Cosmochimica Acta* **20**, 4411-4422.
- Blake, R. E. (1997) Experimental investigations of organic and microbially mediated reactions of aluminosilicates and phosphates. p.H. D. thesis, University of Michigan, 213p.
- Blake, R. E., O'Neil, J. R. and Surkov, A. (2005) Biogeochemical cycling of phosphorus: Insights from oxygen isotope effects of phosphoenzymes. *American Journal of Science* **305**, 596-620.
- Blake, R. E., Chang, S. J. and Lepland, A. (2010) Phosphate oxygen isotopic evidence for a temperate and biologically active Archaean ocean. *Nature* **464**, 1029-1032.
- Bryant, J., Luz, B. and Froelich, P. (1994) Oxygen isotopic composition of fossil horse tooth phosphate as a record of continental paleoclimate. *Paleogeography, Paleoclimatology, Paleoecology* **107**, 303-316.
- Bryant J. D., Koch P. L., Froelich P. N., Showers W. J. and Genna B. J. (1996) Oxygen isotope partitioning between phosphate and carbonate in mammalian apatite. *Geochimica et Cosmochimica Acta* **60**, 5145-5148.

- Chang, S. J. and Blake, R. E. (2015) Precise calibration of equilibrium oxygen isotope fractionations between dissolved phosphate and water from 3 to 37 °C. *Geochemica et Cosmochimica Acta* **150**, 314-329.
- Crowson, R. A., Wright, E. K. and Hoering, T. C. (1991) Preparation of phosphate samples for oxygen isotope analysis. *Anal. Chem.* **63**, 2397-2400.
- Dettman, D. L., Kohn, M. J., Quade, J., Ryerson, F. J., Ojha, T. P. and Hamidullah, S. (2001) Seasonal stable isotope evidence for a strong Asian monsoon throughout the past 10.7 myr. *Geology* **29**, 31-34.
- Eagle, R. A., Schauble, E. A., Tripathi, A. K., Tutken, T., Hulbert, R. and Eiler, J. M. (2010) Body temperatures of modern and extinct vertebrates from ^{13}C - ^{18}O bond abundances in bioapatite. *Proceedings of the National Academy of Sciences of the United States of America* **107**, 10377-10382.
- Eagle R. A., Tutken T., Martin T. S., Aradhna K. T., Fricke H. C., Connely M., Cifelli R. L. and Eiler J. M. (2011) Dinosaur body temperatures determined from isotopic (^{13}C - ^{18}O) ordering in fossil biominerals. *Science* **333**, 443.
- Eiler, J. M. (2007) “Clumped-isotope” geochemistry- The study of naturally-occurring, multiply-substituted isotopologues. *Earth and Planetary Science Letters* **262**, 309-327.
- Elliot, J. C. (1994) Structure and chemistry of the apatites and other calcium orthophosphates. Elsevier, Amsterdam.
- Epstein, S., Buchsbaum, R., Lowenstam, H. and Urey, H. C. (1951) Carbonate-water isotopic temperature scale. *Bulletin of the Geology Society of America* **62**, 417-426.
- Fricke H. C., William C. C., O’Neil J. R. and Gingerich P. D. (1998a) Evidence for rapid climate change in North America during the latest Paleocene thermal maximum: oxygen isotope compositions of biogenic phosphate then the Bighorn Basin (Wyoming). *Earth and Planetary Science Letters* **160**, 193-208.
- Fricke H. C., Clyde W. C. and O’Neil, J. R. (1998b) Intra-tooth variations in $\delta^{18}\text{O}$ (PO_4) of mammalian tooth enamel as a record of seasonal variations in continental climate variables. *Geochimica et Cosmochimica Acta* **62**, 1839-1850.
- Fricke, D. C. and Rogers, R. R. (2000) Multiple taxon-multiple locality approach to providing oxygen isotope evidence for warm-blooded theropod dinosaurs. *Geology* **28**, 799-802.

- Ghosh, P., Adkins, J., Affek, H., Balta, B., Guo, W., Schauble, E. A., Schrag, D. and Eiler, J. M. (2006) ^{13}C - ^{18}O bonds in carbonate minerals: A new kind of paleothermometer. *Geochimica et Cosmochimica Acta* **70**, 1439-1456.
- Iacumin, P., Cominatto, D. and Longinelli, A. (1996) A stable isotope study of mammal skeletal remains of mid-Pleistocene age, Arago cave, eastern Pyrenees, France. Evidence of taphonomic and diagenetic effects. *Plaeogeogr. Plaeoclimatol. Palaeoecol.* **126**, 151-160.
- Joachimski, M., (2006) Constraints on Pennsylvannian glacioeustatic sea-level changes using oxygen isotopes of conodont apatite. *Geology* **34**, 277-280.
- Kim S-T. and O'Neil J. R. (1997) Equilibrium and nonequilibrium oxygen isotope effects in synthetic carbonates. *Geochimica et Cosmochimica Acta* **61**, 3461-3475.
- Koch, P. L., Tuross, N. and Fogel, M. L. (1997) The effects of sample treatment and diagenesis on the isotopic integrity of carbonate in biogenic hydroxyapatite. *J. Archeol. Sci.* **24**, 417-429.
- Kohn, M. J., Rakovan, J. and Hughes, J. M. (2002) Phosphates: Geochemical, geobiological, and material importance. *Reviews in Mineralogy and Geochemistry*, **48**. Mineralogical Society of America, Washington, DC.
- Kohn, M. J. and Cerling, T. E. (2002) Stable isotope compositions of biological apatite. In Phosphates, Geochemical, Geobiological, and Materials Importance. *Reviews in Mineralogy and Geochemistry*, **48** (eds. M. J. Kohn, J. Rakovan and J. M. Hughes). Mineralogical Society of America, Washington, DC, pp. 455–488.
- Kohn, M. J., Miselis, J. L. and Fremd, T. J. (2003) Oxygen isotope evidence for progressive uplift of the cascade range, Oregon. *Earth Planet Science Letter*.
- Kolodny Y., Luc B. and Navon O. (1983) Oxygen isotope variations in phosphate of biogenic apatites, I. Fish bone apatite- rechecking the rules of the game. *Earth and Planetary Science Letters* **64**, 398-404.
- LaPorte, D. F., Holmden, C., Patterson, W. P., Prokopiuk, T. and Eglinton, B. M. (2008) Oxygen isotope analysis of phosphate: improved precision using TC/EA CF-IRMS. *Journal of Mass Spectrometry* **44**, 879-890.
- Lécuyer C., Grandjean P. and Emig C. C. (1996) Determination of oxygen isotope fractionation between water and phosphate from living lingulids: potential application to paleoenvironmental studies. *Paleogeography, Paleoclimatology, Paleocology* **126**, 101-108.

- Lécuyer C., Grandjean P. and Sheppard S. M. (1999) Oxygen isotope exchange between dissolved phosphate and water at temperatures $\leq 135^{\circ}\text{C}$: Inorganic versus biological fractionations. *Geochimica et Cosmochimica Acta* **63**, 855-862.
- Lécuyer, C. (2004) Oxygen isotope analysis of phosphate. *Handbook of Stable Isotope Analytical Techniques* **Vol. 1** (Chp 22), 482-496.
- Lécuyer C., Balter V., Martineau F., Fourel F., Bernard A., Amiot R., Gardien V., Otero O., Legendre S., Panczer G., Simon L. and Martini R. (2010) Oxygen isotopes fractionation between apatite-bound carbonate and water determined from controlled experiments with synthetic apatites precipitated at 10-37 °C. *Geochimica et Cosmochimica Acta* **74**, 2072-2081.
- Lécuyer, C., Amiot, R., Touzaeu, A. and Trotter J. (2013) Calibration of the phosphate $\delta^{18}\text{O}$ thermometer with carbonate-water oxygen isotope fractionation equations. *Chem. Geol.* **347**, 217-226.
- Liang, Y. and Blake, R. E. (2009) Compound- and enzyme-specific phosphodiester hydrolysis mechanisms revealed by ^{18}O of dissolved inorganic phosphate: implications for marine P cycling. *Geochimica et Cosmochimica Acta* **73**, 3782-3794.
- Longinelli, A. (1966) Ratios of oxygen-18: Oxygen-16 in phosphate and carbonate from living and fossil marine organisms. *Nature* **211**, 923-927.
- Longinelli, A. (1984) Oxygen isotopes in mammal bone phosphate: A new tool for paleohydrological and paleoclimatological research?. *Geochimica et Cosmochimica Acta* **48**, 385-390.
- Longinelli, A. and Nuti, S. (1973a) Revised phosphate-water isotopic temperature scale. *Earth and Planetary Science Letters* **19**, 373-376.
- Longinelli, A. and Nuti, S. (1973b) Oxygen isotope measurements of phosphate from fish teeth and bones. *Earth and Planetary Science Letters* **20**, 337-340.
- McCrea, J. M. (1953) Revised on the isotopic chemistry of carbonates and a paleotemperature scale. *The Journal of Chemical Physics* **18**, 849-857.
- Northrop, D. A. and Clayton, R. N. (1966) Oxygen isotope fractionations in systems containing dolomite. *J. Geol.* **74**, 174-196.
- O'Neil, J. R., Roe, L. J., Reinhard, E. and Blake, R. E. (1994) A rapid and precise method of oxygen isotope analysis of biogenic phosphate. *Isr. J. Earth Sci.* **43**, 203-212.

- O'Neil, J. R., Vennemann, T. W. and McKenzie, W. F. (2003) Effects of speciation on equilibrium fractionations and rates of oxygen isotope exchange between $(\text{PO}_4)_{\text{ag}}$ and H_2O . *Geochimica et Cosmochimica Acta* **67**, 3135-3144.
- Puceat, E., Lécuyer, C., Sheppard, S. M. F., Dromart, G., Reboulet, S. and Grandjean, P. (2003) Thermal evolution of Cretaceous Tethyan marine waters inferred from oxygen isotope composition of fish tooth enamels. *Palaeoceanography* **18**, 1029.
- Puceat, E., Joachimski, M., Bouilloux, A., Monna, F., Bonin, A., Motruil, S., Moriniere, P., Henard, S., Mourin, J., Dera, G. and Quesne, D. (2010) Revised phosphate-water fractionation equation reassessing paleotemperatures derived from biogenic apatite. *Earth and Planetary Science Letters* **298**, 135-142.
- Shemesh A. (1990) Crystallinity and diagenesis of sedimentary apatites. *Geochimica et Cosmochimica Acta* **54**, 2433-2438.
- Spencer, C. and Kim, S-T. (2015) Carbonate clumped isotope paleothermometry: A review of recent advances in CO_2 gas evolution, purification, measurement and standardization techniques. *Geosciences Journal* **19**, 257-274.
- Stuart-Williams H. L. and Schwarz H. P. (1997) Oxygen isotopic determination of climatic variation using phosphate from beaver bone, tooth enamel, and dentine. *Geochimica et Cosmochimica Acta* **61**, 2539-2550.
- Straight, W. H., Davis, G. L., Skinner, C. W., Haims, A., McClennan, B. and Tanke, D. H. (2009) Bone lesions in Hadrosaurs: computed tomographic imaging as a guide for paleohistologic and stable isotopic analysis. *Journal of Vertebrate Paleontology* **29**, 315-325.
- Suarez, M. B. and Passey, B. H. (2014) Assessment of the clumped isotope composition of fossil bone carbonate as a recorder of subsurface temperatures. *Geochimica et Cosmochimica Acta* **140**, 142-159.
- Tudge, A. (1960) A method of analysis of oxygen isotopes in orthophosphate- its use in the measurement of paleotemperatures. *Geochemica et Cosmochimica Acta* **18**, 81-93.
- Trotter, J. A., Williams, I. S., Barnes, C. R., Lécuyer, C. and Nicoll, R. S. (2008) Did cooling oceans trigger Ordovician biodiversification? Evidence from conodont thermometry. *Science* **321**, 550-554.
- Urey, H. C. (1947) The thermodynamic properties of isotopic substances. *Journal of the Chemical Society*, 562-581.

- Vennemann, T. W., Fricke, H. C., Blake, R. E., O'Neil, J. R. and Colman, A. (2002) Oxygen isotope analysis of phosphate: a comparison of techniques for analysis of Ag_3PO_4 . *Chemical Geology* **185**, 321-336.
- Wenzel, B., Lecuyer, C. and Joachimski, M. (2000) Comparing oxygen isotope records of Silurian calcite and phosphate- $\delta^{18}\text{O}$ compositions of brachiopods and conodonts. *Geochimica et Cosmochimica Acta* **64**, 1859-1872.
- Zachos, J. C., Stott, L. D. and Lohmann, K. C. (1994) Evolution of early Cenozoic marine temperatures. *Paleoceanography* **9**, 353.
- Zazzo, A., Lécuyer, C. and Mariotti, A. (2004) Experimentally controlled carbon and oxygen isotope exchange between bioapatites and water under inorganic and microbially-mediated conditions. *Geochimica et Cosmochimica Acta* **68**, 1-12.
- Zheng, Y-F. (1996) Oxygen isotope fractionation involving apatites: Application to paleotemperature determination. *Chemical Geology* **127**, 177-187.
- Zheng, Y-F. (2015) Oxygen isotope fractionation in phosphates: the role of dissolved complex anions in isotope exchange. *Isotopes in Environmental and Health Studies*, 1-16.

CHAPTER 2:

Synthesis of carbonate-bearing hydroxyapatite at 25 °C

Synthesis of carbonate-bearing hydroxyapatite at 25 °C

Kesia Ie^a, Julianne Bagg^b and Sang-Tae Kim^a

^aSchool of Geography and Earth Sciences, McMaster University, 1280 Main Street West, Hamilton, ON L8S 4K1, Canada

^bFaculty of Medicine, University of Toronto, 1 King's College Circle, Toronto, ON M5S 1A8, Canada

Abstract

For the synthesis of inorganic hydroxyapatite crystals and hydroxyapatite-bound carbonate, two mixing techniques (instantaneous and slow) were employed. In order to develop a simple method to synthesize hydroxyapatite ($\text{Ca}_{10}(\text{PO}_4)_6(\text{OH})_2$), the experimental protocol proposed by Lécuyer et al. (2010) was modified. Samples of crystalline hydroxyapatite were prepared at 25 °C by precipitation from starting solutions under a variety of experimental conditions (variation of initial and final pH, variation of rates of addition and maturation of the mixed solutions, and variation of concentrations of NaHCO_3 used). At a pH above 6.7 the instantaneous mixing experiment produced a single phase of pure hydroxyapatite (as shown by XRD analysis); however, at a pH between 5.5 and 6.4 the same mixing rate produced a mixture of brushite, octacalcium phosphate, and hydroxyapatite. Under the slow mixing technique, XRD patterns were indicative of the presence of a secondary phase, octacalcium phosphate ($\text{Ca}_8\text{H}_2(\text{PO}_4)_6 \cdot 5\text{H}_2\text{O}$), with a pH value above 6.7. Furthermore, the effect of concentrations of NaHCO_3 is important in order to yield sufficient amount of structural carbonates (% wt) in HAP. It was found that under the instantaneous mixing method, the amounts of structural carbonates in HAP were relatively lower compared to the slow mixing experiment. The apparent trend from the influence of the slow mixing experiment is slightly close to the expected values of the natural carbonate yield from biogenic apatite samples. From the experimental processes and the characterization of the crystals produced, it was concluded that the mixing rates, the effect of pH, and the concentrations of NaHCO_3 are critical for the purity of the final product of hydroxyapatite and hydroxyapatite-bound carbonate and its crystallographic characteristics.

2.1 Introduction

There are a relatively large number of calcium phosphate minerals, but hydroxyapatite ($\text{Ca}_{10}(\text{PO}_4)_6(\text{OH})_2$), otherwise known as HAP, is the most abundant and stable form of the calcium phosphate mineral. It has the solubility of 1.67 (Table 2.1) and occurs from a $\text{pH} > 9$ (neutral to basic) (Dorozhkin, 2007). HAP is widely used in the fields of earth sciences, biology, and anthropology because it is a major component of hard tissues, such as bones and tooth enamel, and fossils, and is often used in the analysis of oxygen isotope composition (Elliot, 1994; Bingol and Durucan, 2011). There are many applications for synthesizing HAP, including in the fields of geochemistry, dentistry, and medicine (Aoba and Moreno, 1984; Inskeep and Silvertooth, 1987; Knabe et al., 2002). For example, Knabe et al. (2002) used HAP as a coating on oral implants to achieve optimal surface geometry and physiochemical properties.

In general, the characteristics of HAP and HAP-bound carbonate can be influenced by control of precipitation rate, nucleation, chemical composition, and morphology. As a result, many different methods have been developed for the synthesis of HAP (Aoba and Moreno, 1984; Nishioka et al., 1986; Inskeep and Silvertooth, 1987; Yamasaki et al., 1990; Ferraz et al., 2004; Balter and Lécuyer, 2004; Earl et al., 2006). The most popular techniques are through solid state reactions (e.g., seeding crystal growth) and wet techniques (e.g., hydrothermal conditions and hydrolysis) (Nancollas and Mohan, 1970; Aoba and Moreno, 1984; Nishioka et al., 1986; Inskeep and Silvertooth, 1987; Yamasaki et al., 1990; Iijima et al., 1997; Ferraz et al., 2004; Earl et al., 2006; Ito et al., 2014). Seeding crystal growth is a method to determine the stoichiometry

of the precipitating phase (Aoba and Moreno, 1984; Inskeep and Silvertooth, 1988). In this scenario, supersaturated calcium phosphate solutions are introduced to a seed crystal of HAP and growth rate is monitored by the concentration of HAP ions in the supersaturated solutions. Supersaturated calcium phosphate solutions are essential to enhance the understanding of the process and mechanisms in the synthesis of seeded crystal growth for HAP (Aoba and Moreno, 1984). Hence, Aoba and Moreno (1984) conducted the seeding crystal growth technique to prepare HAP powders with different particle sizes where the specific surface areas of the resulting seeded crystal growth can be controlled. Nevertheless, the precipitation of HAP is highly dependent on the degree of supersaturated solutions on HAP. In essence, the surface properties of the seed crystals are highly affected by small differences in the supersaturated solutions and kinetic runs in producing substantial amounts of HAP (Aoba and Moreno, 1984). Nancollas and Mohan (1970) proposed an alternative method of synthesizing the HAP seed crystals under a constant pH of 7.4 and using a calcium phosphate solution supersaturated with respect to HAP, which is similar to the technique characterized by Aoba and Moreno (1984). They determined the growth rate of HAP crystals, which was monitored by the concentration of lattice ions in supersaturated solutions. Moreover, Inskeep and Silvertooth (1988) also conducted the technique of seed HAP crystal growth under pH conditions using several empirical rate equations that were suggested by Nancollas and Mohan (1970). These empirical rate equations are used to explain the rate of synthetic HAP from calcium, phosphate, and hydroxide (Inskeep and Silvertooth, 1988).

Another approach to examine HAP synthesis is via hydrothermal methods, as originally suggested by Earl et al. (2006). HAP was synthesized at a high temperature of 200 °C in a hydrothermal reactor for approximately 1 to 3 days, yielding different isotopic compositions of HAP (Earl et al., 2006). Instead of regular physiological apatite, nanosized particles were obtained for the purpose of the mitigation of hypersensitivity in dentinal tubules (Earl et al., 2006). Recent study to synthesize HAP via the hydrothermal method was also used by Bingol and Durucan (2011). Bingol and Durucan (2011) suggested that hydrothermal conditions make the synthesis of HAP more efficient as the reaction kinetics are greatly enhanced.

Lécuyer et al. (2010) recently reported their method for the synthesis of inorganic carbonate-bearing HAP. To identify the mineralogy of their precipitations, they used infrared spectroscopy and electron microscopy. Lécuyer et al. (2010) prepared two aqueous solutions (KNaCO₃ mixed with Na₂HPO₄•2H₂O and CaCl₂•2H₂O) with a pH of 7.4 and constant temperatures of 10°C, 15°C, 20°C, 25°C, 30°C, and 37°C. This method is similar to the method employed by Nancollas and Mohan (1970) that maintained a constant physiological pH of 7.4 at 25 °C to study the growth of HAP crystals. After mixing the two aqueous solutions, Lécuyer et al. (2010) followed the technique used by Balter and Lécuyer (2004) for the maturation of the solutions for 96 hours. Below 10 °C, carbonate-bearing HAP did not precipitate. Conversely, above 10 °C, carbonate-bearing HAP was identified (Balter and Lécuyer, 2004; Lécuyer et al., 2010). As a result, Lécuyer et al. (2010) concluded that pH and temperature were important in order to obtain well-crystallized HAP growth and HAP-bound carbonate.

Krajewski et al. (2005) reported that HAP has two different sites within its structure that can hold carbonate ions: the A-type carbonate apatite is where the crystal planes have a positive charge and the CO_3^{2-} ions are substituted with OH^- ions, whereas the B-type is where the PO_4^{3-} ions can be substituted by the CO_3^{2-} ions in the apatite lattice (Elliot, 1994; Krajewski et al., 2005; Goto et al., 2012). HAP that has A-type carbonate apatites are usually prepared by passing CO_2 gas over HAP at high temperatures under dry conditions (LeGeros, 1991). In contrast, hydrolysis and precipitation techniques are typically employed in the preparation of B-type carbonate apatites (LeGeros, 1991). The utilization of X-ray diffraction (XRD) and infrared spectroscopy (IR) are important in order to differentiate these two types of carbonate-bearing HAP (Elliot, 1994; Krajewski et al., 2005). For instance, Wilson et al. (1999) detected direct substitution of the B-type carbonate-bearing HAP from powder XRD data. Krajewski et al. (2005) also identified the types of compounds obtained through XRD. Certain peaks will be present in IR spectra if the samples run are HAP-bound carbonate. Bands associated with calcium phosphates ($1090\text{-}1040\text{ cm}^{-1}$) should be present with those characteristics of a CO_3^{2-} ion in the B-type ($1457\text{-}1420\text{ cm}^{-1}$) or a CO_3^{2-} ion in the A-type (1550 cm^{-1}) (Krajewski et al., 2005). It has been observed that as carbonate content increases, the presence of A-type carbonate is reduced and the presence of B-type is increased (Krajewski et al., 2005, Goto et al., 2012).

The main purpose of this study is therefore to develop and refine the synthesis method for carbonate-bearing HAP proposed by Lécuyer et al. (2010) at $25\text{ }^\circ\text{C}$. The synthesis of HAP-bound carbonate at various experimental conditions (e.g., mixing rates,

pH, and concentrations of NaHCO_3) is essential prior to the characterization of the oxygen isotope systematics in the HAP-bound carbonate and water. In addition, XRD analysis is employed to provide information on crystallographic characteristics of the samples, which allow us to define experimental conditions necessary to synthesize pure HAP crystals.

2.2 Experimental methods

2.2.1 Inorganic precipitation of carbonate-bearing hydroxyapatite

Carbonate-bearing HAP was synthesized in this study by modifying Lécuyer et al. (2010)'s protocol. They mixed two chemically distinct solutions and subsequently matured the mixed solution for 4 days at specific temperatures ranging between 10 and 37 °C.

In this study, synthesis of carbonate-bearing HAP was carried out at 25 °C. The phosphate-carbonate containing solution (PC) was prepared by adding ACS-grade Na_2HPO_4 and NaHCO_3 to 500 mL deionized water and then thermally equilibrating the solution for a minimum of 7 days. Table 2.1. shows the final concentration of the PC solutions. Initially 0.5 mL of a NaHCO_3 solution of either 100 mmolal or 200 mmolal concentration was used as a source of the carbonate phase. However, this was later changed to a higher volume and concentration in order to ensure a sufficient amount of structural carbonates within the HAP. About 1 or 2 mL of 2% HCl was used to adjust the pH of the PC solution. However, this pH adjustment was also later discontinued because this step was found to be unnecessary to synthesize pure HAP.

The calcium-containing solution (CA) was prepared by dissolving 10 mmol of $\text{CaCl}_2 \cdot 2\text{H}_2\text{O}$ to 1 L of deionized water. The CA solution was also stored for a minimum of 7 days at 25 °C prior to its use. Subsequently, 100 mL from each of the CA and PC solutions were mixed instantaneously and then the mixed solution was matured for 4 to 14 days in a temperature-controlled water bath at 25 ± 0.01 °C (Fig. 2.1 and Table 2.2). The reason for this long-term maturation period is to yield well-crystalized HAP based upon Lécuyer et al. (2010)'s experimental observations. They reported that amorphous calcium phosphate (ACP) formed when the mixed solution was matured less than 96 hours (Balter and Lécuyer, 2004; Lécuyer et al., 2010). Subsequently, the mixed solution was filtered through a 0.45 μm membrane filter by using a vacuum filtration system. The collected precipitates were first washed with deionized water ($\sim 18 \text{ M}\Omega \text{ cm}$) and then methanol before they were dried at room temperature or 70 °C for at least 1 day. Furthermore, in order to examine the influence of the mixing rate for the synthesis of carbonate-bearing HAP, a series of slow-rate mixing experiments were performed in this study (Fig. 2.2 and Table 2.3). In this case, the PC solution was injected into the CA solution by using a syringe pump either at an injection rate of 2.08 mL/hr (2 days) or 0.594 mL/hr (7 days). Thereafter, the slowly mixed solutions were either matured for 7 days or filtered immediately for sampling. The reason for the two different maturation periods is to investigate the conditions necessary to synthesize HAP under slow precipitation rates.

2.2.2 pH measurements

In order to identify the pH conditions required to form HAP-bound carbonate, PC solutions of various compositions were prepared at different pH values (5.5 to 7.4). The pH of the solutions was determined by using a Thermo Scientific Orion combination pH electrode connected to a Radiometer PHM 84 pH meter. The electrode was calibrated using three NIST-traceable buffers (e.g., pH = 4.00, pH = 7.02, and pH = 10.05) at 25 °C. All of the pH measurements were undertaken right after the mixture of the PC and the CA solutions were prepared (initial pH), and right before the filtration of the mixed solution after a given period of maturation (final pH). For some solutions from the early fast precipitation experiments (i.e., MRSI-Bagg-20 to Ie-11C), the pH was measured using pH paper (Table 2.2).

2.2.3 X-ray diffraction

X-ray diffraction (XRD) was used to determine the mineralogy of the precipitates in this study. XRD data was collected using a Bruker Smart 6000 CCD area detector, a Bruker 3-Circle D8 Goniometer, a Rigaku RU 200 CuK α rotating anode source, and a Goebel cross-couple parallel focusing mirror at the McMaster Analytical X-Ray Diffraction Facility. A total of 26 samples were analyzed, representing a range of different experimental conditions. Four frames were collected for each sample to get a continuous 2θ range from 5 ° to 70 ° with an exposure time of 300 seconds. The majority of phosphate and carbonate peaks are within this range and the scattering intensity decreases towards a higher angle.

XRD is a technique that examines x-ray diffraction from crystalline compounds. In general, XRD works on the principle that a crystalline solid produces a unique diffraction pattern based on its crystal structure. The position and the intensity of the diffraction patterns or the peaks produced indicate a certain crystal phase (Glusker and Trueblood, 2010). XRD was used in this study to identify phosphate crystals obtained from different experimental conditions and to define experimental conditions for the synthesis of pure HAP.

2.2.4 Quantification of structural carbonate (CO_3^{2-}) in HAP

The amount of structural CO_3^{2-} within HAP precipitate was determined using a VG-optima isotope ratio mass spectrometer (IRMS) that is equipped with an automated IsoCarb or a Gas Bench II headspace auto-sampler with a Thermo Finnigan Delta plus XP isotope ratio mass spectrometer at McMaster University. For samples MRSI-Ie-8A to MRSI-Ie-15, approximately 2.5 mg (2500 μg) were weighed and reacted with anhydrous phosphoric acid at 90 °C. All other CO_2 measurements of HAP-bound carbonates (MRSI-Ie-16A to MRSI-Ie-35SP4) were analyzed using a Gas Bench II system. The samples were weighed to approximately 10 to 14 mg in order to detect structural CO_3^{2-} within the HAP samples. The amount of structural carbonate (CO_3^{2-}) was estimated by calibrating the mass 44 peaks area (Fig. 3) based on four different weights (0.05, 0.10, 0.15, and 0.20 mg) of internal laboratory standard, Carrara. Structural CO_3^{2-} content in the HAP samples ranged from 0.12 to 3.44 wt %.

2.3 Results and discussion

2.3.1 Lécuyer et al. (2010) vs. this study

Lécuyer et al. (2010) adapted the synthesis method used by Balter and Lécuyer (2004) where two solutions were employed at a specific temperature between 10 to 37 °C (Table 2.4). The first starting solution (PC) was prepared by adding 0.5 mL of 20 mmolal KNaCO_3 to 500 mL of 20 mmolal $\text{Na}_2\text{HPO}_4 \cdot 2\text{H}_2\text{O}$, and the second starting solution (CA) was made by using 20 mmolal of $\text{CaCl}_2 \cdot 2\text{H}_2\text{O}$. Each starting solution was matured for two days to ensure that the carbonate in the PC solution was in isotopical equilibrium with the ambient water (Lécuyer et al., 2010). The pH of the mixed PC and the CA solution was adjusted to approximately 7.4 by adding 0.3% HNO_3 to the PC solution before mixing the two starting solutions together. Indeed, Beck et al. (2005) suggested that in a pure carbonate system the equilibration time between bicarbonate (HCO_3^-) and water at 15, 25, and 40 °C are expected to be ~24, 9, and 2 hours respectively. Moreover, to obtain well-crystallized HAP crystals, Lécuyer et al. (2010) matured the resulting mixed solution for at least 4 days because Balter and Lécuyer (2004) reported that ACP transformed to HAP after 4 days based upon their XRD study.

According to Balter and Lécuyer (2004) and Lécuyer et al. (2010), carbonate-bearing HAP did not form below 10 °C. Instead, brushite was precipitated because there was no transformation of HAP from ACP at 10 °C even after 4 days of maturation. Brushite, also known as dicalcium phosphate dehydrate ($\text{CaHPO}_4 \cdot 2\text{H}_2\text{O}$), is a precursor to apatite (Kumta et al., 2005). Above 10 °C, carbonate-bearing HAP was observed (Lécuyer et al., 2010). The chemical concentrations of PC and CA solutions employed by Lécuyer et al. (2010) also differed from those used for this study where 0.5 to 15 mmolal

of NaHCO_3 and 10 mmolal of NaHPO_4 for the PC solution, and 10 mmolal of $\text{CaCl}_2 \cdot 2\text{H}_2\text{O}$ for the CA solution were used to produce sufficient amount of carbonate in the HAP precipitate. Moreover, both starting solutions of CA and PC for this study were aged for at least 1 to 14 days before mixing. The final pH value varied from 5.5 to 7.4 in this study, whereas Lécuyer et al. (2010) used a pH value of 7.4. In addition, it is important to note that two different mixing rates (instantaneous vs. slow) were used to synthesize HAP-bound carbonate in this study. Table 4 shows the intricate differences between the methods developed in this study and Lécuyer et al. (2010), which affected the samples' final pH, mineralogy, and the precipitations of carbonate in HAP.

2.3.2 Effect of pH on carbonate-bearing HAP

The final pH value of the mixed solution is the most important factor in order to synthesize pure inorganic HAP. Samples MRSI-Bagg-20 to MRSI-Bagg-22 had a final pH value of 5.5 to 6.4, and sample MRSI-Bagg-23 had a final pH value of 7.0. Samples MRSI-Ie-8a to MRSI-Ie-11C had a final pH value of approximately 6.4 to 6.8 (Table 2.2). Samples MRSI-Ie-12 to MRSI-Ie -35SP4 shown in Tables 2.2 and 2.3 were different from other samples because 2% HCl was not added to the PC solution prior to the mixing, which made their final pH significantly higher (pH of 6.7 to 7.4) and thus yielded pure HAP minerals (Tables 2.2 and 2.3).

HAP has the lowest solubility relative to the majority of other calcium phosphate minerals and is preferentially formed under neutral or basic conditions (Johnsson and Nancollas, 1992; Koutsopoulos, 2002). In contrast, octacalcium phosphate (OCP) and

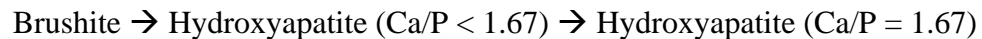
brushite are in fact found in more acidic solutions with a pH value of about 4 to 6 and have a higher solubility than HAP (1.33 and 1 Ca/P ratio) (Koutsoukos and Nancollas, 1981; Johnson and Nancollas, 1992). These three calcium phosphate phases: brushite, OCP, and HAP can be synthesized by methods similar to what was performed in Lécuyer et al. (2010) and this study.

Our XRD analyses showed that MRSI-Bagg-20 that had a final pH value below 6.0 was pure brushite (Fig. 2.4). Samples, such as MRSI-Bagg-21 and MRSI-Bagg-22 that had a final pH value between 6.0 to 6.4, were determined to be a mixture of brushite, OCP, and HAP. When the final pH of the mixed solutions (MRSI-Ie-12 to MRSI-Ie-15) was approximately 6.8 to 7.0, a mixture of OCP and HAP occurred (Fig. 2.4).

Furthermore, a higher pH value was achieved when 2 % HCl was not used, as is the case in samples MRSI-Ie-12 to MRSI-Ie-15, and therefore more HAP crystals were obtained as supported based on the percentile of mineral phases from XRD analyses (Table 2.5 and Fig. 2.4). The rest of the instantaneous mixing methods were found to yield pure HAP when the final pH of the mixed solution is above 7.0 (Fig. 2.5). In contrast, most of the samples (MRSI-Ie-29SP to MRSI-Ie- 35SP4) from the slow mixing experiments were a mixture of OCP and HAP even though the final pH value was above 6.7 (Table 2.5 and Fig. 2.6). It has been documented that HAP is harder to precipitate directly at a pH value below 7 because normally OCP initially nucleates and precipitates before HAP (Elliot et al., 1994; Iijima et al., 1997; Xia et al., 2012; Ito et al., 2014). Nevertheless, MRSI-Ie-28SP and MRSI-Ie-30SP were found to be pure OCP and pure HAP, respectively (Fig.

2.7). Standard reference XRD peaks for HAP, OCP, and brushite are shown in Fig. 2.8 respectively.

Brushite is favourably precipitated in weak acidic environments with a pH value of 4 to 6, and it is usually synthesized by the drop-wise addition of CaCl_2 to ammonium or sodium phosphate at room temperature (Kumta et al., 2005). Brushite can also be synthesized by the neutralization of dilute H_3PO_4 by the addition of calcium succrate at a temperature below 10°C (Elliot, 1994). It is reported that brushite transforms into apatite at a pH value of 7 to 7.5, but will remain stable at this pH range if it is magnesium substituted (Kumta et al., 2005). There are methods for converting brushite into HAP. One hydrolysis method involves first, the structural change of brushite into HAP and second, an increase in the Ca/P ratio (Monma and Kamiya, 1987). This conversion is represented as:



Monma and Kamiya (1987) demonstrated that HAP formed most readily at a pH range between 7.5 and 8 during the first step of structural conversion. During the first step, brushite was suspended in distilled water by bubbling nitrogen gas while the temperature was kept between 40°C and 80°C and pH was between 7.5 and 8. During the second step, the product of the first step was treated in an alkaline solution containing $\text{CaCl}_2 \cdot 2\text{H}_2\text{O}$ (Monma and Kamiya, 1987). Similarly, a recent analysis by Karpikhin et al. (2016) assessed HAP crystal structure via brushite hydrolysis at 60°C . Another method used to convert brushite to HAP is through the boiling of brushite in a solution of sodium hydroxide (Redepenning et al., 1996).

Transformation of OCP to HAP has also been studied by several researchers (Brown et al. 1962; Iijima et al., 1977; Ito et al., 2010; Goto et al., 2012; Ito et al., 2014; Zheng et al., 2015). The methods that are most often used to transform OCP to HAP are by either a hydrothermal treatment or a hydrolysis method. Both methods prompting significant changes in the solution and are suitable to obtain plate-shaped HAP crystals from OCP as proposed by Kamitakahara et al. (2009) and Ito et al. (2010). During the hydrothermal treatment, OCP was treated in distilled water while the temperature was kept between 120 to 240 °C and pH was at 5.5. Kamitakahara et al. (2009) were able to convert OCP to HAP after 3 hours. Conversely, Brown et al. (1962) transformed OCP to HAP using boiling temperature after 72 hours, whereas Nelson and McLean (1984) were able to convert HAP from OCP after 14 hours at 70 °C. All of these hydrothermal conditions kept HAP crystals in a plate-like morphology. Both Iijima et al. (1997) and Ito et al. (2014) proposed transitioning of OCP to HAP via hydrolysis of lattice ions in distilled water at a temperature of 37 °C and a pH of 7.4. These studies via the hydrolysis technique also observed significant changes in the morphology during the transition of OCP, which also showed plate-like crystal characteristics.

The results of our XRD analyses enabled us to define experimental conditions to synthesize pure HAP. Our results suggest that the final pH of the PC solution should be kept at or above 7.0 for the synthesis of 100% HAP (Table 2.5). All of the samples synthesized with a final pH of 7.0 to 7.3 at 25 °C were pure HAP. However, MRSI-Bagg-23 and MRSI-Ie-12 to MRSI-Ie-15 were determined to be a mixture between HAP and OCP because of their final pH values between 6.4 and 6.8. Also, MRSI-Bagg-20 and

MRSI-Bagg-21 were found to be a mixture of brushite, OCP, and HAP (Fig. 2.4) or pure brushite (Fig. 2.5) respectively, due to a low final pH value of 5.5 to 6.0 of their mixed solutions (Table 2.5). Lécuyer et al. (2010) adjusted the pH of their mixed solutions to 7.4 by adding 0.1 M NaOH to the $\text{CaCl}_2 \cdot 2\text{H}_2\text{O}$ solution to precipitate pure HAP instead of brushite. This finding also corresponds to Tas (2002)'s study which utilized the synthesis of biomimetic Ca-HAP powders via synthetic body fluids at 37 °C at a pH value of 7.4. Tas (2002) found that Ca-HAP crystals were synthesized when the pH was reduced from 11 to 7.4 with the addition of 1 M of HCl, whereas whitlockite ($\text{Ca}_9(\text{MgFe})(\text{PO}_4)_6\text{PO}_3\text{OH}$) crystals were precipitated instead when the pH was below 7.4. Koutsopoulos (2002) also synthesized HAP crystals at a pH value between 7 to 8 by adding NH_3 solution and KOH to the HAP solutions. Therefore, all of these studies suggest that a neutral to basic pH is a prerequisite for the synthesis of pure HAP.

2.3.3. Effect of mixing rate on carbonate-bearing HAP

Elliot (1994) proposed that HAP usually does not form directly, but it is more likely to form via an unstable intermediate of OCP or from the precursor of OCP. The reason for this proposal is because OCP nucleates and precipitates more easily than HAP as discussed in section 2.3.2. OCP is a thermodynamically metastable phase of HAP. Therefore, both HAP and OCP have close crystal structures and morphologies, and they are often misinterpreted particularly in the substitution of structural CO_3^{2-} (Johnsson and Nancollas, 1992; Elliot, 1994; Xia et al., 2012). The replacement of structural CO_3^{2-} was found to reduce the crystallinity of HAP, which often leads to changes in the HAP crystal

structure from needle-like to plate-like crystals (Shemesh, 1990; Kohn et al., 1999; Xia et al., 2012). As a result, this will reduce the stability of HAP crystals by increasing its solubility (Table 2.1). Generally, apatite crystallinity is associated with the amount of yield structural carbonates in the apatite (Shemesh, 1990; Zazzo et al., 2004), which means if the amount of structural carbonates decreases, this would lead to an increase in the crystallinity of HAP and vice versa. In general, synthesized HAP crystals are always plate, planar, sheet-like morphologies because these crystals grow *c*-axis in the plane of the plate and lie in the direction of the plate's longest dimension (Elliot, 1994; Dorozhkin, 2007; Xia et al., 2012). Koutsopoulos (2002) and Lécuyer et al. (2010) also showed that all HAP precipitated form subhedral hexagonal crystals by using scanning electron microscope (SEM) and infrared spectroscopy. Using infrared spectroscopy, they were able to note three characteristic absorbance peaks of carbonate-bound to HAP (1456, 1423, and 873 cm^{-1}) (Lécuyer et al., 2010).

Lécuyer et al. (2010) did not specify the mixing rate of their two starting solutions in order to precipitate carbonate-bearing HAP. It is therefore assumed that Lécuyer et al. (2010) only employed an instantaneous mixing experiment to precipitate carbonate-bearing HAP. Krajewski et al. (2005) hypothesized that the formation of apatite and the incorporation of CO_3^{2-} ions into the apatite could be achieved when utilizing a slower mixing method between the two aqueous solutions. Therefore, we tested the effect of mixing of the two starting solutions on the synthesis of pure HAP.

One of the significant factors in the precipitation of carbonate-bearing HAP is the mixing rate of the two starting solutions (i.e., PC to CA), which affects the rate of HAP

nucleation and crystal growth. In this study, a total of 45 samples were prepared by the instantaneous mixing method under various initial NaHCO_3 concentrations, maturation periods, and pH values of the mixed solutions (Table 2.2). An additional 17 samples were prepared by using the slow mixing rate method (Table 2.3). In both instantaneous and slow mixing experiments, once the PC and CA solutions were mixed, a cloudy white precipitation appeared in the mixed solution. It could be that amorphous calcium phosphate(s) immediately precipitated after instantaneously mixing the two starting solutions together based on the proportion of the synthesized apatite phase(s) from XRD analyses. In contrast, in the case of the slow mixing experiments, the PC solution was slowly injected into the CA solution at a given rate per hour (2.08 mL/hr or 0.594 mL/hr), after both the CA and the PC solution were matured for 7 days. From this slow mixing method, it was discovered that calcium phosphate precipitated slower and less amount of precipitation was produced in comparison to the instantaneous mixing experiments. After the mixed solutions from the instantaneous mixing methods were filtered and the precipitates were weighed, all of the precipitates appeared as thick opaque white planar sheets under the microscope (Fig. 2.9 to 2.12). The pure brushite sample (MRSI-Bagg-20) obtained from the instantaneous mixing method appeared as a cloudy needle-shaped precipitation in solution, but as clear, glass-like crystals under the microscope (Fig. 2.13). In contrast, all of the samples from the slow mixing methods appeared as thick light powders that are clumped together under the microscope (Fig. 2.11). They had similar crystal structures to the pure OCP that was produced by the slow mixing method (Fig. 2.13).

Table 5 shows that solid samples that were precipitated under the instantaneous mixing method were either pure HAP or a mixture of HAP and OCP. Conversely, almost all of the precipitates that were prepared under the slow mixing method appeared to be a mixture of OCP and HAP phases. These observations imply that the mixing rate between the two starting solutions is essential to obtain well-crystallized HAP. The difference in mixing rates and maturation times improved the proportion of HAP crystals (Table 2.2 and Table 2.3). Indeed, Koutsopoulos (2002) concluded that precipitation rates and maturation times of the aqueous solutions are “critical for the purity of the product and its crystallographic characteristics” (Koutsopoulos, 2002).

2.3.4 Effect of NaHCO₃ concentration on carbonate phase in HAP

The concentration of NaHCO₃ in the PC solution is another important factor for the precipitation of carbonate-bearing HAP. It was discovered that when the concentration of NaHCO₃ in the PC solution was lower than 5 mmolal, such as the case for MRSI-Bagg-20 to MRSI-Bagg-23, no carbonate phase was detected as shown in Table 2.2. However, a detectable carbonate phase was found with pure HAP when a minimum of 5 mmolal NaHCO₃ in the PC solution was used. The amount of structural CO₃²⁻ in HAP was estimated by calibrating the mass 44 peak area of CO₂ gas (Fig. 2.3) from four different weights (0.05, 0.10, 0.15, 0.20 mg) of McMaster’s internal laboratory standard, Carrara. CO₃²⁻ content in HAP ranges from 0.12 to 3.44 wt% (Tables 2.2 and 2.3). This observation corresponds to the hypothesis proposed by Shemesh (1990) and Kohn et al. (1999) that the amount of structural CO₃²⁻ that substitutes phosphate decreases

when the crystallinity of apatite increases, as indicated by IR-spectroscopy spectra (Shemesh, 1990; Kohn et al., 1999). As shown in Table 2.2, all of the precipitates from the instantaneous mixing rate method have a smaller amount of structural CO_3^{2-} than those from the slow mixing rates method (Table 2.3). Thus, these results demonstrated the increase in HAP crystallinity in comparison to the slow mixing experiments.

Unfortunately, all of the XRD results from this study did not show typical peaks of carbonate minerals. This observation is believed to be related to the relatively low carbonate content of 0.12 to 3.44 wt% in HAP. Lécuyer et al. (2010) synthesized carbonate-bearing HAP samples with 0.05 to 0.23 wt% of CO_3^{2-} and observed peaks of the solid phase of carbonate-bearing HAP through IR-spectroscopy spectra. Therefore, it would be ideal to analyze our samples through IR-spectroscopy spectra in order to show the mineral phases/characteristics other than HAP that were precipitated. Future work with the crystals produced in this study could seek to determine the effectiveness of IR-spectroscopy spectra and to potentially use scanning electron microscope (SEM) to show the mineral phases that were precipitated are well-crystallized HAP.

2.3.5. Effect of NaHCO_3 concentration on carbonate-bearing HAP

The initial NaHCO_3 concentration in the PC solution for the slow mixing method is an essential element in addition to the maturation period and the pH of the mixed solutions for the preparation of carbonate-bound HAP. Based on our XRD results, all of the concentrations of NaHCO_3 in the PC solution from the instantaneous mixing method produced pure HAP crystals with an exception of 5 mmolal of NaHCO_3 samples that were

a mixture of HAP and OCP crystals. On the other hand, under the slow mixing method with an injection rate of 2.08 mL/hr, only pure OCP precipitated from the NaHCO₃ concentration of 5 mmolal (Table 2.3 and Fig. 2.7). At the initial NaHCO₃ concentration of 10 mmolal under both injection rates of 2.08 mL/hr and 0.594 mL/hr, a mixture of OCP and HAP formed although more OCP crystals were found than HAP. Interestingly, it appears that at initial NaHCO₃ concentrations of 15 mmolal, the slow mixing of 2.08 mL/hr and 0.594 mL/hr, did allow sufficient time to allow the precipitation of more HAP than OCP (Table 2.5). For this reason, the higher concentration of NaHCO₃ (15 mmolal) yielded more HAP than OCP at both slow mixing experiments.

As discussed in section 2.3.5, based on the mass 44 area calibration of CO₂ gas there was no distinct relationship found between the effect of NaHCO₃ concentrations and the amount of structural CO₃²⁻ in HAP from the instantaneous mixing method (Table 2.2). The amounts of structural CO₃²⁻ in HAP that were precipitated in this study under this condition was observed from 0.27 up to 1.88 % wt of CO₃²⁻. The reason for the non-relationship between the effect of NaHCO₃ concentrations and the low amount of structural CO₃²⁻ in HAP is rather surprising. A partial explanation for this difference comes from the fact that synthetic apatites have a high degree of crystallization due to a lack of organic matrix (Shemesh, 1990; Kohn et al., 1999; Lécuyer et al., 2010). One drawback to consider for the results of the analysis of carbonate-bearing HAP is that most bioapatites have higher amounts of carbonate than inorganic HAP (Lécuyer et al., 2010). This could potentially pose an issue surrounding the legitimacy of a comparison between the oxygen isotope composition in inorganic HAP and bioapatites. Koch et al. (1997)

reported carbonate amounts around 3.4 to 4.0 wt% for untreated tooth enamel samples, whereas HAP crystals produced by Lécuyer et al. (2010) only had about 0.05 to 0.23 wt% of carbonate.

On the other hand, under the slow mixing method at both injection rates, it appears that the effect of concentration of NaHCO_3 influenced the precipitation amount of structural CO_3^{2-} in HAP. For instance, the 15 mmolal of NaHCO_3 precipitated a higher amount of structural CO_3^{2-} (1.40 to 3.44 % wt of CO_3^{2-}) in HAP samples compared to the 10 mmolal of NaHCO_3 (0.86 to 1.81% wt of CO_3^{2-}) (Table 2.3). Indeed, the average of individual structural CO_3^{2-} from the 15 mmolal NaHCO_3 at an injection rate of 2.08 mL/hr in our experiment is 3.38 ± 0.05 % wt of CO_3^{2-} (Table 2.3), which is nearly identical to the average individual structural CO_3^{2-} in biogenic apatite from untreated teeth enamel (ranges from 3.2 to 4.6 % wt of CO_3^{2-}) that was reported by Koch et al. (1997) and Zazzo et al. (2004). As a result, future studies need to investigate the correlation between the amount of carbonates yielded in inorganic HAP and the effect of NaHCO_3 .

2.4 Conclusions

The calcium phosphate system is very complex as there are many different phosphate and apatite phases involved (Kumta et al., 2005). There are many methodologies that have been described in the literature in order to synthesize HAP crystals. Our findings reveal that the following variations in conditions must be carefully considered to achieve inorganic HAP-bound carbonate: the final pH, the mixing rate to

combine the various solutions, and the concentration of NaHCO_3 . This study attempts to highlight the importance of these conditions (summarized in Table 2.6).

The precipitation of inorganic carbonate-bearing HAP followed a similar protocol that was developed by Lécuyer et al. (2010). Since there was no indication given in Lécuyer et al. (2010) as to how slowly or quickly the two starting solutions were mixed, in this study two different mixing rates were utilized to characterize well-crystallized HAP and HAP-bound carbonate. The final pH of the mixed solution is the most necessary condition to synthesize pure HAP crystals. It was found that when the final pH is less than 6.0, HAP would not synthesize, instead, brushite precipitated. When the final pH is between 6.7 to 7.3, our findings revealed that pure HAP crystals were able to precipitate under the instantaneous mixing experiments. However, for the slow mixing method, a mixture of OCP and HAP was discovered at a final pH above 6.7. Further studies should continue to examine a clear delineation of the pH at which OCP stops being synthesized and HAP starts to form under the slow mixing methods.

Another significant condition to precipitate HAP-bound carbonate was the concentration of NaHCO_3 that was added to each PC solution. All of the samples under the instantaneous mixing method demonstrated pure HAP crystals when the initial concentration of NaHCO_3 was 5, 10, or 15 mmolal. Under slow mixing experiments, using a concentration of 5 mmolal of NaHCO_3 showed only pure OCP crystals; however, with a concentration of 10 mmolal of NaHCO_3 all of the samples appeared to be a mixture of OCP and HAP crystals. Our findings showed no relationship with the yield amount of structural CO_3^{2-} in HAP under the instantaneous mixing method. However, under the

slow mixing method, the amount of structural CO_3^{2-} in HAP increased with an increasing concentration of NaHCO_3 . As a result, further studies are needed to investigate the correlation between the amount of carbonates yielded in inorganic HAP and the concentration of NaHCO_3 . The influence of mixing rate should also be examined as it is possible that at slower mixing and higher concentrations of NaHCO_3 (above 15 mmolal) would lead to an increasing amount of structural CO_3^{2-} in HAP, reaching values that are similar to the natural carbonate yield from bioapatites.

Acknowledgement

Thank you to the members of McMaster Research Group for Stable Isotopologues (MRSI), with a particular mention to Dr. Sang-Tae Kim and Julianne Bagg for their assistance in the sample preparations and feedback on this research paper. Thank you to Martin Kynf and Mohammed El Shenawy for their amazing support in laboratory analyses. Finally, extended thank you to the McMaster Analytical X-Ray Diffraction Facility (MAX), especially to Vicky Jarvis, for their help with analyzing my samples throughout this entire research.

References

- Aoba T. and Moreno E. C. (1984) Preparation of hydroxyapatite crystals and their behavior as seeds for crystal growth. *Journal of Dental Research* **63**, 874-880.
- Balter V. and Lécuyer C. (2004) Determination of Sr and Ba partition coefficients between apatite and water from 5 °C to 60 °C: A potential new thermometer for aquatic paleoenvironments. *Geochimica et Cosmochimica Acta* **68**, 423-432.
- Balter V. and Lécuyer C. (2010) Determination of Sr and Ba partition coefficients between apatite from fish (*Sparus aurata*) and seawater: The influence of temperature. *Geochimica et Cosmochimica Acta* **74**, 3449-3458.
- Beck, W. C., Grossman, E. L. and Morse, J. W. (2005) Experimental studies of oxygen isotope fractionation in the carbonic acid system at 15 °, 25 °, and 40 °C. *Geochimica et Cosmochimica Acta* **69**, 3493-3503.
- Brown, W. E., Smith, J. P., Lehr, J. R. and Ferris, J. S. (1962) Crystallographic and chemical relations between octacalcium phosphate and hydroxyapatite. *Nature* **196**, 1050-1055.
- Brown, W. E., Eidelman, N. and Tomazic, B. (1987) Octacalcium phosphate as a precursor in biomineral formation. *Advances in Dental Research* **1**, 306-313.
- Coreno, J., Coreno, O., Cruz, J. and Rodriguez, C. (2005) Mechanochemical synthesis of nanocrystalline carbonate-substituted hydroxyapatite. *Optical Materials* **27**, 1281-1285.
- Dorozhkin, S. V. (2007) Calcium orthophosphates. *Journal of Materials Science* **42**, 1061-1095.
- Earl J. S., Wood D. J. and Milne S. J. (2006) Hydrothermal and synthesis of hydroxyapatite. *Journal of Physics* **26**, 268-271.
- Elliot, J. C. (1994) Structure and chemistry of the apatites and other calcium orthophosphates. *Elsevier*, Amsterdam.
- Ferraz M. P., Monteiro F. J. and Manuel C. M. (2004) Hydroxyapatite nanoparticles: A review of preparation methodologies. *Journal of Applied Biomaterials & Biomechanics* **2**, 74-80.
- Fricke H. C., William C. C., O'Neil J. R. and Gingerich P. D. (1998) Evidence for rapid climate change in North America during the latest Paleocene thermal maximum:

- oxygen isotope compositions of biogenic phosphate then the Bighorn Basin (Wyoming). *Earth and Planetary Science Letters* **160**, 193-208.
- Goto, T., Kim, I. Y., Kikuta, K. and Ohtsuki, C. (2012) Comparative study of hydroxyapatite formation from α - and β -tricalcium phosphates under hydrothermal conditions. *Journal of the Ceramic Society of Japan* **120**, 131-137.
- Halas S., Skrzypek G., Meier-Augenstein W., Pelc A. and Kemp H. F. (2011) Inter-laboratory calibration of new silver orthophosphate comparison materials for the stable oxygen isotope analysis of phosphates. *Rapid Communications in Mass Spectrometry* **25**, 579-584.
- Iijima, M., Kamemizu, H., Wakamatsu, N., Goto, T., Doi, Y. and Moriwaki, Y. (1997) Transition of octacalcium phosphate to hydroxyapatite in solution at pH 7.4 and 37 °C. *Journal of Crystal Growth* **181**, 70-78.
- Inskeep W. P. and Silvertooth J. C. (1988) Kinetics of hydroxyapatite precipitation at pH 7.4 to 8.4*. *Geochimica et Cosmochimica Acta* **52**, 1883-1893.
- Ito, N., Kamitakahara, M. and Murakami, S. (2010) Hydrothermal synthesis and characterization of hydroxyapatite from octacalcium phosphate. *Journal of the Ceramic Society of Japan* **118**, 762-766.
- Ito, N., Kamitakahara, M., Yoshimura, M. and Ioku, K. (2014) Importance of nucleation in transformation of octacalcium phosphate to hydroxyapatite. *Materials Science and Engineering* **40**, 121-126.
- Johnsson. M. S. and Nancollas. G. H. (1972) The role of brushite and octacalcium phosphate in apatite formation. *Critical Reviews in Oral Biology and Medicine* **3**, 61-82
- Kamitakahara, M., Ito, N., Murakami, S., Watanabe, N. and Ioku, K. (2009) Hydrothermal synthesis of hydroxyapatite from octacalcium phosphate: effect of hydrothermal temperature. *Journal of Ceramic the society of Japan* **117**, 385-387.
- Karpikhin, A. E., Fedotov, A. Y., Komlev, V. S., Barinov, S. M., Sirotinkin, V. P., Gordeev, A. S. and Shamrai, V. F. (2016) Structure of hydroxyapatite powders prepared through dicalcium phosphate dehydrate hydrolysis. *Inorganic Materials* **52**, 170-175.
- Kim J-W., Kogure T., Yang K., Kim S-T., Jang Y-N., Baik H-S. and Geesey G. (2012) The characterization of CaCO₃ in a geothermal environment: A SEM/TEM-eels study. *Clays and Clay Minerals* **60**, 484-495.

- Knabe C., Klar F., Fitzner R., Radlanski R. J. and Gross U. (2002) In vitro investigation of titanium and hydroxyapatite dental implant surfaces using a rat bone marrow stromal cell culture system. *Biomaterials* **23**, 3235-3245.
- Koch P. L., Tuross N. and Fogel M. L. (1997) The effects of sample treatment and diagenesis on the isotopic integrity of carbonate in biogenic hydroxyapatite. *Journal of Archaeological Science* **24**, 417-429.
- Kohn, M. J., Schoeninger, M. J. and Barker, W. W. (1999) Altered states: Effects of diagenesis in fossil tooth chemistry. *Geochimica et Cosmochimica Acta* **63**, 2737-2747.
- Kohn M. J., Schoeninger M. J. and Valley J. W. (1996) Herbivore tooth oxygen isotope compositions: Effects of diet and physiology. *Geochimica et Cosmochimica Acta* **60**, 3889-3896.
- Kohn, M. J., Rakovan, J. and Hughes, J. M. (2002) Phosphates: Geochemical, geobiological, and material importance. *Reviews in Mineralogy and Geochemistry*, **48**. Mineralogical Society of America, Washington, DC.
- Kolodny Y., Luc B. and Navon O. (1983) Oxygen isotope variations in phosphate of biogenic apatites, I. Fish bone apatite- rechecking the rules of the game. *Earth and Planetary Science Letters* **64**, 398-404.
- Koutsopoulos, S. (2002) Synthesis and characterization of hydroxyapatite crystals: A review study on the analytical methods. *Journal of Biomedical Materials Research* **62**, 600-612.
- Krajewski, A., Mazzocchi, M., Buldini, P. L., Ravagliolo, A., Tinti, A., Taddei, P. and Fagnano, C. (2005) Synthesis of carbonated hydroxyapatites: Efficiency of the substitution critical evaluation of analytical methods. *Journal of Molecular Structure* **744-747**, 221-228.
- Kumta, P. N., Sfeir, C., Lee, D. H., Olton, D. and Choi, D. (2005) Nanostructured calcium phosphates for biomedical application: novel synthesis and characterization. *Acta Biomaterialia* **1**, 65-83.
- Lécuyer C., Grandjean P. and Emig C. C. (1996) Determination of oxygen isotope fractionation between water and phosphate from living lingulids: potential application to paleoenvironmental studies. *Paleogeography, Paleoclimatology, Paleoecology* **126**, 101-108.

- Lécuyer C., Grandjean P. and Sheppard S. M. (1999) Oxygen isotope exchange between dissolved phosphate and water at temperatures $\leq 135^{\circ}\text{C}$: Inorganic versus biological fractionations. *Geochimica et Cosmochimica Acta* **63**, 855-862.
- Lécuyer C., Balter V., Martineau F., Fourel F., Bernard A., Amiot R., Gardien V., Otero O., Legendre S., Panczer G., Simon L. and Martini R. (2010) Oxygen isotopes fractionation between apatite-bound carbonate and water determined from controlled experiments with synthetic apatites precipitated at 10-37 $^{\circ}\text{C}$. *Geochimica et Cosmochimica Acta* **74**, 2072-2081.
- LeGeros, R. Z. (1991) *Calcium Phosphates in Oral Biology and Medicine* (1st ed.). New York: Karger.
- Longinelli A. (1984) Oxygen isotopes in mammal bone phosphate: A new tool for paleohydrological and paleoclimatological research?. *Geochimica et Cosmochimica Acta* **48**, 385-390.
- Longinelli A. and Nuti S. (1973) Revised phosphate-water isotopic temperature scale. *Earth and Planetary Science Letters* **19**, 373-376.
- Monma, H. and Kamiya, T. (1987) Preparation of hydroxyapatite by the hydrolysis of brushite. *Journal of Materials Science* **22**, 4247-4250.
- Nancollas G. H. and Mohan M. S. (1970) The growth of hydroxyapatite crystals. *Archives of Oral Biology* **15**, 731-745.
- Nelson, D. G. and McLean, J. D (1984) High-resolution electron microscopy of octacalcium phosphate and its hydrolysis products. *Calcif. Tissue Int.* **36**, 219-326.
- Nishioka, M., Yanagisawa, K. and Yamasaki, N. (1986) Solidification of glass powder by a hydrothermal hot-pressing technique. *Yogyo Kyokaishi* **94**, 1119-1124.
- Redepenning, J., Schlessinger, T., Burnham, S., Lippiello, L. and Miyano, J. (1996) Characterization of electrolytically prepared brushite and hydroxyapatite coatings on orthopedic alloys. *Journal of Biomedical Materials Research* **30**, 287-297.
- Sharma V. K., Johnsson M., Sallis J. D. and Nancollas G. H. (1992) Influence of citrate of phosphocitrate on the crystallization of octacalcium phosphate. *Langmuir* **8**, 676-679.
- Shemesh A. (1990) Crystallinity and diagenesis of sedimentary apatites. *Geochimica et Cosmochimica Acta* **54**, 2433-2438.

- Stuart-Williams H. L. and Schwarz H. P. (1997) Oxygen isotopic determination of climatic variation using phosphate from beaver bone, tooth enamel, and dentine. *Geochimica et Cosmochimica Acta* **61**, 2539-2550.
- Tas, A. C. (2000) Synthesis of biomimetic Ca-hydroxyapatite powders at 37 °C in synthetic body fluids. *Biomaterials* **21**, 1429-1438.
- Wilson, R. M., Elliot, J. C. and Dowker, S. E. P. (1999) Rietveld refinement of the crystallographic structure of human dental enamel apatites. *American Mineralogist* **84**, 1406-1414.
- Xia, W., Lin, K., Gou, Z. and Engqvist, H. (2012) Morphology control of hydroxyapatite crystal and its aggregates. *Hydroxyapatite: Synthesis, Properties, and Applications* (Eds. V. S. Gshalaev and A. C. Demirchan). Nova Science Publishers, pp. 243-264.
- Yamasaki, N., Kai, T., Nishioka, K., Yanagisawa, K. and Loku, K. (1990) Porous hydroxyapatite Ceramics prepared by hydrothermal hot-pressing. *Journal of Materials Science Letters* **9**, 1150-1151.
- Zazzo, A., Lécuyer, C. and Mariotti, A. (2004) Experimentally controlled carbon and oxygen isotope exchange between bioapatites and water under inorganic and microbially-mediated conditions. *Geochemica et Cosmochimica Acta* **68**, 1-12.
- Zheng Y-F. (1996) Oxygen isotope fractionations involving apatites: Application to paleotemperature determination. *Chemical Geology* **127**, 177-187.
- Zheng, Y., Dong, G., He, L., Wu, G., Zheng, H. and Deng, C. (2016) In Vitro study of calcium phosphate layers on hydroxyapatite ceramics surface mineralized in different solutions. *Ceramics International* **42**, 1660-1665.

Table 2.1. Different phases of calcium phosphates, in order from the most soluble to the least soluble (Modified from Johnsson and Nancollas, 1992; Elliot, 1994).

Minerals	Empirical formula	Abbreviation	Ca/P ratio
Monohydrate calcium phosphate	$\text{Ca}(\text{H}_2\text{PO}_4)_2 \cdot \text{H}_2\text{O}$	MCP	0.5
Monocalcium phosphate	$\text{Ca}(\text{H}_2\text{PO}_4)_2$	MP	0.5
Dicalcium phosphate dihydrate (Brushite)	$\text{Ca}(\text{HPO}_4) \cdot 2\text{H}_2\text{O}$	Brushite	1
Octacalcium phosphate	$\text{Ca}_8(\text{H}_2\text{PO}_4)_6 \cdot 5\text{H}_2\text{O}$	OCP	1.33
Tricalcium phosphate	$\alpha\text{- and } \beta\text{- Ca}_3(\text{PO}_4)_2$	TCP	1.5
Amarphous calcium phosphate	$\text{Ca}_9(\text{PO}_4)_6 \cdot \text{H}_2\text{O}$	ACP	1.5
Hydroxyapatite	$\text{Ca}_{10}(\text{PO}_4)_6(\text{OH})_2$	HAP	1.67
Fluoroapatite	$\text{Ca}_{10}(\text{PO}_4)_6\text{F}_2$	FAP	1.67

Table 2.2 Solution chemistry of all instantaneous mixing experiments at 25 °C.

Sample #	CA/PC CaCl ₂ ·2H ₂ O/HPO ₄ ⁻ +HCO ₃ [*] (mmolal)	Stage I	Stage II	Stage III		CA pH	PC Ini. pH	PC Fin. pH	XRD HAP %	CO ₃ ²⁻ %wt
		Maturation (Days) of a single solution	Maturation (Days) of mixed solutions	T (°C)	Dry Time (D)					
MRSI-Bagg-20	20/10+1 ^a	1	4	RT	2	5.6	6.2	~5.5-6.0	0	N/A
MRSI-Bagg-21	20/10+1	1	4	RT	3	5.6	6.6	~6.0-6.4	59.06	N/A
MRSI-Bagg-22	10/10+0.5	1	4	RT	2	5.6	6.5	~6.4	41.15	N/A
MRSI-Bagg-23	10/10+0.5	1	4	RT	3	5.6	7.9	~7.0-7.2	100	N/A
MRSI-Ie-8-A	10/10+7 ^b	7	7	RT	7	5.0	7.2	6.8		4.70E-08
MRSI-Ie-8-B	10/10+7	7	7	RT	7	5.0	7.2	6.8		5.40E-08
MRSI-Ie-8-C	10/10+7	7	7	RT	7	5.0	7.2	6.8		4.50E-08
MRSI-Ie-9-A	10/10+10	7	7	RT	7	5.0	~7.2-7.6	6.4-6.8		4.90E-08
MRSI-Ie-9-B	10/10+10	7	7	RT	7	5.0	~7.2-7.6	6.8		5.00E-08
MRSI-Ie-9-C	10/10+10	7	7	RT	7	5.0	~7.2-7.6	6.4-6.8		4.90E-08
MRSI-Ie-10-A	10/10+15	7	7	RT	7	5.0	~7.2	6.8		6.20E-08
MRSI-Ie-10-B	10/10+15	7	7	RT	7	5.0	~7.2	6.8		5.70E-08
MRSI-Ie-10-C	10/10+15	7	7	RT	7	5.0	~7.2	6.8		5.60E-08
MRSI-Ie-11-A	10/10+5	7	7	RT	7	5.0	~7.2	6.4-6.8		4.20E-08
MRSI-Ie-11-B	10/10+5	7	7	RT	7	5.0	~7.2	6.4-6.8		3.80E-08
MRSI-Ie-11-C	10/10+5	7	7	RT	7	5.0	~7.2	6.4-6.8		3.80E-08
MRSI-Ie-12	10/10+7	7	7	RT	7	5.0	~7.6	6.8-7.0	94.8	1.5
MRSI-Ie-13	10/10+10	7	7	RT	7	5.0	~7.6	6.8-7.0	97.7	1.9
MRSI-Ie-14	10/10+15	7	7	RT	7	5.0	~7.6	6.8-7.0	96.1	1.6
MRSI-Ie-15	10/10+5	7	7	RT	7	5.0	~7.6	6.8-7.0	96.4	1.6
MRSI-Ie-16-A 1	10/10+5	7	7	RT	7	5.5	8.6	7.2		1.3
MRSI-Ie-16-A 2	10/10+5	7	7	70	1	5.9	8.7	7		0.4
MRSI-Ie-16-A 3	10/10+5	7	7	70	7	5.9	8.7	7		0.3
MRSI-Ie-17-A 1	10/10+10	7	7	70	7	5.5	8.6	7	100	1.7
MRSI-Ie-17-A 2	10/10+10	7	7	70	1	5.9	8.6	7		1.1
MRSI-Ie-17-A 3	10/10+10	7	7	70	1	5.9	8.6	7		0.5
MRSI-Ie-18-A2 1	10/10+15	7	7	70	7	5.5	8.5	7		0.9
MRSI-Ie-18-A2 2	10/10+15	7	7	70	1	5.9	8.5	7		0.7
MRSI-Ie-16B 1	10/10+5	14	14	70	1	5.5	8.5	7.2		1.2
MRSI-Ie-16B 2	10/10+5	14	14	70	1	5.9	8.8	7.02		1.1
MRSI-Ie-16B 3	10/10+5	14	14	70	1	5.9	8.8	7.02		1.0
MRSI-Ie-17B 1	10/10+10	14	14	70	1	5.5	8.6	7.3	100	1.3
MRSI-Ie-17B 2	10/10+10	14	14	70	1	5.9	8.7	7.2		0.7
MRSI-Ie-17B 3	10/10+10	14	14	70	1	5.9	8.7	7.2		0.7
MRSI-Ie-18B 1	10/10+15	14	14	70	1	5.5	8.5	7.3		1.8
MRSI-Ie-18B 2	10/10+15	14	14	70	1	5.9	8.6	7.3		1.4
MRSI-Ie-18B 3	10/10+15	14	14	70	1	5.9	8.6	7.3		0.8
MRSI-Ie-1-TS	10/10+10	2 hr	0	70	1	5.8	8.6	7.1	100	0.4
MRSI-Ie-2-TS	10/10+10	4 hr	0	70	1	5.8	8.6	7.2		0.3
MRSI-Ie-3-TS	10/10+10	6 hr	0	70	1	5.8	8.6	7.2		1.0
MRSI-Ie-4-TS	10/10+10	12 hr	0	70	1	5.8	8.6	7.2		0.2
MRSI-Ie-5-TS	10/10+10	1	0	70	1	5.8	8.6	7.2		0.1
MRSI-Ie-6-TS	10/10+10	2	0	70	1	5.8	8.6	7.2		0.1
MRSI-Ie-7-TS	10/10+10	5	0	70	1	5.8	8.6	7.1		0.2
MRSI-Ie-8-TS	10/10+10	7	0	70	1	5.8	8.6	7.1	100	0.5

CA= Calcium

PC= Phosphate Carbonate

Ini. pH= Initial pH

Fin. pH= Final pH of the mixed solution

T= Temperature

HAP= Hydroxyapatite

N.A= Not Available

^{*}HPO₄⁻+HCO₃⁻ denotes Na₂HPO₄⁻+ NaHCO₃^a 20/10+1 denotes 20 mmolal CaCl₂·2H₂O/10 mmolal Na₂HPO₄⁻+ 1 mmolal NaHCO₃^b 10/10+5 denotes 10 mmolal CaCl₂·2H₂O/10 mmolal Na₂HPO₄⁻+ 5 mmolal NaHCO₃

Table 2.3 Solution chemistry of all slow mixing experiments at 25 °C.

Sample #	CA/PC CaCl ₂ ·2H ₂ O/HPO ₄ +HCO ₃ * (mmolal)	Stage I		Stage II			Stage III		CA pH	PC Fin. pH	XRD HAP%	CO ₃ ²⁻ %wt
		Maturation (D) of a single solution	Injection rate ml/hr	Injection (D)	Maturation (D) of mixed solutions	T (°C)	Dry Time (D)					
MRSI-Ie-28-SP	10/10+5**	1	2.08	2	7	70	1	4.6	6.67	0	0.6	
MRSI-Ie-29-SP	10/10+10	5	2.08	2	7	70	1	4.6	6.86		1.1	
MRSI-Ie-29-SP (2)	10/10+10	5	2.08	2	7	70	1	5.8	7		1.4	
MRSI-Ie-29-SP (3)	10/10+10	5	2.08	2	7	70	1	5.8	7		1.5	
MRSI-Ie-29-SP (2) 2	10/10+10	5	2.08	2	7	70	1	6.0	6.80		1.8	
MRSI-Ie-29-SP (3) 3	10/10+10	5	2.08	2	7	70	1	6.0	6.80		1.4	
MRSI-Ie-30-SP	10/10+15	5	2.08	2	7	70	1	5.7	7.13	100	3.4	
MRSI-Ie-30-SP (2)	10/10+15	5	2.08	2	7	70	1	6	7		3.4	
MRSI-Ie-30-SP (3)	10/10+15	5	2.08	2	7	70	1	6	7		3.3	
MRSI-Ie-34-SP	10/10+10	7	0.58	8	0	70	1	5.7	7	29.43	1.3	
MRSI-Ie-34-SP 2	10/10+10	7	0.594	7	0	70	1	5.3	6.7	36.02	0.9	
MRSI-Ie-34-SP 3	10/10+10	7	0.594	7	0	70	1	5.8	6.9		1.3	
MRSI-Ie-34-SP 4	10/10+10	7	0.594	7	0	70	1	6.0	6.9		1.1	
MRSI-Ie-35-SP	10/10+15	7	0.58	8	0	70	1	5.7	7.33	80.04	3.4	
MRSI-Ie-35-SP2	10/10+15	7	0.594	7	0	70	1	5.3	6.9	67	1.7	
MRSI-Ie-35-SP3	10/10+15	7	0.594	7	0	70	1	5.8	7		1.4	
MRSI-Ie-35-SP4	10/10+15	7	0.594	7	0	70	1	6.0	7		1.8	

CA= Calcium

PC= Phosphate Carbonate

Ini. pH= Initial pH

Fin. pH= Final pH

D= Days

T= Temperature

HAP= Hydroxyapatite

N.A= Not Available

*HPO₄+HCO₃ denotes Na₂HPO₄+ NaHCO₃** 10/10+5 denotes 10 mmolal CaCl₂·2H₂O/10 mmolal Na₂HPO₄+ 5 mmolal NaHCO₃

Table 2.4. Comparison of experimental conditions employed by Lécuyer et al. (2010) and this study.

	Lécuyer et al. (2010)		This study	
Temp. (°C)	10, 15, 20, 25, 30, and 37		25	
CA solution	100/10 ^d	Ini. pH= Unknown	10 ^c	Ini. pH= 5.0-5.5
PC solution	100/10 ^p	Ini. pH= Unknown	10/0.5, 10/1,10/5, 10/7, 10/10, and 10/15 ^d	Ini. pH= 6.2-8.8
Mixing CA+PC solutions	Before mixing, PC solutions were held at a given temperature (10-37 °C) for approximately 2 days. Then equal volumes of PC and CA solutions were mixed at a given temperature.		Before mixing, both CA and PC were aged for at least 14 days at a given temperature. 100 ml of CA was added into 250 ml beaker and then 100 ml of PC was added.	
pH adjustment	0.3% HNO ₃ was added into PC solutions		2% HCl was added into some of the PC solutions	
Final pH	7.4		5.5 to 7.4	
Maturation	4 days		4 to 14 days	
Filtration	The solid phase was separated from supernatant by centrifugation, washed with distilled water and dried at room temperature. The aqueous solutions were filtered through a 0.22 µm filter		The solutions were matured for 7 days before filtration. The solutions were filtered through a 0.45 µm filter. MQ water and methanol were used to rinse the samples after which they were dried at room temperature or at 70 °C for at least 1 day.	
Wt% CaCO₃	0.05-0.23		0.12-3.44	

Temp.= Temperature

Ini. pH= Initial pH

^a100/10 denotes 100 mmolal NaOH + 10 mmolal CaCl₂•2H₂O^b100/10 denotes 100 mmolal KNaCO₃ + 10 mmolal Na₂HPO₄•H₂O^c 10 mmolal CaCl₂•2H₂O^d10/0.5 denotes 10 mmolal Na₂HPO₄ + 0.5 mmolal NaHCO₃

Table 2.5. Initial and final pH and mineralogy based on XRD results from this study for synthesizing HAP crystals.

Precipitation	Sample #	Ini. pH	Fin. pH	Mineralogy (%)			Maturation* Stage II (days)	
				HAP	OCP	Brushite		
Instantaneous	MRSI-Bagg-20	6.2	~5.5-6.0	0	0	100	4	
	MRSI-Bagg-21	6.6	~6.0-6.4	59	38	3	4	
	MRSI-Bagg-22	6.5	~6.4	41	59	0	4	
	MRSI-Bagg-23	7.9	~7.0-7.2	100	0	0	4	
	MRSI-Ie-12	~7.6	6.8	95	5	0	7	
	MRSI-Ie-13	~7.6	6.8	98	2	0	7	
	MRSI-Ie-14	~7.6	6.8	96	4	0	7	
	MRSI-Ie-15	~7.6	6.8	96	4	0	7	
	MRSI-Ie-17A2	8.6	7.0	100	0	0	7	
	MRSI-Ie-17B1	8.6	7.3	100	0	0	14	
	MRSI-Ie-1TS	8.6	7.0	100	0	0	0	
	MRSI-Ie-8TS	8.6	7.0	100	0	0	0	
	Slow 2.08 mL/hr	MRSI-Ie-28SP	8.6	6.7	0	100	0	7
MRSI-Ie-29SP2		8.6	7.0	49	51	0	7	
MRSI-Ie-29SP3		8.6	7.0	56	44	0	7	
MRSI-Ie-30SP		8.5	7.1	100	0	0	7	
MRSI-Ie-30SP2		8.5	7.0	90	10	0	7	
MRSI-Ie-30SP3		8.5	7.0	94	6	0	7	
0.594 mL/hr		MRSI-Ie-34SP	8.4	7.0	29	71	0	0
		MRSI-Ie-34SP2	8.6	6.7	36	64	0	0
		MRSI-Ie-34SP4	8.6	6.9	51	49	0	0
		MRSI-Ie-35SP	8.5	7.3	80	20	0	0
MRSI-Ie-35SP2	8.5	7.0	67	33	0	0		
MRSI-Ie-35SP3	8.5	7.0	79	21	0	0		
MRSI-Ie-35SP4	8.5	7.0	74	26	0	0		

Ini. pH= Initial pH

Fin. pH= Final pH of the mixed solution

HAP= Hydroxyapatite

OCP= Octacalcium phosphate

*Maturation of the mixed solutions

Table 2.6. Various calcium phosphate phases and their corresponding synthesis conditions at 25 °C.

Phase	Concentration	Precipitation	Solution			
			Maturation		PC	Mixed
			Each solution	Mixed solution	Ini. pH	Fin. pH
HAP	A	Instantaneous	0 to 14	7 and 14	8.4 to 8.7	6.7-7.4
HAP/OCP	A+B+C	Instantaneous/slow	0 to 14	7 and 14	8.4 to 8.7	6.4 -7
OCP	A	Slow	7	7	8.6	6.7
Brushite	D	Instantaneous	1	4	6.2	5.5-6.0*
HAP/OCP/Brushite	D	Instantaneous	1	4	6.6	6.0-6.4*

HAP= Hydroxyapatite

OCP= Octacalcium phosphate

* Measured using pH paper

A= 10 mmolal $\text{CaCl}_2 \cdot 2\text{H}_2\text{O}$ /10 mmolal Na_2HPO_4 + 5/10/15 mmolal NaHCO_3

B= 10 mmolal $\text{CaCl}_2 \cdot 2\text{H}_2\text{O}$ /10 mmolal Na_2HPO_4 + 1 mmolal NaHCO_3

C= 10 mmolal $\text{CaCl}_2 \cdot 2\text{H}_2\text{O}$ /10 mmolal Na_2HPO_4 + 0.5 mmolal NaHCO_3

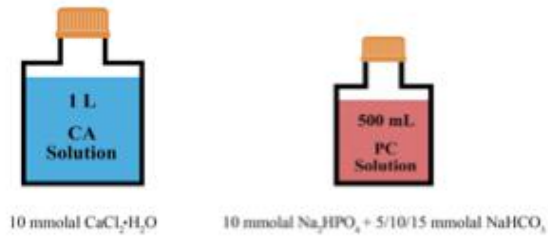
D= 20 mmolal $\text{CaCl}_2 \cdot 2\text{H}_2\text{O}$ /10 mmolal Na_2HPO_4 + 1 mmolal NaHCO_3

Ini. pH= Initial pH from the PC solutions

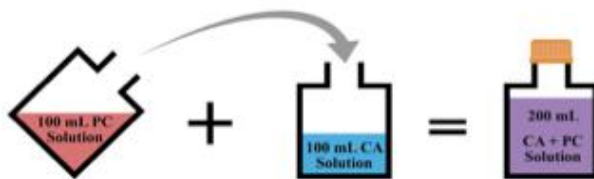
Fin. pH= Final pH of the mixed solutions

Instantaneous Mixing Experiments: 25 °C

Stage I: Maturation of CA and PC solutions before instantaneous mixing



Stage II: Instantaneous mixing solutions and maturations



Stage III: Filtration + Drying

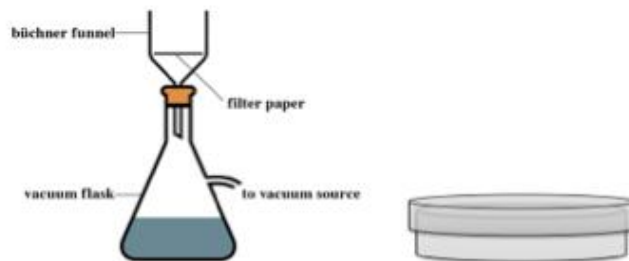


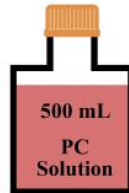
Figure 2.1. Schematic illustration for the instantaneous mixing experiment used in this study to synthesize HAP-bound carbonate at 25°C.

Slow Mixing Experiments: 25 °C

Stage I: Preparation and maturation of CA and PC solutions for 7 days before slow mixing



10 mmolal $\text{CaCl}_2 \cdot \text{H}_2\text{O}$

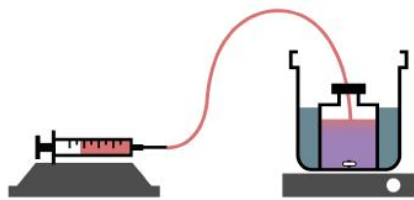


10 mmolal Na_2HPO_4 + 5/10/15 mmolal NaHCO_3

7 days

Stage II: Mixing solutions and maturations

I. Injection PC to CA



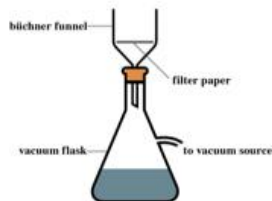
Rate: 2.08 mL/hr 100 cc syringe
0.594 mL/hr 100 cc syringe

II. Maturations



7 days
0 day

Stage III: Filtration and drying



Vacuum filter, rinse with DI water and methanol. Stored in 70 °C over for 1 day

Figure 2.2. Schematic illustration for the slow mixing experiment employed in this study to synthesize HAP-bound carbonate at 25 °C.

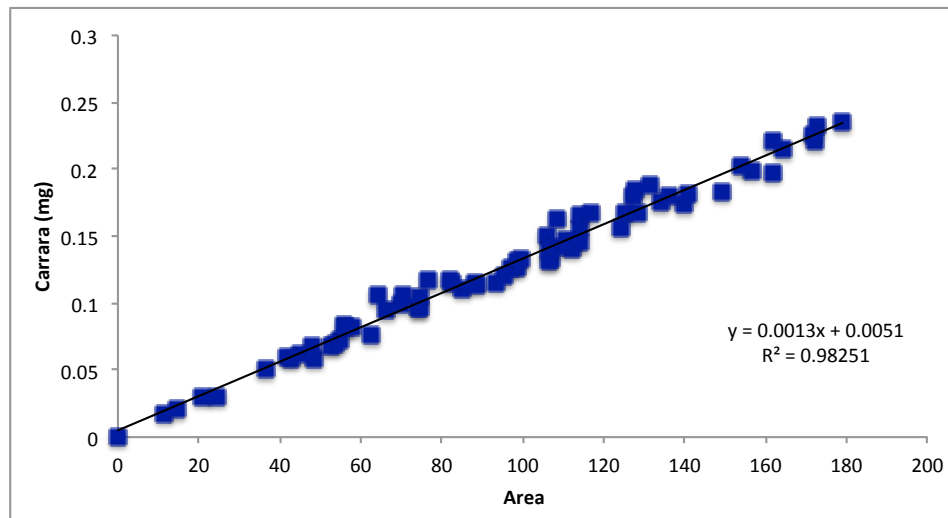


Figure 2.3. The calibration of mass-44 peak area based on different weights of laboratory standard Carrara marble.

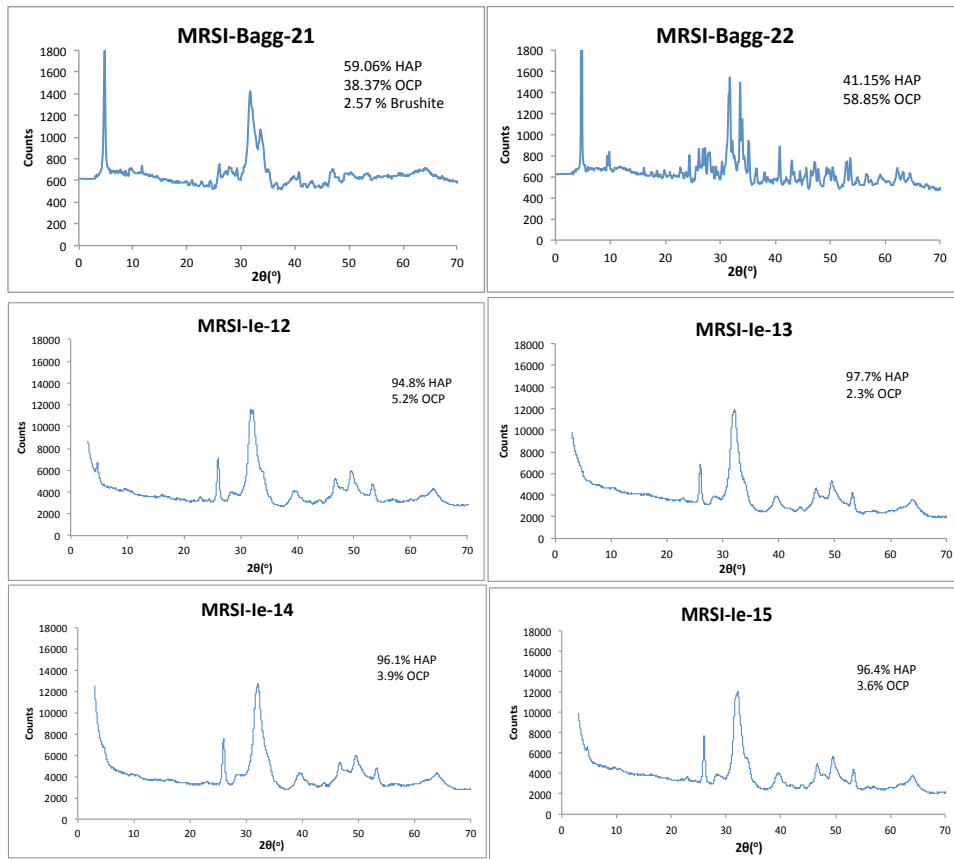


Figure 2.4. XRD results from the instantaneous mixing experiments at 25 °C. Different maturation periods, initial concentrations of NaHCO_3 , and low final pH values induced mixtures of OCP, brushite, and HAP.

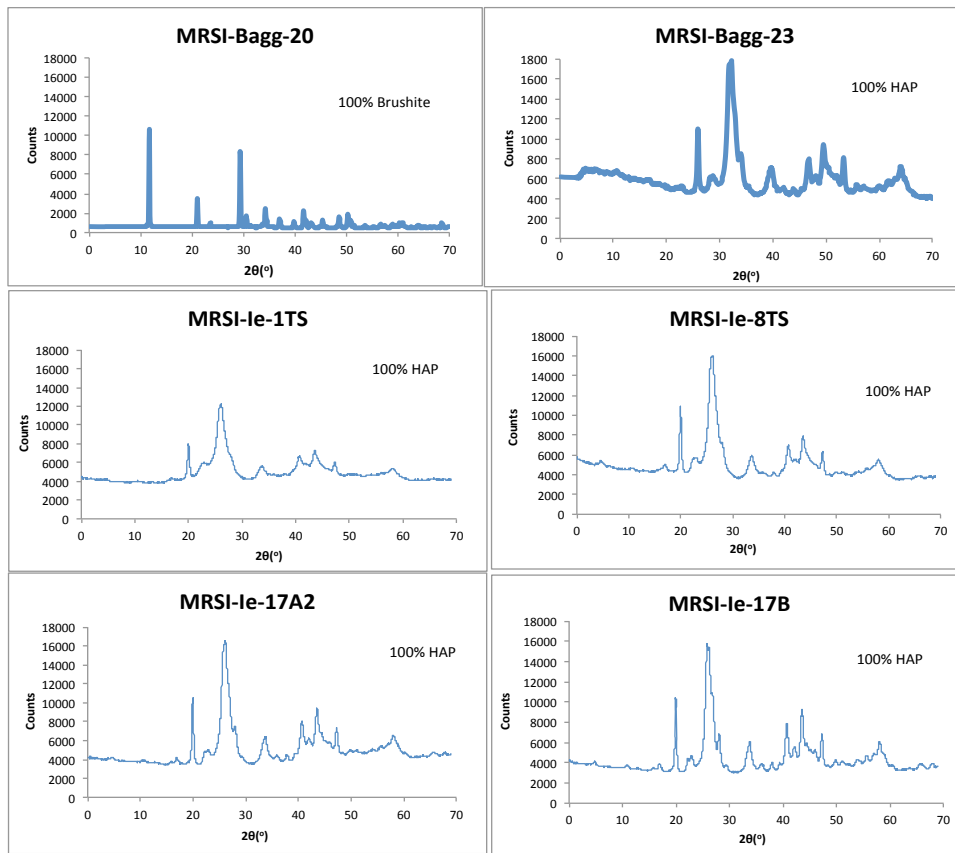


Figure 2.5. XRD results from the instantaneous mixing at 25 °C from different maturations, initial concentrations of NaHCO₃, and high final pH that demonstrated pure brushite (MRSI-Bagg-20) and pure HAP crystals.

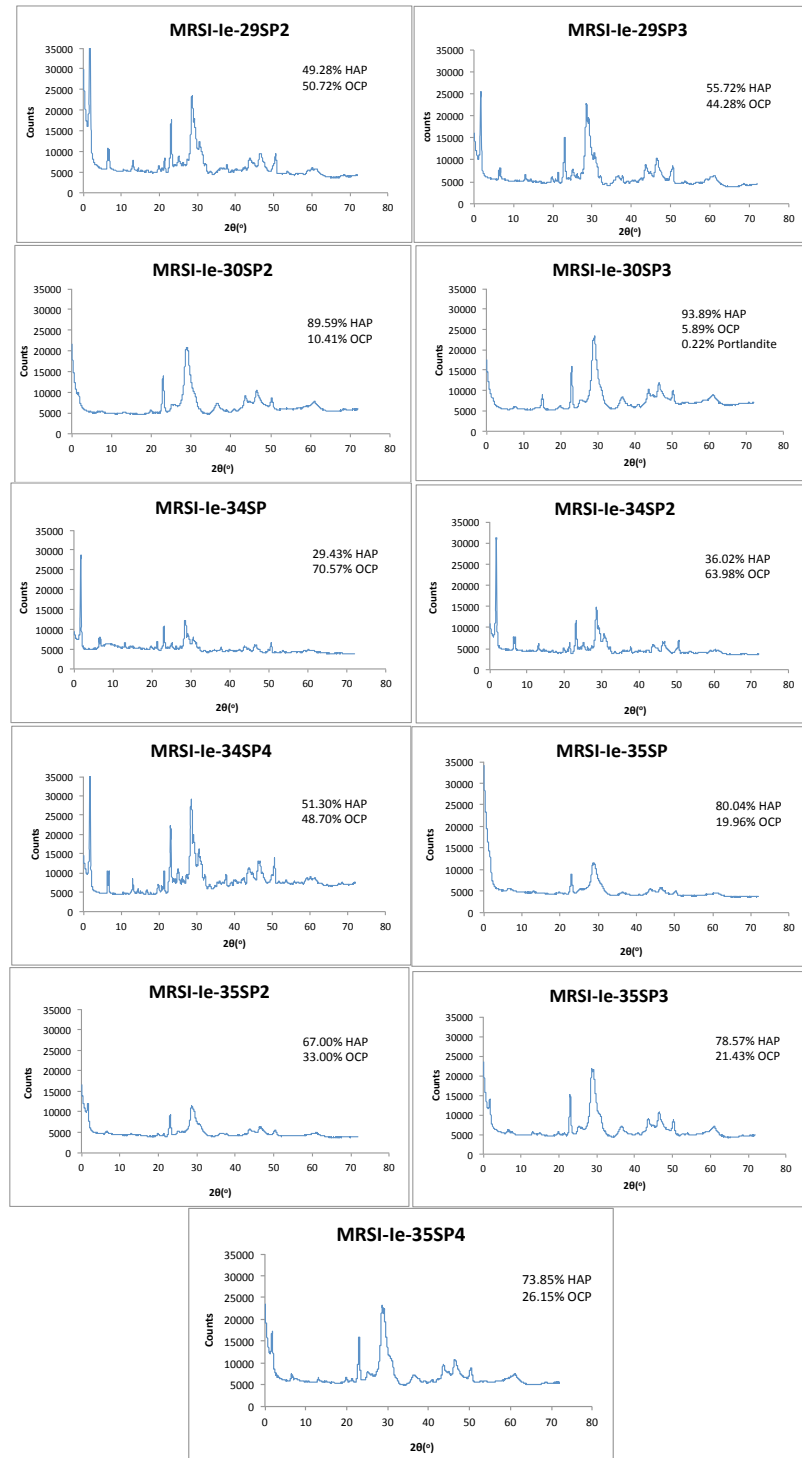


Figure 2.6. XRD results from all of the slow mixing experiments that demonstrated mixtures of OCP and HAP crystal.

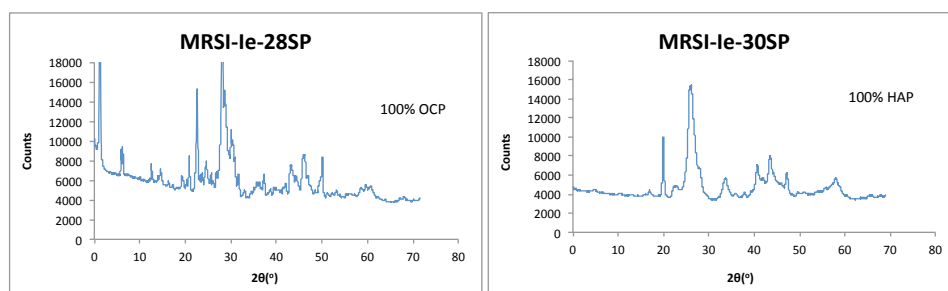


Figure 2.7. XRD results that demonstrated pure OCP (left) and pure HAP (right), both under slow mixing of 2.08 mL/hr (2 days) and 7 days of maturation of the mixed solutions.

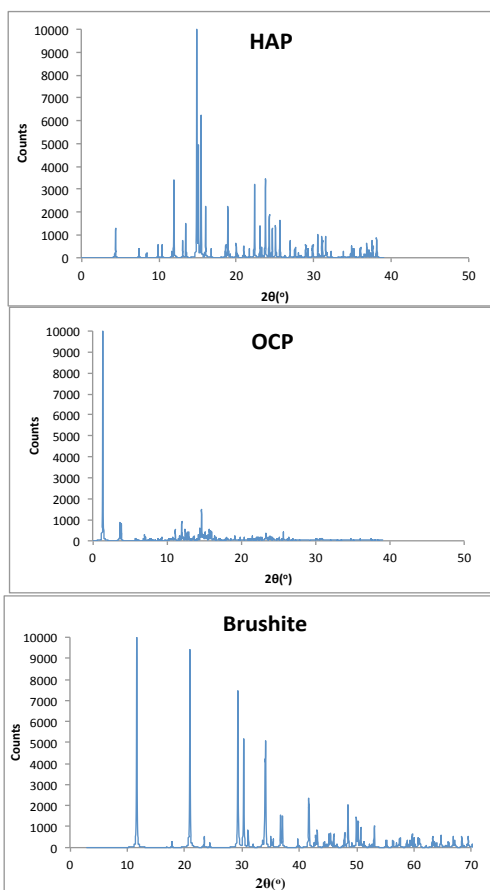


Figure 2.8. Reference standard XRD peaks of HAP phase (top), OCP phase (middle), and brushite phase (bottom).



Figure 2.9. Dried samples of the instantaneous mixing (left) and slow mixing (right).

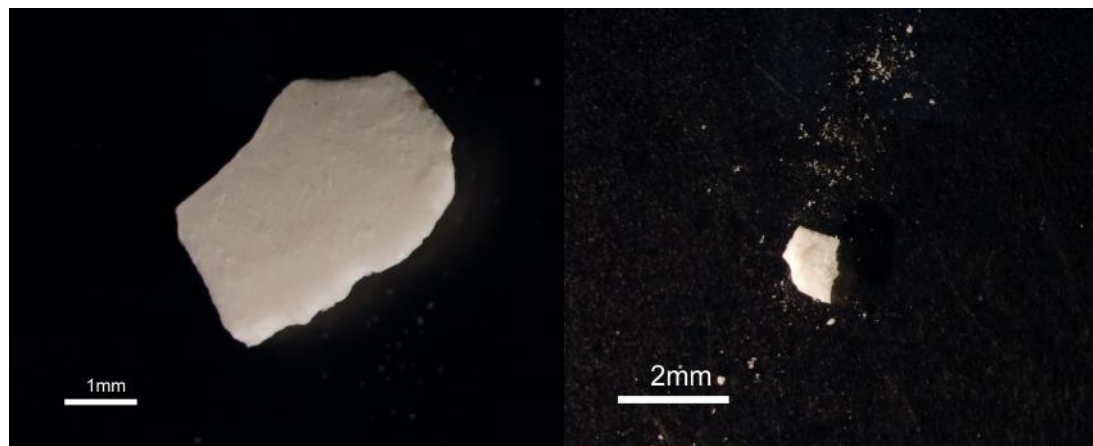


Figure 2.10. Mixtures of HAP and OCP under microscope from the instantaneous mixing experiments: MRSI-Ie-8 (left) and MRSI-Ie-12 (right).

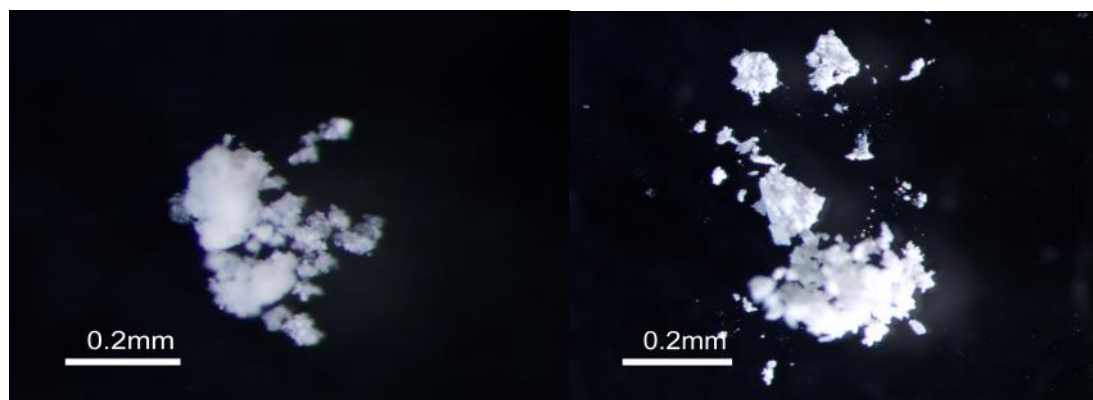


Figure 2.11. Mixtures of HAP and OCP under microscope from slow mixing experiments: MRSI- Ie-34SP (left) and MRSI-Ie-35SP (right).

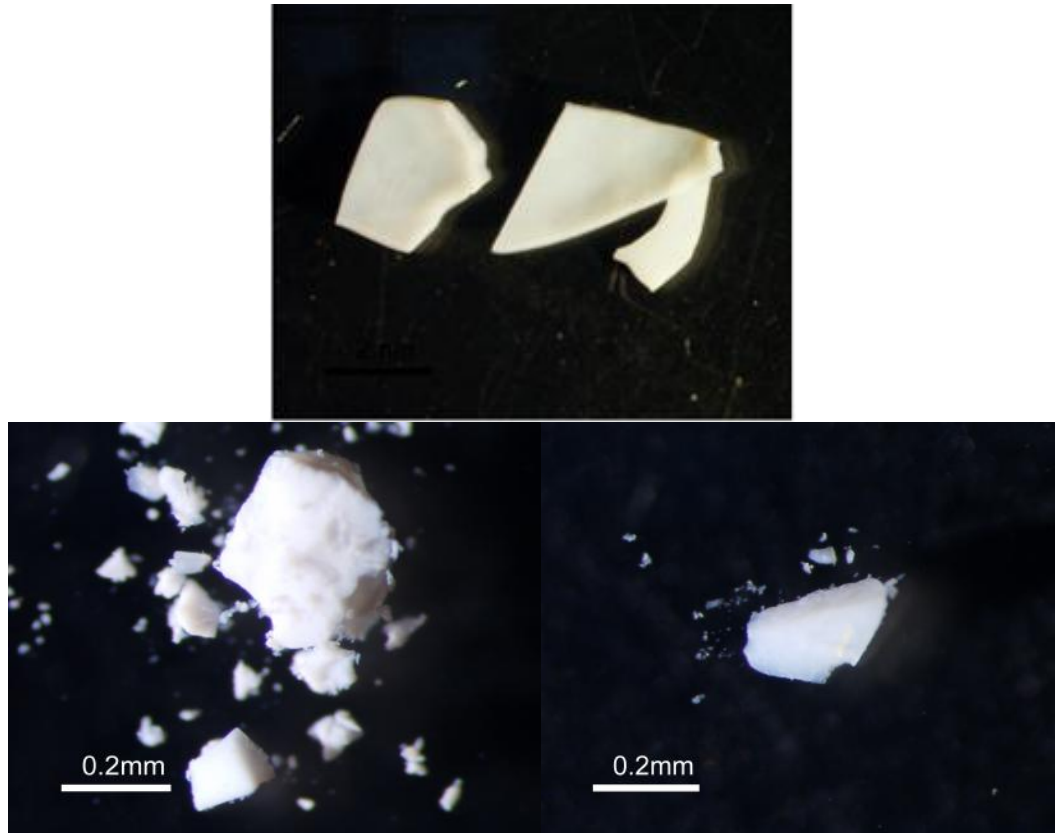


Figure 2.12. All of the pure HAP crystals under microscope from the instantaneous mixing experiments: TOP: MRSI-Bagg-23, BOTTOM: MRSI-Ie-1TS (left) and MRSI-Ie-17B (right).

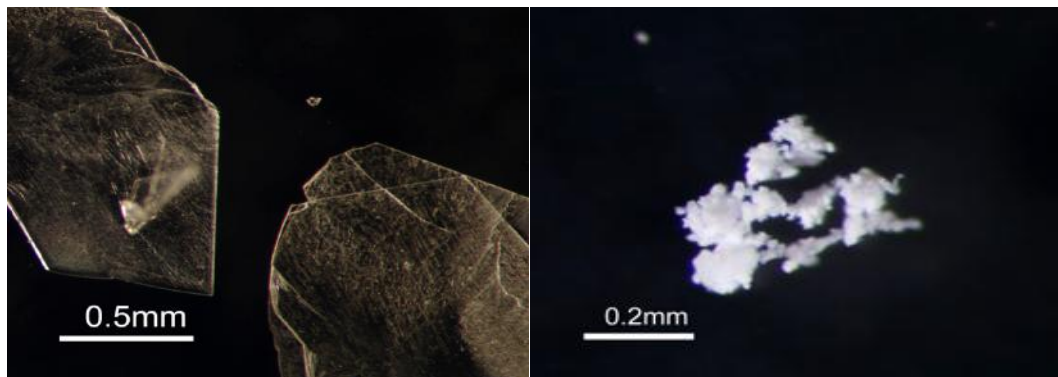


Figure 2.13. Pure brushite crystals from the instantaneous mixing experiment: MRSI-Bagg-20 (left) and pure OCP crystals from the slow mixing experiment: MRSI-Ie-28SP (right)

CHAPTER 3:

Oxygen isotope fractionation between hydroxyapatite (HAP)-bound carbonate and water at 10, 25, and 40 °C

Oxygen isotope fractionation between Hydroxyapatite (HAP)-bound carbonate and water at 10, 25, and 40 °C

Kesia Ie^a and Sang-Tae Kim^a

^aSchool of Geography and Earth Sciences, McMaster University, 1280 Main Street West, Hamilton, ON L8S 4K1, Canada

Abstract

Oxygen isotope fractionation was measured experimentally between inorganically precipitated hydroxyapatite-bound carbonate and water at 10, 25, and 40 °C. In this study, the measured oxygen isotope fractionation between hydroxyapatite-bound carbonate and water positively deviated from the nominal equilibrium oxygen isotope fractionation between carbonate and water that was defined by Kim and O'Neil (1997). This indicates that hydroxyapatite-bound carbonates were influenced by non-equilibrium oxygen isotope effects which were found to increase with temperature. In addition, the maturation of the starting solutions and initial concentration of NaHCO_3 were the most likely cause of the non-equilibrium oxygen isotope effect in our study. The oxygen isotope fractionation obtained from experiments with a longer maturation (14 days) of the starting solutions and a higher concentration (15 mmolal) of NaHCO_3 was closer to the oxygen isotope fractionation value proposed by Kim and O'Neil (1997). In contrast, those with a shorter maturation (7 days) and a lower initial concentration (5 mmolal) of NaHCO_3 were more isotopically enriched compared Kim and O'Neil (1997).

3.1 Introduction

Calcium phosphates, especially apatites, are a critical nutrient for biological processes which exist in natural aqueous systems (i.e., rivers, lakes, ocean, and soil/groundwater), minerals, as well as organic matters. These calcium phosphates can be found in the form of salt in phosphoric acid (H_3PO_4 , H_2PO_4^- , HPO_4^{2-} , and PO_4^{3-}), and their speciations are highly dependent on the pH condition (Elliot, 1994). For example, phosphate species like H_3PO_4 and H_2PO_4^- are dominant in an acidic condition, whereas HPO_4^{2-} and PO_4^{3-} occur in neutral to basic conditions (Elliot, 1994; O'Neil et al., 2003). Typically, phosphate containing apatite ($\text{Ca}_5(\text{PO}_4, \text{CO}_3, \text{F})_3(\text{OH}, \text{F}, \text{Cl}, \text{CO}_3)$) is very tolerant with ionic substitutions of F^- (for fluorapatite), OH^- (for hydroxyapatite) or Cl^- (for chlorapatite). Fluorapatite is a mineral that is present in small quantities in many igneous and metamorphic rocks and is a major component of tooth enamel. The mineral fluorapatite is similar to hydroxyapatite (HAP) that sometimes contains carbonates, and is commonly found in the mineral of bones and teeth from terrestrial and marine environments (Elliot, 1994; Kohn et al., 2002). In aqueous systems, there are a relatively large amount of calcium phosphates containing apatite that vary in solubility (Table 3.1) and have hexagonal crystal structures (Kohn et al., 2002).

Both apatite and phosphate minerals have a great application in an interdisciplinary field of sciences, including biology, geology, medicine, and chemistry. For example, over the last two decades, phosphate minerals have been used for the reconstruction of past environmental changes based upon stable isotope-based thermometry (Tudge, 1960, Longinelli and Nuti, 1973a;b). The temperature dependence of oxygen isotope fractionation factor between phosphate and water (or $1000\ln\alpha_{\text{PO}_4\text{-H}_2\text{O}}$) was investigated by Longinelli and Nuti (1973a; b) and was later modified by Kolodny et al. (1983). These earlier, as well as

follow-up empirical studies have demonstrated a considerable promise of the phosphate-based paleothermometry, providing an alternative to biogenic carbonates, for tracking changes in the Earth's past climate and environmental changes (Longinelli and Nuti 1973a; b; Kolodny et al., 1983; Lécuyer et al., 1996; Fricke et al., 1998a; b; Lécuyer, 2004; Amiot et al., 2007; Puceat et al., 2010).

In general, phosphorus (P) bonds with oxygen (O) where three oxygen isotopes are stable (^{16}O , ^{17}O , and ^{18}O) (Hoefs, 2009). The bonds between P and O in phosphates are covalently strong which influence the oxygen isotopic exchange rate between phosphates and water, particularly at low temperatures unless enzymes (i.e., enzyme inorganic pyrophosphatase) break the P-O bonds. Once these bonds are broken, the oxygen will rapidly exchange with oxygens in water (Blake et al., 1997; Lécuyer et al., 1999; Chang and Blake, 2015). Similarly to the pure carbonate and water system, the isotopic exchange between inorganic phosphates and water will increase rapidly at high temperatures (Lécuyer et al., 1999; Kim and O'Neil, 1997; O'Neil et al., 2003), although in a pure phosphate system, the isotopic exchange rates could take months to equilibrate with water due to strong P-O bonds (Lécuyer et al., 1999; O'Neil et al., 2003). Additionally, the preservation of bioapatite is more resistant than biogenic carbonate because biogenic carbonates are more prone to diagenetic alteration (Blake et al., 1997; Puceat et al., 2003; Trotter et al., 2008; Puceat et al., 2010). Therefore, the study of oxygen isotope fractionation between bioapatites and water has helped to elucidate the issues, such as dinosaur thermoregulation (Fricke and Rogers, 2000; Straight et al., 2009; Eagle et al., 2011), mammalian biology/physiology (Amiot et al., 2007; Eagle et al., 2010), and studies of climate change from oxygen isotope evidence using bones and teeth enamel of extinct vertebrate (Dettman et al., 2001; Kohn et al., 2003).

Bioapatite, especially HAP, also contains oxygen in structural carbonate (CO_3^{2-}), and the isotopic compositions of this structural CO_3^{2-} can be used as a climatic signal (Bryant et al., 1996; Iacumin et al., 1996). The carbon and oxygen isotope compositions of the structural CO_3^{2-} component in HAP can be determined by reacting the structural CO_3^{2-} in apatite with H_3PO_4 , which is similar to the analytical method proposed by McCrea (1953) for carbonate minerals. Moreover, Shemesh (1990) hypothesized that the amount of structural CO_3^{2-} decreases with increasing apatite crystallinity and these structural CO_3^{2-} have been used as indicators of tooth enamel and bone diagenesis (Shemesh, 1990; Bryant et al., 1994; Lécuyer et al., 2010). Based on this hypothesis, Bryant et al. (1994) observed that diagenesis alteration exists in some tooth fossil, as detected by increased apatite crystallinity and decreased in apatite concentration relative to modern tooth enamel. The isotopic compositions of both structural CO_3^{2-} and apatite are better preserved by well-crystallized tooth enamel rather than by poorly crystallized dentine/bone apatite (Shemesh, 1990; Ayliffe et al., 1992; Iacumin et al., 1996). In fact, HAP occurs mostly in the mineral from teeth enamel compared to bone because HAP is a major component of tooth enamel whereas bone is mostly made of calcium phosphate and minor amounts of calcium carbonate (Elliot, 1994; Zazzo et al., 2004). In the carbonate-bearing apatite of living vertebrates, $\delta^{18}\text{O}$ values of structural CO_3^{2-} and apatite are linearly correlated with a nearly constant difference of 8.56 ‰ and 8.86 ‰ (Bryant et al., 1996; Iacumin et al., 1996; Zazzo et al., 2004). Unfortunately, according to Bryant et al. (1996), $\delta^{18}\text{O}$ values of structural CO_3^{2-} and phosphate in the samples of terrestrial mammals do not show a constant difference even though their body temperature is near constant ($T = 37 \pm 2 \text{ }^\circ\text{C}$) (Bryant et al., 1996; Iacumin et al., 1996; Zazzo

et al., 2004). This is due to the large isotopic difference (~ 8 to 11 ‰) between structural CO_3^{2-} and phosphate from biogenic materials.

While numerous studies have been undertaken to measure the oxygen isotope fractionation between bioapatite and water, only a few researchers have investigated the oxygen isotope systematics on the inorganic HAP-bound carbonate-water system. Lécuyer et al. (2010) was the first to examine the oxygen isotope fractionation between the structural CO_3^{2-} of inorganically precipitated HAP and water between 10 and 37 °C. They observed that oxygen isotope fractionation factor between HAP-bound carbonate and water ($1000\ln\alpha_{\text{HAPBC-H}_2\text{O}}$) decreased from 32.46 - 32.80 ‰ at 10 °C to 24.50 - 25.24‰ at 37 °C. However, Kim and O'Neil (1997)'s temperature-dependent oxygen isotope fractionation relation between calcite and water has a shallower slope than Lécuyer et al. (2010)'s temperature-dependent of the $1000\ln\alpha_{\text{HAPBC-H}_2\text{O}}$. For this reason, Lécuyer et al. (2010) concluded that the oxygen isotope equilibrium between precipitated HAP-bound carbonate and water could not be demonstrated and that the $1000\ln\alpha_{\text{HAPBC-H}_2\text{O}}$ at 37 °C are independent of the $\delta^{18}\text{O}$ value of water (Lécuyer et al., 2010).

However, an apparent drawback of synthesizing inorganic HAP-bound carbonate is the inability to precipitate sufficient amounts of CO_3^{2-} within HAP. According to Lécuyer et al. (2010), inorganically induced HAP-bound carbonate have a higher degree of crystallization than biogenically induced HAP-bound carbonate due to the lack of organic matrix. The carbonate content of inorganic HAP ranges from 0.05 to 0.23 wt % while 3.4 to 4.0 wt % was observed from biogenically induced HAP-bound carbonates (e.g., fossils and tooth enamel) (Koch et al., 1997; Zazzo et al., 2004; Lécuyer et al., 2010).

In this study, we refined the synthesis method reported by Lécuyer et al. (2010) to precipitate inorganically induced HAP-bound carbonate between 10 and 40 °C. The objective of this study is to investigate the oxygen isotope systematics in the inorganically induced carbonate-bearing HAP and water system under controlled experimental conditions (i.e., pH, NaHCO₃ concentration, mixing rates and maturation of the mixed solution). It is crucial to understand the oxygen isotope fractionation between HAP-bound carbonate and water because it will provide basic information, such as formation temperature and climate shifts, when studying natural carbonate-bearing HAP for the reconstruction of terrestrial and marine environments. As a result, the synthesis of HAP-bound carbonate from various experimental conditions (i.e., temperature, pH, maturation and mixing rates, and concentration of NaHCO₃) is a prerequisite to characterize the oxygen isotope systematics in the HAP-bound carbonate and water.

3.2 Experimental Methods

3.2.1. Overall experimental stages

HAP-bound carbonate was synthesized by adapting the protocol reported by Lécuyer et al. (2010). Instantaneous mixing- and slow mixing- experiments were employed to determine approximately when isotopic equilibrium between dissolved inorganic carbonate (DIC) and water was reached under the chosen experimental conditions (i.e., effect of pH and concentration of NaHCO₃, mixing rates and maturation of the solutions); These experimental conditions are shown in this study as:

Stage I: The maturation of a starting solution (CA and PC) is essential for its thermal equilibration with water, as well as for complete isotopic equilibration between DIC species and water as suggested by Beck et al. (2005).

Stage II: The addition of PC into CA solution and the maturation of the mixed solution (both at an instantaneous or at a slow rate).

Stage III: The filtration of the HAP-containing solution and the drying of the precipitates. Subsequently, an aliquot of the solution was taken for $\delta^{18}\text{O}$ measurement and the precipitates were sent out for XRD analyses.

3.2.2 Solution preparation

3.2.2.1. Instantaneous mixing experiments

The phosphate-carbonate containing solution (PC) was prepared by adding ACS-grade Na_2HPO_4 and NaHCO_3 to 500 mL deionized water. In the second solutions, the calcium-containing solution (CA) was prepared by dissolving 10 mmol of $\text{CaCO}_3 \cdot 2\text{H}_2\text{O}$ to 1 L of deionized water. During Stage I of the instantaneous mixing experiment, both CA and PC solutions were matured for 7 or 14 days (Fig. 3.1). Specifically, all of labelled ‘A’ samples were matured for 7 days and all of labelled ‘B’ samples were matured for 14 days. These solutions were stored in a closed glass bottle and placed in a constant temperature bath (10, 25, and 40 ± 0.01 °C) until their thermal and isotopic equilibria were established at a given temperature. In stage II, 100 mL of the PC solution was mixed instantaneously with 100 ml of the CA solution. The mixed solution was matured for additional 7 and 14 days in a constant temperature bath at a given temperature.

3.2.2.2. Time-series experiments

A time-series experiment for the instantaneous mixing was conducted at 25 °C. The solutions were prepared only by adding 20 mmolal of NaHCO₃ and Na₂HPO₄ to 500 mL of deionized water at 25 °C. The second starting solution (CA) was also prepared by adding 10 mmolal of CaCl₂·2H₂O to 1L of deionized water. After the preparation of each PC and CA solutions, the solutions were then matured for 2 hours to 7 days (Stage I, Fig. 3.2) to ensure their thermal equilibrium before the precipitation and to assess the oxygen isotope exchange between DIC and water. Once the two starting solutions were matured, 100 mL of the PC solution was instantaneously added into 100 ml of the CA solution. There was no maturation of the mixed solution (Stage II) since the purpose of this time-series experiment is to evaluate the time needed for a complete isotopic exchange between DIC and water prior to the mixing of the two starting solutions.

3.2.2.3. Slow mixing experiments

The CA and PC solutions were prepared similarly to those for the instantaneous mixing experiment. Both PC and CA solutions were matured for 7 days and stored in a closed glass bottle in a growth chamber at 25 ± 0.05 °C (Stage I). Prior to Stage II, 100 mL of the CA solution was added into a new glass bottle, which was placed on top of a magnetic stirrer to maintain the chemical and isotopic homogeneity of the CA solution. Subsequently, 100 mL of the PC solution was transferred into a 60 mL plastic syringe. Afterward, two PC solution-containing syringes were positioned on a syringe pump that dispenses the PC solution into the CA solution (Stage II, Fig. 3.3). Two predetermined slow rates of 2.08 mL/hr and 0.594 mL/hr were used in this study in order to identify the optimum time to

synthesize pure HAP. After the PC solution was injected to the CA solution, the mixed solution at a rate 2.08 mL/hr was matured for 7 days, whereas the mixed solution at a rate 0.594 mL/hr was immediately proceeded to stage III. The reason for these differences in maturation period for the mixed solution is to determine how long it would take for the solutions to reach isotopic equilibrium with the ambient water at a slower mixing rate.

Finally, all matured mixed solutions were filtered using a vacuum filtration system through a 0.45 μm Durapore® membrane filter to separate the solid phase from the liquid phase. All of the filtered solid phases were rinsed with deionized water and methanol and then put in petri dishes and dried in a 70 °C oven for 1 day prior to storage for XRD and isotopic analyses.

3.2.3 pH calibration

The pH of the solution was measured with a Thermo Scientific Orion combination pH electrode connected to a Radiometer PHM 84 pH meter. The electrode was calibrated with three NIST-traceable buffers (i.e., pH 4.00, pH 7.00, and pH 10.00 at 25 °C) which were stored in a temperature controlled water bath of 10, 25, and 40 \pm 0.01 °C to ensure consistency between all experimental solutions. Electrode values were recorded after placing the electrode in a buffer and waited for ~ 3 minutes. Afterward, recorded values for the three buffers were plotted in Excel to determine a relationship between pH and millivolts (mV). All of the pH values were measured at the beginning of Stage I (the initial pH of the aqueous solution) and right before Stage III filtration (the final pH of the mixed solution).

3.2.4 Oxygen isotope analysis of HAP-bound carbonate ($\delta^{18}O_{\text{HAPBC}}$)

The oxygen isotope composition of HAP-bound carbonate was determined using either an IsoCarb attached to a VG-optima isotope ratio mass spectrometer (IRMS) or a Gas Bench II headspace auto-sampler with a Thermo Finnigan Delta plus XP isotope ratio mass spectrometer at McMaster University. For samples MRSI-Ie-12 to -15, approximately 2.5 mg (2500 μg) of HAP-bound carbonate was weighed and reacted with anhydrous phosphoric acid at 90 °C using the IsoCarb system. All other oxygen isotope analyses of HAP-bound carbonate (MRSI-Ie-16A to – 35SP4) were conducted using the Gas Bench II system, where approximately 10 to 14 mg of the sample was required in order to detect structural carbonate ions (CO_3^{2-}) within the HAP sample. Oxygen isotope compositions are reported in permil (‰) relative to VSMOW using the delta (δ) notation. For HAP-bound carbonate, $\delta^{18}\text{O}$ values were normalized to the current (2014) IUPAC-recommended values for NBS-19 and NBS-18 of +28.65‰ and +7.20‰ relative to VSMOW, respectively. The acid fractionation factor used in this paper is 1.01025 for calcite (Kim et al., 2015). Reproducibility of the $\delta^{18}\text{O}$ measurement based on the multiple analyse of the both standards was $\pm 0.15\text{‰}$ (1σ). The amount of structural CO_3^{2-} was estimated by calibrating a mass 44 peaks area (Fig.4) on the basis of four different weights (0.05, 0.10, 0.15, and 0.20 mg) of our internal laboratory standard, Carrara. Structural CO_3^{2-} content in the HAP sample ranges from 0.12 to 3.44 wt%.

3.2.5 Oxygen isotope analysis of water ($\delta^{18}O_{\text{H}_2\text{O}}$)

All oxygen isotope measurements for water samples from HAP-bound carbonate synthesis experiments were performed using the Gas Bench II headspace autosampler with a Thermo Finnigan Delta plus XP isotope ratio mass spectrometer at McMaster University.

The first step was to flush and fill reaction vials with a 0.2 % CO₂ and 99.8 % He mixture with a double needle at a flow rate of 100 mL/min. Subsequently, 0.2 mL of the water sample was dispensed into each reaction vial using a 1 mL syringe. After twenty-four hours was allotted for isotopic equilibration at 25 °C, CO₂ in the headspace was analyzed for oxygen isotopes. All of the water analyses were run as duplicates, and all of the standard analyzed as triplicates. The $\delta^{18}\text{O}$ values of water were normalized using the laboratory water standards, MRSI-STD-W1 (+0.58 ‰) and MRSI-STD-W2 (+28.08 ‰) which were analyzed at the beginning and end of each session. They are reported relative to VSMOW and the reproducibility (1σ) of $\delta^{18}\text{O}$ analysis for water, based on replicate analyses of the water standards, was ± 0.08 ‰.

3.2.6 Oxygen isotopic analysis of phosphate ($\delta^{18}\text{O}_{\text{PO}_4}$)

Inorganic HAP was analyzed by adapting the protocol from Bassett et al. (2007). In this study, 14 inorganic HAP samples were analyzed and were converted to Ag₃PO₄ and analyzed using high-temperature reduction as proposed by Vennemann et al. (2002) and Bassett et al. (2007). The volume of the acids (i.e., HNO₃, KOH, KF, and silver amine) in this study were adjusted from that used by Bassett et al. (2007) according to our sample weight relative to the amount of the concentrations of the acid used. The HAP samples were weighed about 1.6 to 2.0 mg and dissolved in 0.15 to 0.20 mL of HNO₃ (0.5 M) into microcentrifuge tubes depending on the weight of each HAP sample. Once the samples were dissolved within approximately 2 hours, the solutions were neutralized with 0.1 mL of 0.5 M KOH. The addition of 0.3 mL of 0.2 M KF is necessary to remove calcium ions out of the solutions. The samples were placed into the centrifuge for ~5 minutes. Then, the samples

were transferred to a new microcentrifuge tube, and 0.45 mL of silver amine was added into the solution. The tubes were placed in a 50 °C drying oven for 48 hours. These samples were then rinsed 5 times with deionized water, dried at 50 °C oven for another 24 hours, and weighed.

To measure $\delta^{18}O_{PO_4}$, the Ag_3PO_4 crystals were weighed of approximately 1.5 mg and transferred to 3.5 x 5 mm silver capsules, which then sealed to reduce the amount of isotopic exchange with CO_2 and other molecules containing oxygen in the atmosphere. These silver capsules were put in a Thermo Finnigan high temperature elemental analyzer (TC/EA) carousel where the silver capsules dropped sequentially into a graphite cubicle at 1450 °C. The oxygen in the sample was converted to CO where the gas was carried in a stream He on a Thermo Finnigan DeltaPlus GC-IRMS in which the isotopic ratios of CO were measured. Moreover, the $\delta^{18}O_{PO_4}$ values were reported relative to VSMOW and they were also calibrated using laboratory standards, IAEA 600 (-3.48 ‰), IAEA 601 (+23.14 ‰), NBS 18 (+7.20 ‰), NBS 19 (+28.65 ‰), and NBS 30 (+5.1 ‰) at the onset and conclusion of each session. The overall reproducibility (1σ) of $\delta^{18}O_{PO_4}$ measurement, based on the replicate analyses of the HAP samples, was ± 0.21 ‰.

3.2.7 X-Ray diffraction (XRD) analysis

XRD analysis was used to determine the mineralogy of the precipitate at analytical X-Ray Diffraction Facility at McMaster University. XRD data was collected using a Bruker Smart 6000 CCD area detector, a Bruker 3-Circle D8 Goniometer, a Rigaku RU 200 $CuK\alpha$ rotating anode source, and Goebel cross-couple parallel focusing mirror (McMaster Analytical X-Ray Diffraction Facility, 2013). A total of 35 samples were analyzed, representing a range

of different experimental conditions. Four frames were collected for each sample to get a continuous 2θ range from 5° to 70° with an exposure time of 300 seconds. The majority of phosphate and carbonate peaks are within this 2θ range, and the scattering intensity decreases towards a higher angle.

3.3 Results

This study used a similar synthesis technique that was developed by Lécuyer et al. (2010) to prepare inorganic HAP and HAP-bound carbonate crystals. It is noteworthy that HAP was not precipitated below 10°C ; however, brushite was precipitated instead because there was no transformation of HAP from amorphous calcium phosphate (ACP) at this temperature as previous studies (Balter and Lécuyer, 2004; Lécuyer et al. 2010) suggested. In our experiments, PC and CA solutions were held at 10, 25, and 40°C in this study unlike Lécuyer et al. (2010) kept their solutions at constant temperatures of 10 to 37°C . Table 3.2 shows the intricate differences between the method developed by Lécuyer et al. (2010) and this study, that eventually affected both the samples' solution and mineralogy, the precipitation of carbonates in HAP, and the oxygen isotope fractionation factor between HAP-bound carbonate and water.

3.3.1. Mineralogy of the precipitates based on XRD analyses

35 samples prepared from different conditions (i.e., mixing rates, pH, temperatures, and initial concentrations of NaHCO_3) were sent for an XRD analysis. XRD results showed that mineral phases formed between 10 and 40°C from the instantaneous mixing experiments with a final pH above 6.7 were pure HAP (Fig. 3.5 and 3.6). In contrast, samples collected

from final pH values between 6.4 and 6.7 were discovered to be a mixture of octacalcium phosphate (OCP) and HAP (Fig. 3.7). It was also observed that most of the slow mixing experiments with an injection rate of 2.08 mL/hr and 0.594 mL/hr were a mixture of OCP and HAP crystals (Table 3.3). The only exception from the slow mixing experiment at 5 mmolal NaHCO₃ yielded pure OCP (Fig. 3.6). Interestingly, no brushite was found from all the experiments when the final pH was above 6.4. Lécuyer et al. (2010) reported the same results when their pH value was 7.4 (Lécuyer et al., 2010). Therefore, the mixing rates and final pH of the mixed solution are the most important factor to synthesize pure HAP.

Furthermore, NaHCO₃ concentration in the PC solution for the slow mixing experiment is an essential element, in addition to the mixing rate, maturation period, and the pH of the mixed solution, for the preparation of pure HAP-bound carbonate. Based on our XRD results, all of the tested NaHCO₃ concentrations in the PC solution for the instantaneous mixing experiment produced pure HAP crystals. The only exception were the 5 mmolal NaHCO₃ samples which discovered to be a mixture of HAP and OCP crystals at a lower final pH (> 6.7) of the mixed solution under the instantaneous mixing rate experiment. In addition, the NaHCO₃ concentration in the PC solution influenced the precipitation of pure HAP crystals under the slow mixing experiments. For example, only the pure OCP was precipitated from the NaHCO₃ concentration of 5 mmolal when the two starting solutions were mixed at an injection rate of 2.08 mL/hr and the mixed solution was matured for 7 days (Table 3.9). At 10 mmolal NaHCO₃ concentration under both injection rates of 2.08 mL/hr and 0.594 mL/hr, a mixture of OCP and HAP formed although OCP crystals were dominant than HAP. Interestingly, it appears that at NaHCO₃ concentrations of 15 mmolal, the slow

mixing rates of 2.08 mL/hr and 0.594 mL/hr, allowed sufficient time to elapse the precipitation of more HAP than OCP (Tables 3.3 and 3.9).

After all of the mixed solutions from the instantaneous mixing experiments were filtered and weighed, all of the samples appeared as thick opaque white planar sheets under the microscope (Fig. 3.8 and 3.9). In contrast, all of the samples from the slow mixing experiments appeared as thick light powders clumped together under the microscope (Fig. 3.10) which had similar crystal structures to the pure OCP that was produced under the slow mixing experiment (Fig. 3.11). In general, synthesized HAP crystals show always plate-, planar-, sheet-like morphologies because they grow *c*-axis in the plane of plate and lying in the direction of the plate's longest dimension (Elliot, 1994; Dorozhkin, 2007; Xia et al., 2012).

3.3.2. Oxygen isotope compositions of hydroxyapatite-bound carbonate ($\delta^{18}\text{O}_{\text{HAPBC}}$)

$\delta^{18}\text{O}_{\text{HAPBC}}$ values from the two sets of synthesis experiments (instantaneous and slow mixing) are shown in Tables 3.4 and 3.6 as a function of temperature, NaHCO_3 concentration, and the final $\delta^{18}\text{O}_{\text{H}_2\text{O}}$ value of the mixed solution. Over the course of the instantaneous mixing experiments, $\delta^{18}\text{O}_{\text{HAPBC}}$ values were varied from 13.83 to 27.53 ‰ (Table 3.6). This large variation in $\delta^{18}\text{O}_{\text{HAPBC}}$ could be caused by the instantaneous mixing of the mixed solutions which led to heterogeneous nucleation of HAP. $\delta^{18}\text{O}_{\text{HAPBC}}$ collected from the slow precipitation experiment at 25 °C ranged from 15.26 to 26.12 ‰. The overall reproducibility (1σ) of $\delta^{18}\text{O}_{\text{HAPBC}}$ measurement, based on the replicate analyses of the HAP-bound carbonate samples, was approximately $\pm 0.23\%$.

3.3.3 Oxygen isotope compositions of waters ($\delta^{18}\text{O}_{\text{H}_2\text{O}}$)

The $\delta^{18}\text{O}_{\text{H}_2\text{O}}$ values of the experimental solutions did not change significantly over the course of this study, varying only from -6.65‰ to -6.37‰ (Tables 3.4 to 3.6). The average of the final $\delta^{18}\text{O}_{\text{H}_2\text{O}}$ values were used to calculate oxygen isotope fractionation between HAP-bound carbonate and water, and that between HAP and water as described in section 3.3.4.

3.3.4 Oxygen isotope fractionation between HAP-bound carbonate and water ($1000\ln\alpha_{\text{HAPBC-H}_2\text{O}}$)

The data presented in Tables 3.4 to 3.6 are divided according to the mixing rate experiments (i.e., Table 3.4 is for the instantaneous mixing, Table 3.5 is for the time-series, Table 3.6 is the slow mixing) for easy comparison with the HAP-bound carbonate samples. Experiments were performed in a restricted NaHCO_3 concentration range and from 10 to 40 °C (Tables 3.7 to 3.9). Moreover, the mixing rates and the maturations of the mixed solutions were varied to investigate how they influence the oxygen isotope fractionation factor between carbonate-bearing HAP and water. The $1000\ln\alpha_{\text{HAPBC-H}_2\text{O}}$ values varied from 23.10 to 33.69 ‰ for the instantaneous mixing experiment and they changed from 21.60 to 32.34 ‰ for the slow mixing experiment.

3.3.4.1 Pure HAP-bound carbonate

Most of the instantaneous mixing experiments yielded pure HAP crystals when the initial pH value of the PC solution was approximately 8.4 to 8.8 and the final pH value of the mixed solution was 6.7 to 7.4. Over the experimental range of the instantaneous mixing experiments performed in this study, the temperature dependence of the oxygen isotope

fractionation factor between HAP-bound carbonate and water showed a shallower slope (Fig. 3.12) compared to that was proposed by Lécuyer et al. (2010). Under the instantaneous mixing method, the oxygen isotope fractionations between HAP-bound carbonate and water were divided into two different maturations of the mixed solutions (7 and 14 days). As shown in Fig. 3.12, the oxygen isotope fractionation determined from the 7-day maturation of the mixed solution appeared to be larger, decreasing from 33.69 ‰ at 10 °C to about 24.50 ‰ at 40 °C. On the other hand, the oxygen isotope fractionation observed from the 14-day maturation of the mixed solutions seemed to have smaller oxygen isotope fractionations from 33.21 ‰ at 10 °C up to 23.10 ‰ at 40 °C. In general, the oxygen isotope fractionation between HAP-bound carbonate and water determined from the 7-day maturation of the mixed solution was about 1‰ larger than that determined from the 14-day maturation. Nonetheless, the temperature dependence of our oxygen isotope fractionation between HAP-bound carbonate and water for both maturation periods is positively deviated from the equilibrium oxygen isotope fractionation between calcite and water proposed by Kim and O'Neil (1997) (Fig. 3.12). However, the oxygen isotope fractionation between HAP-bound carbonate and water that was determined from the 14-day maturation of the mixed solution is closer to the predicted equilibrium oxygen isotope relationship by Kim and O'Neil. (1997), particularly at 10 °C. This supports our hypothesis that the longer the maturation of the mixed solution (or the DIC in the solution), the closer HAP-bound carbonate will reach the isotopic equilibrium with water. Noticeably, Fig 3.12 shows that some data points under 7-day maturation lie slightly above Beck et al. (2005)'s equilibrium oxygen isotope fractionation between HCO_3^- and water at 25 and 40 °C. This observation will be further discussed in section 3.4.1. The spread of the isotopic data are also (i.e., sample variance

under the sample temperature conditions) more pronounced with increasing temperature as presented in Fig. 3.12. This is potentially caused by the rapid exchange between DIC and water at higher temperatures which led to insufficient time for HAP-bound carbonate to reach equilibrium with water.

3.3.4.2 Non-pure HAP-bound carbonate (mixture of OCP and HAP)

Based on XRD analyses, all of the precipitates from the slow mixing experiments were turned out to be a mixture of HAP and OCP crystals. Fig. 3.13 shows that the oxygen isotope fractionation between non-pure HAP-bound carbonate and water displays slightly larger values (32.34 ‰ to 26.19 ‰) when the injection rate was 0.594 mL/hr and the mixed solution was not matured. Whereas the injection rate of 2.08 mL/hr along with the addition of 7-day maturation of the mixed solutions, demonstrate smaller fractionation values (31.17 ‰ to 25.53 ‰). These oxygen isotope fractionation from both slow mixing experiments lied within the fractionation values from the instantaneous mixing experiment at 25 °C (Fig. 3.14). Thus, our results suggest that the maturation period of the mixed solutions (Stage II) is necessary in order for the HAP-bound carbonate to reach closer to isotopic equilibrium with water.

3.3.5 Oxygen isotope fractionation between HAP and water

Fourteen samples of pure HAP and a mixture of HAP and OCP were selected from several different experimental conditions (i.e., pH, NaHCO₃ concentration, mixing rates and maturation of the mixed solution) in order to measured the oxygen isotope fractionation between HAP and water (Table 3.10). The $\delta^{18}\text{O}_{\text{PO}_4}$ values of HAP from all experiments did

not show any dependence with experimental conditions (i.e., pH, NaHCO₃ concentration, mixing rates and maturation of the mixed solution) over the course of experiments, varying only from 12.71‰ to 10.42‰. The resulting oxygen isotope fractionation between HAP and water also were smaller by ~2 to 7‰ compared to those already established between dissolved inorganic phosphate (DIP) and water using microbial enzyme (Blake et al., 1997; Chang and Blake, 2015) (Fig. 3.15).

3.4 Discussion

3.4.1 Oxygen isotope fractionation between HAP-bound carbonate and water ($1000\ln\alpha_{\text{HAPBC-H}_2\text{O}}$)

Tables 3.4 and 3.7 show that the oxygen isotope fractionation between HAP-bound carbonate and water are functions of maturation of the mixed solutions and NaHCO₃ concentration. The temperature dependence of $1000\ln\alpha_{\text{HAPBC-H}_2\text{O}}$ is presented in Fig. 3.12. A clear relation between the $1000\ln\alpha_{\text{HAPBC-H}_2\text{O}}$ and temperatures is observed from data collected from both 7- and 14 day-maturation of the mixed solutions, with $1000\ln\alpha_{\text{HAPBC-H}_2\text{O}}$ increasing with decreasing temperatures. Oxygen isotope equilibrium between HAP-bound carbonate and water during the precipitation of carbonate-bearing HAP was tested under various temperatures, mixing rates and maturation periods of the mixed solution, pH values, as well as NaHCO₃ concentrations. The temperature dependence relationship of $1000\ln\alpha_{\text{HAPBC-H}_2\text{O}}$ in our study was compared with that determined by Lécuyer et al. (2010) (Eq. 1) and that for calcite and water by Kim and O'Neil (1997) (Eq. 2):

$$1000\ln\alpha(\text{HAPBC-H}_2\text{O}) = 25.19 (10^3/T) - 56.47 \quad \text{Equation 1}$$

$$1000\ln\alpha(\text{Calcite-H}_2\text{O}) = 18.03 (10^3/T) - 32.43 \quad \text{Equation 2}$$

In general, temperature is important in investigating equilibrium and kinetic oxygen isotope effects, which has been extensively studied theoretically and experimentally in both the carbonate and water system (O'Neil et al., 1969; Kim and O'Neil, 1997; Zeebe, 1999; Beck et al., 2005; Kim et al., 2006), and the phosphate and water system (Blake et al., 1997; Lécuyer et al., 1999; O'Neil et al., 2003; Chang and Blake, 2015). According to Beck et al. (2005), oxygen isotope exchange between DIC species and water increases with increasing temperature and decreasing pH, similar to those established between phosphate-water systems (Lécuyer et al., 1999; O'Neil et al., 2003). For example, O'Neil et al. (2003) observed that at low pH and high temperature, the isotopic exchange between phosphate and water is much more rapid than at high pH and low temperature conditions. Beck et al. (2005) showed that the equilibration time between HCO_3^- and water is expected to be ~24, 9, and 2 hours at 15, 25, and 40 °C. On the other hand, O'Neil et al. (2003) demonstrated the isotopic equilibration time of H_2PO_4^- and HPO_4^{2-} with water is estimated to be ~2.5 years, 32 days, 19 days, and 12 days at 70, 115, 150 and 180 °C, respectively. Zeebe (1999) and Kim et al. (2006) also suggested that the oxygen isotope composition of a carbonate mineral (both synthetic and biogenic carbonates) is not only dependent on formation temperature, the speciation of DIC species, and pH, but also the effect of precipitation rate. As a result, instantaneous and slow mixing experiments were employed in this study in addition to two different maturation periods for the starting solution and mixed solution.

3.4.1.1 Effect of mixing rates and maturations on oxygen isotope fractionation between HAP-bound carbonate and water.

The mixing rate of the mixed solution was varied to investigate equilibrium oxygen isotope effects on HAP-bound carbonate and water. The $1000\ln\alpha_{\text{HAPBC-H}_2\text{O}}$ values, particularly with the 14 day-maturation, has a slightly similar slope with that determined between calcite and water (Kim and O'Neil, 1997) and DIC and water (Beck et al., 2005) (Fig. 3.12). On the other hand, it appears that the oxygen isotope fractionation determined from the 7 day-maturation of the mixed solution did not allow a sufficient time for the DIC to isotopically equilibrate with water. However, both of the temperature dependence of the $1000\ln\alpha_{\text{HAPBC-H}_2\text{O}}$ values from this study have shallower slopes compared to the oxygen isotope fractionation between HAP-bound carbonate and water that was proposed by Lécuyer et al. (2010). The followings are several possible scenarios:

1. Lécuyer et al. (2010) matured the starting solutions only for 2 days at 10 to 37 °C and the mixed solutions for 4 days at 10 to 37 °C. In this case, the HAP-bound carbonate solutions in Lécuyer et al. (2010) might not be in isotopic equilibrium with the parent water. In contrast, the starting and the mixed solutions were matured for 7 and 14 days at 10, 25, and 40 °C, respectively in this study. Fig. 3.12 shows the $1000\ln\alpha_{\text{HAPBC-H}_2\text{O}}$ values, determined from our instantaneous mixing experiments for both 7- and 14-day maturation periods, are up to ~3‰ larger at 40 °C than those from 4 day maturation of the mixed solution by Lécuyer et al. (2010). Since phosphate was present in the carbonate-water system in our study as well as Lécuyer et al. (2010), the precipitation of HAP-bound carbonate may slow down the equilibration time between DIC and water due to the strong P-O bonds at low

temperatures especially if microbial enzyme is absent (Lécuyer et al. 1999; O’Neil et al., 2003). Therefore, the longer the maturation of the starting and mixed solutions in the phosphate-carbonate-water system, the closer it would reach oxygen isotope equilibrium with parent water.

Consequently, the slopes and the fractionation factors of HAP-bound carbonate and water are closer to that proposed by Kim and O’Neil (1997), particularly at 10 °C where a small isotopic difference of ~0.05 ‰ was observed. However, the $1000\ln\alpha_{\text{HAPBC-H}_2\text{O}}$ value at 40 °C shows a positive oxygen isotope fractionation up to ~2.5 ‰ above the calcite-water equilibrium line by Kim and O’Neil (1997). This observation is compatible with the hypothesis in the carbonate-water systems (Beck et al., 2005) that determined the exchange between DIC and water decreases at low temperature, which yield to smaller isotopic fractionations values. Furthermore, according to Lécuyer et al. (2010), their $1000\ln\alpha_{\text{HAPBC-H}_2\text{O}}$ value at low temperatures could not demonstrate oxygen isotope equilibrium between precipitated HAP-bound carbonate and water. However, Lécuyer et al. (2010)’s oxygen isotope fractionation between HAP-bound carbonate and water is close to that established between calcite and water that was proposed by Kim and O’Neil (1997). Lécuyer et al. (2010)’s findings of the non-equilibrium in the $1000\ln\alpha_{\text{HAPBC-H}_2\text{O}}$ support the proposition by Kim and O’Neil (1997). In which Kim and O’Neil (1997) suggested that the steeper slope of the temperature dependence of oxygen isotope fractionations in carbonate-water system, the oxygen isotope fractionation curves would be further or positively deviated from the “assume” equilibrium between calcite and water that was reported by Kim and O’Neil (1997). Therefore, the differences in the maturations of the starting and the mixed solutions

experiments are critical to reach closer to equilibrium oxygen isotope fractionation towards Kim and O'Neil (1997).

2. Differences in solution chemistry among Kim and O'Neil (1997), Lécuyer et al (2010) and this study might lead to a different slope in temperature dependence of the $1000\ln\alpha_{\text{HAPBC-H}_2\text{O}}$ values, and influence the oxygen isotope composition of HAP-bound carbonate. This hypothesis will be further discussed in section 3.4.1.2.
3. Possible oxygen isotope effects observed during the precipitation of HAP-bound carbonate can be attributed to the preferential deprotonation of isotopically heavy HCO_3^- ions and the incorporation of isotopically light CO_3^{2-} during the mineral growth of HAP-bound carbonate (Beck et al., 2005). Furthermore, some of the oxygen isotope fractionation determined from the 7 day-maturation of the mixed solution lie above the equilibrium line of HCO_3^- and water at 25 and 40 °C, which may be due to the large analytical uncertainties of ± 0.23 ‰ based on the replicated analyses between HAP-bound carbonate samples. This can generate non-equilibrium conditions between carbonate-bearing HAP and water. The non-equilibrium conditions can be explained by the rapid precipitation at higher temperatures and low pH in both phosphate-water and carbonate-water system along with the instantaneous mixing rate of the mixed solutions, which did not allow sufficient time to achieve isotopic equilibrium between HAP-bound carbonate and water (O'Neil et al., 2003).

As a result, slower mixing experiments were employed in an attempt to minimize the kinetic isotope effects while synthesizing HAP-bound carbonate. Unfortunately, XRD results showed that both the slow mixing experiments yielded a mixture of HAP and OCP at 25 °C. As presented in Fig. 3.13 and 3.14, there are no distinct trends in oxygen isotope fractionation between HAP-bound carbonate and water from the slow mixing experiments at

25 °C as a function of maturation of the mixed solution, temperature, and pH. Ultimately, the oxygen isotope fractionations between HAP-bound carbonate and water from the slow mixing experiments are within the range of the fractionation observed from the instantaneous mixing experiments at 25 °C. It is noteworthy that most of the replicate analyses among HAP-bound carbonate samples had large analytical errors up to $\sim \pm 1.2$ ‰ (Fig. 3.14), which caused some $1000\ln\alpha_{\text{HAPBC-H}_2\text{O}}$ values lie above DIC and water that was reported by Beck et al. (2005). Additionally, since phosphate is incorporated within the carbonate sample in our experiments, the isotopic exchange between HAP-bound carbonate and water was not rapid enough to reach isotopic equilibrium with water. Therefore, a future study is necessary to investigate the necessary conditions (i.e., mixing rates and maturations of the starting and mixed solutions) for the HAP-bound carbonate to have a complete isotopic exchange with water, particularly at low temperatures.

3.4.1.2 Effect of NaHCO_3 concentrations on oxygen isotope fractionation between HAP-bound carbonate and water.

Fig. 3.17 shows a temperature dependence of the oxygen isotope fractionation factor between HAP-bound carbonate and water. Kim and O'Neil (1997) reported that, this equilibrium oxygen isotope effects between calcite and water increases with increasing the DIC concentration at a given temperature. In contrast, we observed the oxygen isotope fractionation between HAP-bound carbonate and water that determined from the 14 day-maturation of the mixed solution which appears to be in the reverse order from Kim and O'Neil (1997) (Fig. 3.17). It is important to note that phosphates was used in our synthesis experiments. Therefore, we expect that the oxygen isotope exchange between DIC and water

in the HAP-bound carbonate and water system would be slower than a system that contain only carbonate and water. As shown in Fig. 3.18, all of the initial concentrations of DIC (5, 10, and 15 mmolal NaCO_3) were not in equilibrium with water, hence we assume that all of the initial concentrations of NaHCO_3 would be below the initial oxygen isotope fractionation between DIC and water. This is because a complete oxygen isotope exchange in the phosphate-water system has not been studied at low temperatures and it is expected to delayed the isotopically equilibration times. In general, the oxygen isotope exchange between DIC and water depends on the size of the DIC reservoir (Beck et al., 2005). In this study, the small DIC reservoir (i.e., 5 mmolal NaHCO_3) reaches faster isotopically exchange to equilibrium with water and slower precipitation rate of CaCO_3 than the larger DIC reservoir (Fig. 3.18). Conversely, the larger DIC reservoir (i.e., 15 mmolal NaHCO_3) shows slower oxygen isotope exchange with water and faster precipitation rate of CaCO_3 due to the high saturation index in the HAP-bound carbonate and water. As shown in Fig. 3.18, the smaller DIC reservoir positively deviated from Kim and O'Neil (1997)'s oxygen isotope fractionation between calcite-water. Also, the smaller DIC reservoir reaches faster to oxygen isotope fractionation equilibrium between HCO_3^- and water by Beck et al. (2005) than the larger DIC reservoir (Fig. 3.18). The larger DIC reservoir (15 mmolal NaHCO_3) isotopically exchange with water slowly and provides sufficient time to reach closer to the equilibrium oxygen isotope fractionation between calcite and water that was observed by Kim and O'Neil (1997). On the other hand, the oxygen isotope fractionation between calcite and water that was determined by Kim and O'Neil (1997) starts at equilibrium between initial DIC and water regardless of the initial NaHCO_3 concentration tested. This is due to the fact that the isotopic equilibration times in the carbonate-water system has been observed at low

temperatures (Halas and Wolacewicz, 1982; Beck et al., 2005). In this case, the smaller DIC reservoir reported to consume more DIC in which resulted in a faster precipitation rate of CaCO_3 . Thus, the smaller DIC reservoir found to reach closer to the “assumed” oxygen isotope fractionation equilibrium between calcite and water by Kim and O’Neil (1997) compared to their larger DIC reservoir. Therefore, it is concluded that the presence of bicarbonates ions in the phosphate-water system in this study possibly lead to slow oxygen isotope exchange between DIC species and water, most notably at higher NaHCO_3 concentrations.

Furthermore, under the 7 day-maturation (both from the starting and mixed solutions) as shown in Fig. 3.17, larger oxygen isotope fractionations between HAP-bound carbonate and water are more pronounced with higher DIC concentrations (10 and 15 mmolal) and decreasing temperatures as suggested by Kim and O’Neil (1997). In this case, we expect faster precipitation of DIC and water, which may induce kinetic isotope effects. As discussed in 3.4.1.1, the precipitation rates at higher temperature are much faster (especially with higher DIC concentrations) compared to those at higher temperature with lower DIC concentrations. Under low temperatures (i.e., 10°C), the precipitation rates are much slower, which will provide sufficient time for the DIC to equilibrate with the water (Fig. 17). The attainment of oxygen isotope equilibrium in the HAP-bound carbonate and water system therefore could not be proven at increases DIC concentrations with increasing temperature. This is due to larger oxygen isotope fractionations which lead to kinetic effects in the phosphate-water and carbonate-water system.

The slower mixing experiments at 25°C with the injection rate of 2.08 mL/hr and 0.594 mL/hr are presented in Fig. 3.19. The large and scattered $1000\ln\alpha_{\text{HAPBC-H}_2\text{O}}$ values

among the mixture of carbonate-bearing HAP and OCP samples are observed in both injection rates. As discussed in section 3.4.1.2, the oxygen isotope fractionation values between HAP-bound carbonate and water that are above to that DIC and water at 25 and 40 °C that was reported by (Beck et al., 2005) are caused by the large analytical error associated with the measurement among the replicate analyses of these samples. Such large analytical uncertainties could result from disequilibrium oxygen isotope fractionation between HAP-bound carbonate and water. At an injection rate of 0.594 mL/hr (7 days), most of the samples are closer to the oxygen isotope equilibrium line reported by Kim and O'Neil (1997) under both the DIC concentrations of 10 and 15 mmolal. This near equilibrium line under 7 days mixing rate indicates faster oxygen isotopic exchange between DIC and water. As a result, insufficient time for the DIC to isotopically exchange with the water indicates the disequilibrium of the oxygen isotope fractionation between HAP-bound carbonate and water, particularly at higher temperature (25 and 40 °C)

3.4.2 Oxygen isotope fractionation between HAP and water ($1000\ln\alpha_{\text{HAP-H}_2\text{O}}$)

In this study, the oxygen isotope fractionation between inorganic HAP and water was observed to have no significant dependence with respect to temperatures, solution maturations, mixing rates, and NaHCO_3 concentration (Fig. 3.20). Fig. 3.20 shows that the $1000\ln\alpha_{\text{HAP-H}_2\text{O}}$ values are approximately 3.4 ‰ to 5.9 ‰ smaller than those between bioapatites and water at low temperatures (25 to 40 °C) (Longinelli ad Nuti 1973a; b; Kolodny et al., 1983; Lécuyer et al., 1996; Puceat et al., 2010). The reason for this large range of isotopic difference might be caused by the heterogeneity of the isotopic data collected from the standard reference materials that were used for the normalization of oxygen isotope

data for HAP and water samples. These standard materials were found to have offsets from ± 1.9 ‰ up to ± 3.2 ‰ from the published values in our study.

Moreover, Chang and Blake (2015) reported that there are some discrepancies in oxygen isotope fractionation between DIP and water depending on the employed analytical methods (BiPO_4 or Ag_3PO_4 , and TC/EA or CF-IRMS) and the normalization bias among different laboratories (Longinelli and Nuti, 1973b; Vennemann et al., 2002; Puceat et al., 2010; Lécuyer et al., 2013). Thus, these analytical technique discrepancies resulted in potential inconsistencies of oxygen isotope fractionation equilibrium between phosphate (biogenic and inorganic) and water, similar to that oxygen isotope fractionation between bioapatite and water observed by Puceat et al (2010). For example, Chang and Blake (2015) observed that there were +0.9 to +2.3‰ offsets in oxygen isotope fractionation between DIP and water based on TC/EA analysis using Ag_3PO_4 , and oxygen isotope fractionation between bioapatite and water using fluorination of BiPO_4 (Longinelli and Nuti, 1973a; b). Additionally, they reported that there was another offset of +0.5 to +0.7 ‰ when using different calibration standards (i.e., SRM 120c) in oxygen isotope fractionation between DIP and water to that established between bioapatite and water fractionation (Puceat et al., 2010). Nonetheless, these studies employed the same analytical techniques using Ag_3PO_4 and TC/EA analysis (Puceat et al. 2010; Chang and Blake, 2015). The inconsistencies in the standard calibrations and the analytical techniques used in different laboratories corresponded to the hypothesis proposed by Zheng (2015), who discussed potential discrepancies in the reported equilibrium oxygen isotope fractionation in the phosphate-water system. Thus, the impact of the analytical protocols (BiPO_4 and Ag_3PO_4) (Vennemann et al., 2002; Chang and Blake, 2015), the oxygen isotope analysis for phosphates (CO_2 or CO gases

and heating method) (Lécuyer, 2004), as well as the oxygen isotope heterogeneity in the standard reference materials (Puceat et al., 2010; Zheng, 2015) play significant roles in the quantification of the equilibrium oxygen isotope fractionation in the phosphate-water system.

3.5 Conclusions

The main goal of this study was to determine the oxygen isotope fractionation between HAP-bound carbonate and water at low temperatures. The synthesis of HAP-bound carbonate from an aqueous solution was developed by testing the effects of the start solution mixing and the maturation period of the mixed solution. Our experimental results indicate that the effect of pH of the mixed solutions and the concentrations of NaHCO_3 are important in the synthesis of pure HAP and HAP-bound carbonate crystals. Moreover, temperatures, the mixing rates and the maturation periods of the mixed solution are also crucial to achieve the oxygen isotope equilibrium between HAP-bound carbonate and parent water.

In this study, pure HAP was synthesized when the two starting solutions were mixed instantaneously and the pH of the mixed solution was between 6.7 and 7.4 regardless of the NaHCO_3 concentration tested. A mixture of HAP, OCP, and brushite was found when the mixed solution has a pH below 6.4. However, when the starting solutions were mixed slowly and the pH of the mixed solution was above 6.7, a mixture of HAP and OCP was yielded at 25 °C and irrespective of the NaHCO_3 concentration. Our study also revealed that the shallow slopes of the temperature dependence of the $1000\ln\alpha_{\text{HAPBC-H}_2\text{O}}$ values obtained from the instantaneous mixing experiment are in a close approximation to Kim and O'Neil (1997)'s temperature dependence of the oxygen isotope fractionation between calcite and water. Whereas Lécuyer et al. (2010) observed a steeper slope between their temperature

dependence of the oxygen isotope fractionation between HAP-bound carbonate and water compared to our study. The steeper slope that was determined by Lécuyer et al. (2010) could be due to the shorter maturations in the mixed solutions and different solution chemistry that may influenced the disequilibrium effect on the oxygen isotope fractionation between HAP-bound carbonate and water.

Furthermore, the initial DIC concentration in the HAP-bound carbonate and water system showed non-equilibrium effect which may simply due to the incorporation of phosphate species that slows down the exchange reactions between DIC and water. The oxygen isotope fractionation between HAP-bound carbonate and water obtained from experiments with 14-day maturations of the starting solutions and larger DIC reservoir (15 mmolal NaHCO_3) were closer to the oxygen isotope fractionation value proposed by Kim and O'Neil (1997). In contrast, the smaller DIC reservoir (5 mmolal NaHCO_3) was more isotopically enriched compared Kim and O'Neil (1997)'s oxygen isotope fractionation between calcite and water.

Therefore, with the adjustments of NaHCO_3 concentration under different maturations and mixing rates of the starting and mixed solutions, one can discriminate in which conditions to reach closer to equilibrium oxygen isotope fractionation between HAP-bound carbonate and water. While the research findings presented in this study advance our understanding of the oxygen isotope systematics between HAP-bound carbonate and water, several amendments can be made to improve the overall precision and further refine the equilibrium effect in HAP-bound carbonate and water system. For example, longer maturations of the starting and mixing solutions above 14 days in HAP-bound carbonate-

water system is necessary for the DIC to be in isotopically equilibrium with the parent water since the presence of phosphate ions slows down the equilibration times.

Our results for the temperature dependence of oxygen isotope fractionation between HAP and water could not be demonstrated. Therefore, future research on the temperature dependence of the oxygen isotope fractionation between HAP and water is required. Moreover, in order to avoid and resolve considerable inconsistencies in the oxygen isotope fractionation analysis between phosphate (biogenic and DIP) and water, much attention has to be made on the geochemical procedures of different analytical protocols (BiPO_4 and Ag_3PO_4) and standard calibrations. Also, longer maturations (above 14 days) are necessary in order to ensure HAP is closer or in equilibrium with the water. These modifications are essential for the quantification of the equilibrium oxygen isotope fractionation in the phosphate-water system.

References

- Amiot, R., Lécuyer, C., Escarguel, G., Billon-Bruyat., J-P., Buffetaut, E., Langlois, C., Martin, S., Martineau, F. and Mazin J-M. (2007) Oxygen isotope fractionation between crocodylian phosphate and water. *Palaogeography, Paleoclimatology, Palaeoecology* **243**, 412-420.
- Ayliffe, L. K., Lister, A. M. and Chivas, A. R. (1992) The preservation of glacial-interglacial climatic signatures in the oxygen isotopes of elephant skeletal phosphate. *Palaeogeology Paleoclimatology Palaeoecology* **99**, 179-191.
- Balter V. and Lécuyer C. (2004) Determination of Sr and Ba partition coefficients between apatite and water from 5 °C to 60 °C: A potential new thermometer for aquatic paleoenvironments. *Geochimica et Cosmochimica Acta* **68**, 423-432.
- Bassett, D., MacLeod, L., Miller, J. and Ethington, R. (2007) Oxygen isotopic composition of biogenic phosphate and the temperature of early ordovician seawater. *Palaios* **22**, 98-103.
- Beck, W. C., Grossman, E. L. and Morse, J. W. (2005) Experimental studies of oxygen isotope fractionation in the carbonic acid system at 15 °, 25 °, and 40 °C. *Geochimica et Cosmochimica Acta* **69**, 3493-3503.
- Blake, R. E., O'Neil, J. R. and Garcia, G. A. (1997) Oxygen isotope systematics of biologically mediated reactions of phosphate: Microbial degradation of organophosphorus compounds. *Geochemica et Cosmochimica Acta* **20**, 4411-4422.
- Bryant, J., Luz, B. and Froelich, P. (1994) Oxygen isotopic composition of fossil horse tooth phosphate as a record of continental paleoclimate. *Paleogeography, Paleoclimatology, Paleoecology* **107**, 303-316.
- Bryant J. D., Koch P. L., Froelich P. N., Showers W. J. and Genna B. J. (1996) Oxygen isotope partitioning between phosphate and carbonate in mammalian apatite. *Geochimica et Cosmochimica Acta* **60**, 5145-5148.
- Chang, S. J. and Blake, R. E. (2015) Precise calibration of equilibrium oxygen isotope fractionations between dissolved phosphate and water from 3 to 37 °C. *Geochemica et Cosmochimica Acta* **150**, 314-329.
- Dettman, D. L., Kohn, M. J., Quade, J., Ryerson, F. J. Ojha, T. P. and Hamidullah, S. (2001) Seasonal stable isotope evidence for a strong Asian monsoon throughout the past 10.7 myr. *Geology* **29**, 31-34.

- Dorozhkin, S. V. (2007) Calcium orthophosphates. *Journal of Materials Science* **42**, 1061-1095.
- Eagle, R. A., Schauble, E. A., Tripathi, A. K., Tutken, T., Hulbert, R. and Eiler, J. M. (2010) Body temperatures of modern and extinct vertebrates from ^{13}C - ^{18}O bond abundances in bioapatite. *Proceedings of the National Academy of Sciences of the United States of America* **107**, 10377-10382.
- Eagle R A., Tutken T., Martin T S., Aradhna K T., Fricke H C., Connely M., Cifelli R L. and Eiler J M. (2011) Dinosaur body temperatures determined from isotopic (^{13}C - ^{18}O) ordering in fossil biominerals. *Science* **333**, 443.
- Elliot, J. C. (1994) Structure and chemistry of the apatites and other calcium orthophosphates. Elsevier, Amsterdam.
- Fricke H. C., William C. C., O'Neil J. R. and Gingerich P. D. (1998a) Evidence for rapid climate change in North America during the latest Paleocene thermal maximum: oxygen isotope compositions of biogenic phosphate then the Bighorn Basin (Wyoming). *Earth and Planetary Science Letters* **160**, 193-208.
- Fricke H. C., Clyde W. C. and O'Neil, J. R. (1998b) Intra-tooth variations in $\delta^{18}\text{O}$ (PO_4) of mammalian tooth enamel as a record of seasonal variations in continental climate variables. *Geochimica et Cosmochimica Acta* **62**, 1839-1850.
- Fricke, D. C. and Rogers. R. R. (2000) Multiple taxon-multiple locality approach to providing oxygen isotope evidence for warm-blooded theropod dinosaurs. *Geology* **28**, 799-802.
- Halas, S. and Wolacewicz, W. (1982) The experimental study of oxygen isotope exchange reaction between dissolved bicarbonate and water. *J. Chem. Phys.* **76**, 5479-5472.
- Hoefs, J. (2009) *Stable Isotope Geochemistry* (6th ed). Berlin; Springer.
- Iacumin, P., Cominatto, D. and Longinelli, A. (1996) A stable isotope study of mammal skeletal remains of mid-Pleistocene age, Arago cave, eastern Pyrenees, France. Evidence of taphonomic and diagenetic effects. *Plaeogeogr. Plaeoclimatol. Palaeoecol.* **126**, 151-160.
- Joachimski, M., (2006) Constraints on Pennsylvannian glacioeustatic sea-level changes using oxygen isotopes of conodont apatite. *Geology* **34**, 277-280.
- Kim S-T. and O'Neil J. R. (1997) Equilibrium and nonequilibrium oxygen isotope effects in synthetic carbonates. *Geochimica et Cosmochimica Acta* **61**, 3461-3475.

- Kim, S-T., Hillaire-Marcel, C. and Mucci, A. (2006) Mechanisms of equilibrium and kinetic oxygen isotope effects in the synthetic aragonite at 25 °C. *Geochimica et Cosmochimica Acta* **70**, 5790-5801.
- Koch, P. L., Tuross, N. and Fogel, M. L. (1997) The effects of sample treatment and diagenesis on the isotopic integrity of carbonate in biogenic hydroxyapatite. *J. Archeol. Sci.* **24**, 417-429.
- Kohn, M. J., Rakovan, J. and Hughes, J. M. (2002) Phosphates: Geochemical, geobiological, and material importance. *Reviews in Mineralogy and Geochemistry*, **48**. Mineralogical Society of America, Washington, DC.
- Kohn, M. J., Miselis, J. L. and Fremd, T. J. (2003) Oxygen isotope evidence for progressive uplift of the cascade range, Oregon. *Earth Planet Science Letter*.
- Kolodny Y., Luc B. and Navon O. (1983) Oxygen isotope variations in phosphate of biogenic apatites, I. Fish bone apatite- rechecking the rules of the game. *Earth and Planetary Science Letters* **64**, 398-404.
- Lécuyer C., Grandjean P. and Emig C. C. (1996) Determination of oxygen isotope fractionation between water and phosphate from living lingulids: potential application to paleoenvironmental studies. *Paleogeography, Paleoclimatology, Paleoecology* **126**, 101-108.
- Lécuyer C., Grandjean P. and Sheppard S. M. (1999) Oxygen isotope exchange between dissolved phosphate and water at temperatures $\leq 135^{\circ}\text{C}$: Inorganic versus biological fractionations. *Geochimica et Cosmochimica Acta* **63**, 855-862.
- Lécuyer C., Balter V., Martineau F., Fourel F., Bernard A., Amiot R., Gardien V., Otero O., Legendre S., Panczer G., Simon L. and Martini R. (2010) Oxygen isotopes fractionation between apatite-bound carbonate and water determined from controlled experiments with synthetic apatites precipitated at 10-37 °C. *Geochimica et Cosmochimica Acta* **74**, 2072-2081.
- Lécuyer, C., Amiot, R., Touzaeu, A. and Trotter J. (2013) Calibration of the phosphate $\delta^{18}\text{O}$ thermometer with carbonate-water oxygen isotope fractionation equations. *Chem. Geol.* **347**, 217-226.
- Longinelli, A. and Nuti, S. (1973a) Revised phosphate-water isotopic temperature scale. *Earth and Planetary Science Letters* **19**, 373-376.
- Longinelli, A. and Nuti, S. (1973b) Oxygen isotope measurements of phosphate from fish teeth and bones. *Earth and Planetary Science Letters* **20**, 337-340.

- McCrea, J. M. (1953) Revised on the isotopic chemistry of carbonates and a paleotemperature scale. *The Journal of Chemical Physics* **18**, 849-857.
- O'Neil, J. R., Clayton R. N. and Mayeda, T. K. (1969) Oxygen isotope fractionation in divalent metal carbonates. *J. Chem. Phys* **51**, 5547-5558.
- O'Neil, J. R., Vennemann, T. W. and McKenzie, W. F. (2003) Effects of speciation on equilibrium fractionations and rates of oxygen isotope exchange between $(\text{PO}_4)_{\text{ag}}$ and H_2O . *Geochimica et Cosmochimica Acta* **67**, 3135-3144.
- Puceat, E., Lécuyer, C., Sheppard, S. M. F., Dromart, G., Reboulet, S. and Grandjean, P. (2003) Thermal evolution of Cretaceous Tethyan marine waters inferred from oxygen isotope composition of fish tooth enamels. *Palaeoceanography* **18**, 1029.
- Puceat, E., Joachimski, M., Bouilloux, A., Monna, F., Bonin, A., Motruil, S., Moriniere, P., Henard, S., Mourin, J., Dera, G. and Quesne, D. (2010) Revised phosphate-water fractionation equation reassessing paleotemperatures derived from biogenic apatite. *Earth and Planetary Science Letters* **298**, 135-142.
- Shemesh A. (1990) Crystallinity and diagenesis of sedimentary apatites. *Geochimica et Cosmochimica Acta* **54**, 2433-2438.
- Straight, W. H., Davis, G. L., Skinner, C. W., Haims, A., McClennan, B. and Tanke, D. H. (2009) Bone lesions in Hadrosaurs: computed tomographic imaging as a guide for paleohistologic and stable isotopic analysis. *Journal of Vertebrate Paleontology* **29**, 315-325.
- Tudge, A. (1960) A method of analysis of oxygen isotopes in orthophosphate- its use in the measurement of paleotemperatures. *Geochemica et Cosmochimica Acta* **18**, 81-93.
- Trotter, J. A., Williams, I. S., Barnes, C. R., Lécuyer, C. and Nicoll, R. S. (2008) Did cooling oceans trigger Ordovician biodiversification? Evidence from conodont thermometry. *Science* **321**, 550-554.
- Vennemann, T. W., Fricke, H. C., Blake, R. E., O'Neil, J. R. and Colman, A. (2002) Oxygen isotope analysis of phosphate: a comparison of techniques for analysis of Ag_3PO_4 . *Chemical Geology* **185**, 321-336.
- Xia, W., Lin, K., Gou, Z. and Engqvist, H. (2012) Morphology control of hydroxyapatite crystal and its aggregates. *Hydroxyapatite: Synthesis, Properties, and Applications* (Eds. V. S. Gshalaev and A. C. Demirchan). Nova Science Publishers, pp. 243-264.

- Zazzo, A., Lécuyer, C. and Mariotti, A. (2004) Experimentally controlled carbon and oxygen isotope exchange exchange between bioapatites and water under inorganic and microbially-mediated conditions. *Geochemica et Cosmochimica Acta* **68**, 1-12.
- Zeebe, R. E, Wolf-Gladrow, D. A. and Jansen, H. (1999) On the time required to establish chemical and isotopic equilibrium in the carbon dioxide system in seawater. *Marine Chemistry* **65**, 135-153.
- Zheng, Y-F. (2015) Oxygen isotope fractionation in phosphates: the role of dissolved complex anions in isotope exchange. *Isotopes in Environmental and Health Studies*, 1-16.

Table 3.1. Different phases of calcium phosphates in order from the most soluble to the least soluble compounds (Modified from Johnsson and Nancollas, 1992; Elliot, 1994)

Minerals	Empirical formula	Abbreviation	Ca/P ratio
Monohydrate calcium phosphate	$\text{Ca}(\text{H}_2\text{PO}_4)_2 \cdot \text{H}_2\text{O}$	MCP	0.5
Monocalcium phosphate	$\text{Ca}(\text{H}_2\text{PO}_4)_2$	MP	0.5
Dicalcium phosphate dihydrate (Brushite)	$\text{Ca}(\text{HPO}_4) \cdot 2\text{H}_2\text{O}$	Brushite	1
Octacalcium phosphate	$\text{Ca}_8(\text{H}_2\text{PO}_4)_6 \cdot 5\text{H}_2\text{O}$	OCP	1.33
Tricalcium phosphate	α - and β - $\text{Ca}_3(\text{PO}_4)_2$	TCP	1.5
Amarphous calcium phosphate	$\text{Ca}_9(\text{PO}_4)_6 \cdot \text{H}_2\text{O}$	ACP	1.5
Hydroxyapatite	$\text{Ca}_{10}(\text{PO}_4)_6(\text{OH})_2$	HAP	1.67
Fluoroapatite	$\text{Ca}_{10}(\text{PO}_4)_6\text{F}_2$	FAP	1.67

Table 3.2. Comparisons between two methods that was developed by Lécuyer et al. (2010) and this study for synthesizing hydroxyapatite crystals.

	Lécuyer et al. (2010)		This study	
T (°C)	10, 15, 20, 25, 30 and 37		Room temperature, 10, 25, and 40	
CA solution	100/10 ^a	Ini. pH= Unknown	10 ^c	Ini. pH= 5.0-5.5
PC solution	100/10 ^b	Ini. pH= Unknown	10/5, 10/7, 10/10, and 10/15 ^d	Ini. pH= 6.2-8.8
Mixing CA+PC solutions	Before mixing, PC solutions were held at a given temperatures (10-37 °C) for approximately 2 days. Then equal volumes of PC and CA solutions were mixed at a given temperature.		Before mixing, both CA and PC were aged for at least 14 days at a given temperature. 100 ml of CA was added into 250 ml beaker then added 100 ml of PC.	
pH adjustment	0.3% HNO ₃ was added into PC solutions		2% HCl was added into some PC solutions	
Final pH	7.4		6.3 to 7.4	
Maturation	4 days		7 and 14 days	
Filtration	The solid phase was separated from supernatant by centrifugation, washed with distilled water and dried at room temperature. The aqueous solutions were filtered through a 0.22 µm filter		The solutions were matured for 7 days before filtration. The solutions were filtered through a 0.45 µm filter. Then MQ water and methanol were used to rinse the samples, then dried at room temperature or at 70 °C for at least 1 day.	
Wt% CaCO₃	0.05-0.23		0.12-3.44	

T= Temperature

Ini. pH= Initial pH

^a 100/10 denotes 100 mmolal NaOH + 10 mmolal CaCl₂•2H₂O^b 100/10 denotes 100 mmolal KNaCO₃ + 10 mmolal Na₂HPO₄•H₂O^c 10 mmolal CaCl₂•2H₂O^d 10/5, 10/7, 10/10, and 10/15 denotes Na₂HPO₄+ NaHCO₃

Table 3.3. Final pH and mineralogy based on XRD results.

Precipitation	Sample #	Ini. pH	Fin. pH	Mineralogy			Maturation* Stage II (days)
				HAP %	OCP %	Brushite	
Instantaneous	MRSI-Ie-3	7.0	6.4	90	10	0	7
	MRSI-Ie-4	~ 7.2-7.6	6.4	95	5	0	7
	MRSI-Ie-5	7.2	6.4	96	4	0	7
	MRSI-Ie-6	7.2	6.4	98	3	0	7
	MRSI-Ie-7	7.0	6.4	93	7	0	7
	MRSI-Ie-12	~7.6	6.8	95	5	0	7
	MRSI-Ie-13	~7.6	6.8	98	2	0	7
	MRSI-Ie-14	~7.6	6.8	96	4	0	7
	MRSI-Ie-15	~7.6	6.8	96	4	0	7
	MRSI-Ie-17A2	8.6	7.0	100	0	0	7
	MRSI-Ie-17B1	8.6	7.3	100	0	0	14
	MRSI-Ie-22B2	8.6	7.2	100	0	0	14
	MRSI-Ie-23A	8.4	6.7	100	0	0	7
	MRSI-Ie-23B	8.4	6.7	100	0	0	14
	MRSI-Ie-25A2	8.4	7.2	100	0	0	7
	MRSI-Ie-25B2	8.6	6.7	100	0	0	14
	MRSI-Ie-26A	8.5	7.4	100	0	0	7
	MRSI-Ie-26B	8.4	6.8	100	0	0	14
	MRSI-Ie-27A2	8.4	7.4	100	0	0	7
	MRSI-Ie-27B2	8.4	7.0	100	0	0	14
	MRSI-Ie-1TS	8.6	7.0	100	0	0	0
	MRSI-Ie-8TS	8.6	7.0	100	0	0	0
	Slow	MRSI-Ie-28SP	8.6	6.7	0	100	0
MRSI-Ie-29SP2		8.6	7.0	49	51	0	7
MRSI-Ie-29SP3		8.6	7.0	56	44	0	7
MRSI-Ie-30SP		8.5	7.1	100	0	0	7
MRSI-Ie-30SP2		8.5	7.0	90	10	0	7
MRSI-Ie-30SP3		8.5	7.0	94	6	0	7
MRSI-Ie-34SP		8.4	7.0	29	71	0	0
MRSI-Ie-34SP2		8.6	6.7	36	64	0	0
MRSI-Ie-34SP4		8.6	6.9	51	49	0	0
MRSI-Ie-35SP		8.5	7.3	80	20	0	0
MRSI-Ie-35SP2		8.5	7.0	67	33	0	0
MRSI-Ie-35SP3		8.5	7.0	79	21	0	0
MRSI-Ie-35SP4		8.5	7.0	74	26	0	0

Ini. pH= Initial pH

Fin. pH= Final pH of the mixed solution

HAP= Hydroxyapatite

OCP= Octacalcium phosphate

SP= Slow precipitation

*Maturation of the mixed solutions

Table 3.4. Oxygen isotope compositions of hydroxyapatite-bound carbonate and water that were inorganically precipitated under the instantaneous mixing at 10, 25, and 40 °C.

Sample #	CA/PC	T (°C)	CO ₃ ²⁻ (wt%)	δ ¹⁸ O (H ₂ O) ⁿ (‰ V-SMOW)	δ ¹⁸ O (HAPBC) ⁿ (‰ V-SMOW)	1000lnα _{HAPBC-H2O}
	CaCl ₂ ·2H ₂ O/HPO ₄ +HCO ₃ [*] (mM)					
MRSI-Ie-16-A 1	10/10+5**	25	1.3	-6.62	25.22	31.54
MRSI-Ie-16-A 2	10/10+5	25	0.4	-6.63	20.65	27.08
MRSI-Ie-16-A 3	10/10+5	25	0.3	-6.63	24.86	31.21
MRSI-Ie-17-A 1	10/10+10	25	1.7	-6.55	23.71	30.00
MRSI-Ie-17-A 2	10/10+10	25	1.1	-6.57	22.93	29.27
MRSI-Ie-17-A 3	10/10+10	25	0.5	-6.57	23.62	29.94
MRSI-Ie-18-A2 1	10/10+15	25	0.9	-6.5	25.93	32.12
MRSI-Ie-18-A2 2	10/10+15	25	0.7	-6.59	17.17	23.63
MRSI-Ie-16B 1	10/10+5	25	1.2	-6.57	23.05	29.38
MRSI-Ie-16B 2	10/10+5	25	1.1	-6.63	24.56	30.91
MRSI-Ie-16B 3	10/10+5	25	1.0	-6.63	23.58	29.96
MRSI-Ie-17B 1	10/10+10	25	1.3	-6.49	23.12	29.36
MRSI-Ie-17B 2	10/10+10	25	0.7	-6.61	16.64	23.12
MRSI-Ie-17B 3	10/10+10	25	0.7	-6.61	22.88	29.25
MRSI-Ie-18B 1	10/10+15	25	1.8	-6.46	24.17	30.36
MRSI-Ie-18B 2	10/10+15	25	1.4	-6.58	23.33	29.67
MRSI-Ie-18B 3	10/10+15	25	0.8	-6.58	21.59	27.96
MRSI-Ie-22A	10/10+5	40	0.9	-6.70	18.76	25.31
MRSI-Ie-22A2	10/10+5	40	0.4	-6.46	22.31	28.55
MRSI-Ie-23A	10/10+10	40	1.5	-6.64	21.23	27.67
MRSI-Ie-23A2	10/10+10	40	1.5	-6.46	21.24	27.50
MRSI-Ie-24A	10/10+15	40	1.8	-6.60	19.16	25.60
MRSI-Ie-24A2	10/10+15	40	0.7	-6.45	22.97	29.18
MRSI-Ie-36B1	10/10+5	40	0.8	-6.44	16.79	23.10
MRSI-Ie-36B2	10/10+5	40	0.6	-6.44	21.68	27.90
MRSI-Ie-36B3	10/10+5	40	0.6	-6.44	21.90	28.12
MRSI-Ie-37B1	10/10+10	40	1.2	-6.42	21.26	27.47
MRSI-Ie-37B2	10/10+10	40	1.3	-6.42	13.83	20.17
MRSI-Ie-37B3	10/10+10	40	1.0	-6.42	20.85	27.08
MRSI-Ie-38B 1	10/10+15	40	2.0	-6.43	21.04	27.27
MRSI-Ie-38B2	10/10+15	40	2.2	-6.43	20.57	26.81
MRSI-Ie-38B3	10/10+15	40	3.0	-6.43	19.30	25.56
MRSI-Ie-25A	10/10+5	10	0.2	-6.59	26.47	32.74
MRSI-Ie-25A2	10/10+5	10	0.1	-6.55	26.04	32.28
MRSI-Ie-25A3	10/10+5	10	0.1	-6.55	25.84	32.08
MRSI-Ie-25B	10/10+5	10	0.8	-6.5	23.73	29.97
MRSI-Ie-25B2	10/10+5	10	0.1	-6.54	24.94	31.20
MRSI-Ie-25B3	10/10+5	10	0.1	-6.54	27.15	33.35
MRSI-Ie-26A	10/10+10	10	0.8	-6.57	24.52	30.81
MRSI-Ie-26A2	10/10+10	10	0.1	-6.51	25.06	31.29
MRSI-Ie-26A3	10/10+10	10	0.1	-6.51	26.43	32.61
MRSI-Ie-26B	10/10+10	10	0.8	-6.49	24.72	31.60
MRSI-Ie-26B2	10/10+10	10	0.1	-6.47	23.58	29.80
MRSI-Ie-26B3	10/10+10	10	0.1	-6.47	25.76	31.93
MRSI-Ie-27A	10/10+15	10	0.9	-6.5	24.23	30.47
MRSI-Ie-27A2	10/10+15	10	0.1	-6.63	27.53	33.67
MRSI-Ie-27A3	10/10+15	10	1.0	-6.63	23.55	29.80
MRSI-Ie-27B	10/10+15	10	0.8	-6.5	24.30	30.87
MRSI-Ie-27B2	10/10+15	10	0.1	-6.63	24.98	31.19
MRSI-Ie-27B3	10/10+15	10	0.1	-6.63	24.99	31.21

CA= Calcium

PC= Phosphate Carbonate

T= Temperature

HAPBC= Hydroxyapatite-bound carbonate

*HPO₄+HCO₃ denotes Na₂HPO₄+ NaHCO₃

** 10/10+5 denotes 10 mmolal CaCl₂·2H₂O/10 mmolal Na₂HPO₄+ 5 mmolal NaHCO₃

n= Each HAP samples has been duplicated for the δ¹⁸O analysis

Table 3.5. Oxygen isotope compositions of hydroxyapatite-bound carbonate and water that were inorganically precipitated from time-series experiments at 25 °C.

Sample #	CA/PC		$\delta^{18}\text{O}$ (H ₂ O) (‰ V-SMOW)	$\delta^{18}\text{O}$ (HAPBC) ⁿ (‰ V-SMOW)	1000ln $\alpha_{\text{HAPBC-H}_2\text{O}}$
	CaCl ₂ ·2H ₂ O/HPO ₄ +HCO ₃ [*] (mmolal)	CO ₃ ²⁻ wt%			
MRSI-Ie-1-TS	10/10+10**	0.4	-6.50	25.91	32.10
MRSI-Ie-2-TS	10/10+10	0.3	-6.47	21.93	28.18
MRSI-Ie-3-TS	10/10+10	1.0	-6.50	24.69	30.91
MRSI-Ie-4-TS	10/10+10	0.2	-6.43	26.00	32.11
MRSI-Ie-5-TS	10/10+10	0.1	-6.48	24.93	31.12
MRSI-Ie-6-TS	10/10+10	0.1	-6.37	25.70	31.77
MRSI-Ie-7-TS	10/10+10	0.2	-6.50	24.78	31.00
MRSI-Ie-8-TS	10/10+10	0.5	-6.45	20.79	27.04

CA= Calcium

PC= Phosphate Carbonate

T= Temperature

HAP= Hydroxyapatit

*HPO₄+HCO₃ denotes Na₂HPO₄+ NaHCO₃

** 10/10+10 denotes 10 mmolal CaCl₂·2H₂O/10 mmolal Na₂HPO₄+ 10 mmolal NaHCO₃

ⁿ= Each HAP samples has been duplicated for the $\delta^{18}\text{O}$ analysis

Table 3.6. Oxygen isotope compositions of hydroxyapatite-bound carbonate and water that were inorganically precipitated under the slow mixing experiment at 25 °C.

Sample #	CA/PC CaCl ₂ ·2H ₂ O/HPO ₄ +HCO ₃ [*] (mmolal)	CO ₃ ²⁻ (wt%)	δ ¹⁸ O (H ₂ O) (‰ V-SMOW)	δ ¹⁸ O (HAPBC) ⁿ (‰ V-SMOW)	1000lnα _{HAPBC-H₂O}
MRSI-Ie-28-SP1	10/10+5**	0.6	-6.47	21.14	27.41
MRSI-Ie-29-SP1	10/10+10	1.1	-6.48	23.62	29.85
MRSI-Ie-29-SP2	10/10+10	1.4	-6.65	23.56	29.96
MRSI-Ie-29-SP3	10/10+10	1.5	-6.65	23.50	29.83
MRSI-Ie-30-SP1	10/10+15	3.4	-6.43	25.02	31.17
MRSI-Ie-30-SP2	10/10+15	3.4	-6.52	19.79	26.14
MRSI-Ie-30-SP3	10/10+15	3.3	-6.52	19.17	25.53
MRSI-Ie-34-SP1	10/10+10	1.3	-6.45	21.25	27.5
MRSI-Ie-34-SP2	10/10+10	0.9	-6.54	26.12	32.34
MRSI-Ie-34-SP3	10/10+10	1.3	-6.47	22.19	28.44
MRSI-Ie-34-SP4	10/10+10	1.1	-6.47	19.89	26.19
MRSI-Ie-35-SP1	10/10+15	3.4	-6.44	15.26	21.6
MRSI-Ie-35-SP2	10/10+15	1.7	-6.55	31.78	37.85
MRSI-Ie-35-SP3	10/10+15	1.4	-6.56	23.76	30.06
MRSI-Ie-35-SP4	10/10+15	1.8	-6.56	20.77	27.14

CA= Calcium

PC= Phosphate Carbonate

HAP= Hydroxyapatite

*HPO₄+HCO₃ denotes Na₂HPO₄+ NaHCO₃** 10/10+5 denotes 10 mmolal CaCl₂·2H₂O/10 mmolal Na₂HPO₄+ 5 mmolal NaHCO₃ⁿ= Each HAP samples has been duplicated for the δ¹⁸O analysis

Table 3.7. Solution chemistry of all of instantaneous mixing experiments.

Sample #	CA/PC CaCl ₂ ·2H ₂ O/HPO ₄ +HCO ₃ [*] (mM)	T (°C)	Stage I	Stage II	Stage III		CA pH	PC Ini. pH	PC Fin. pH	Sample size (mg)	XRD (HAP %)
			Maturation (D) of a single solution	Maturation (D) of mixed solutions	T (°C)	Dry Time (D)					
MRSI-Ie-16-A 1	10/10+5**	25	7	7	RT	7	5.5	8.6	7.2	101.35	54.92
MRSI-Ie-16-A 2	10/10+5	25	7	7	70	1	5.9	8.7	7	100.27	
MRSI-Ie-16-A 3	10/10+5	25	7	7	70	7	5.9	8.7	7	101.35	
MRSI-Ie-17-A 1	10/10+10	25	7	7	70	7	5.5	8.6	7	106.68	100
MRSI-Ie-17-A 2	10/10+10	25	7	7	70	1	5.9	8.6	7	105.7	
MRSI-Ie-17-A 3	10/10+10	25	7	7	70	1	5.9	8.6	7	104.8	
MRSI-Ie-18-A2 1	10/10+15	25	7	7	70	7	5.5	8.5	7	120.01	
MRSI-Ie-18-A2 2	10/10+15	25	7	7	70	1	5.9	8.5	7	117.27	
MRSI-Ie-16B 1	10/10+5	25	14	14	70	1	5.5	8.5	7.2	94.33	
MRSI-Ie-16B 2	10/10+5	25	14	14	70	1	5.9	8.8	7.02	92.61	
MRSI-Ie-16B 3	10/10+5	25	14	14	70	1	5.9	8.8	7.02	88.27	
MRSI-Ie-17B 1	10/10+10	25	14	14	70	1	5.5	8.6	7.3	61.46	100
MRSI-Ie-17B 2	10/10+10	25	14	14	70	1	5.9	8.7	7.2	97.6	
MRSI-Ie-17B 3	10/10+10	25	14	14	70	1	5.9	8.7	7.2	101.24	
MRSI-Ie-18B 1	10/10+15	25	14	14	70	1	5.5	8.5	7.3	101.27	
MRSI-Ie-18B 2	10/10+15	25	14	14	70	1	5.9	8.6	7.3	94.16	
MRSI-Ie-18B 3	10/10+15	25	14	14	70	1	5.9	8.6	7.3	98.19	
MRSI-Ie-22A	10/10+5	40	7	7	70	1	5.9	8.5	6.3	100.97	
MRSI-Ie-22A2	10/10+5	40	7	7	70	1	5	8.6	7.2	104.15	
MRSI-Ie-22B	10/10+5	40	7	14	70	1	5.9	8.5	6.3	101.71	
MRSI-Ie-22B2	10/10+5	40	7	14	70	1	5	8.6	7.2	105.86	100
MRSI-Ie-23A	10/10+10	40	7	7	70	1	5.9	8.4	6.7	100.03	100
MRSI-Ie-23A2	10/10+10	40	7	7	70	1	5	8.5	6.8	108.28	
MRSI-Ie-23B	10/10+10	40	7	14	70	1	5.9	8.4	6.7	145.05	100
MRSI-Ie-23B2	10/10+10	40	7	14	70	1	5	8.5	6.8	104.81	
MRSI-Ie-24A	10/10+15	40	7	7	70	1	5.9	8.5	6.9	101.9	
MRSI-Ie-24A2	10/10+15	40	7	7	70	1	5	8.5	6.9	109.02	
MRSI-Ie-24B	10/10+15	40	7	14	70	1	5.9	8.5	6.9	106.36	
MRSI-Ie-24B2	10/10+15	40	7	14	70	1	5	8.5	6.9	107.67	
MRSI-Ie-25A	10/10+5	10	7	7	70	1	5.1	8.5	6.9	88.51	
MRSI-Ie-25A2	10/10+5	10	7	7	70	1	5	8.6	7.4	88.78	67.12
MRSI-Ie-25A3	10/10+5	10	7	7	70	1	5	8.4	7.2	89.01	
MRSI-Ie-25B	10/10+5	10	14	14	70	1	5.1	8.6	6.6	89.54	
MRSI-Ie-25B2	10/10+5	10	14	14	70	1	5	8.4	7.2	90.01	100
MRSI-Ie-25B3	10/10+5	10	14	14	70	1	5	8.4	7.2	89.7	
MRSI-Ie-26A	10/10+10	10	7	7	70	1	5.1	8.5	7.4	91.66	100
MRSI-Ie-26A2	10/10+10	10	7	7	70	1	5	8.6	6.7	92.77	
MRSI-Ie-26A3	10/10+10	10	7	7	70	1	5	8.6	6.8	91.8	
MRSI-Ie-26B	10/10+10	10	14	14	70	1	5.1	8.4	6.8	93.54	100
MRSI-Ie-26B2	10/10+10	10	14	14	70	1	5	8.5	6.8	92.74	
MRSI-Ie-26B3	10/10+10	10	14	14	70	1	5	8.5	6.8	93.78	

Table 3.7. Continued

Sample #	CA/PC CaCl ₂ ·2H ₂ O/HPO ₄ +HCO ₃ * (mM)	T (°C)	Stage I	Stage II	Stage III		CA pH	PC Ini. pH	PC Fin. pH	Mass (mg)	XRD (HAP %)
			Maturation (D) of a single solution	Maturation (D) of mixed solutions	T (°C)	Dry Time (D)					
MRSI-Ie-27A	10/10+15	10	7	7	70	1	5.1	8.5	7.4	95.77	
MRSI-Ie-27A2	10/10+15	10	7	7	70	1	5	8.4	7.4	96.68	100
MRSI-Ie-27A3	10/10+15	10	7	7	70	1	5	8.4	7.4	97.78	
MRSI-Ie-27B	10/10+15	10	14	14	70	1	5.1	8.5	7	95.78	
MRSI-Ie-27B2	10/10+15	10	14	14	70	1	5	8.4	7	95.78	100
MRSI-Ie-27B3	10/10+15	10	14	14	70	1	5	8.4	7	91.78	

CA= Calcium

PC= Phosphate Carbonate

Ini. pH= Initial pH

Fin. pH= Final pH

T= Temperature

RT= Room Temperature

HAP= Hydroxyapatite

N.A= Not Available

*HPO₄+HCO₃ denotes Na₂HPO₄+ NaHCO₃** 10/10+5 denotes 10 mmolal CaCl₂·2H₂O/10 mmolal Na₂HPO₄+ 5 mmolal NaHCO₃

Table 3.8. Solution chemistry of all of instantaneous mixing rate for the time-series experiments at 25 °C.

Sample #	CA/PC		CA pH	PC Ini. pH	PC Fin. pH	Stage I	Stage II	Stage III		Sample size (mg)	XRD HAP%	CO ₃ ²⁻ wt%
	CaCl ₂ ·2H ₂ O/HPO ₄ +HCO ₃ * (mmolal)	Maturation (D) of a single solution				Maturation (D) of mixed solutions	T (°C)	Dry Time (D)				
MRSI-Ie-1-TS	10/10+10**	5.8	8.6	7.1	2 hr***	0	70	1	57.49	100	0.4	
MRSI-Ie-2-TS	10/10+10	5.8	8.6	7.2	4 hr	0	70	1	56.5		0.3	
MRSI-Ie-3-TS	10/10+10	5.8	8.6	7.2	6 hr	0	70	1	62.72		1.0	
MRSI-Ie-4-TS	10/10+10	5.8	8.6	7.2	12 hr	0	70	1	62.26		0.2	
MRSI-Ie-5-TS	10/10+10	5.8	8.6	7.2	1	0	70	1	61.85		0.1	
MRSI-Ie-6-TS	10/10+10	5.8	8.6	7.2	2	0	70	1	60.79		0.1	
MRSI-Ie-7-TS	10/10+10	5.8	8.6	7.1	5	0	70	1	65.07		0.2	
MRSI-Ie-8-TS	10/10+10	5.8	8.6	7.1	7	0	70	1	89.81	100	0.5	

CA= Calcium

PC= Phosphate Carbonate

Ini. pH= Initial pH

Fin. pH= Final pH

HAP= Hydroxyapatit

*HPO₄+HCO₃ denotes Na₂HPO₄+ NaHCO₃

** 10/10+10 denotes 10 mmolal CaCl₂·2H₂O/10 mmolal Na₂HPO₄+ 10 mmolal NaHCO₃

*** hour

Table 3.9. Solution chemistry of all slow mixing experiments at 25 °C.

Sample #	CA/PC CaCl ₂ ·2H ₂ O/HPO ₄ +HCO ₃ [*] (mmolal)	Stage I		Stage II		Stage III		CA pH	PC Ini. pH	PC Fin. pH	Sample size (mg)	XRD (HAP%)	CO ₃ ²⁻ (wt%)
		Maturation (D) of a single solution	Injection rate ml/hr	Injection (D)	Maturation (D) of mixed solutions	T (°C)	Dry Time (D)						
MRSI-Ie-28-SP1	10/10+5**	1	2.08	2	7	70	1	4.6	8.57	6.7	39.52	0	0.6
MRSI-Ie-29-SP1	10/10+10	5	2.08	2	7	70	1	4.6	8.47	6.9	53.66		1.1
MRSI-Ie-29-SP2	10/10+10	5	2.08	2	7	70	1	5.8	8.6	7.0	75.47		1.4
MRSI-Ie-29-SP3	10/10+10	5	2.08	2	7	70	1	5.8	8.6	7.0	58.33		1.5
MRSI-Ie-30-SP1	10/10+15	5	2.08	2	7	70	1	5.7	8.5	7.1	54.88	100	3.4
MRSI-Ie-30-SP2	10/10+15	5	2.08	2	7	70	1	6.0	8.5	7.0	45.69		3.4
MRSI-Ie-30-SP3	10/10+15	5	2.08	2	7	70	1	6.0	8.5	7.0	46.71		3.3
MRSI-Ie-34-SP1	10/10+10	7	0.58	8	0	70	1	5.7	8.7	7.0	61.04	29.43	1.3
MRSI-Ie-34-SP2	10/10+10	7	0.594	7	0	70	1	5.3	8.6	6.7	78.76	36.02	0.9
MRSI-Ie-34-SP3	10/10+10	7	0.594	7	0	70	1	5.8	8.6	6.9	35.96		1.3
MRSI-Ie-34-SP4	10/10+10	7	0.594	7	0	70	1	6.0	8.6	6.9	39.90		1.1
MRSI-Ie-35-SP1	10/10+15	7	0.594	8	0	70	1	5.7	8.5	7.3	45.97	80.04	3.4
MRSI-Ie-35-SP2	10/10+15	7	0.594	7	0	70	1	5.3	8.5	6.9	76.78	67.00	1.7
MRSI-Ie-35-SP3	10/10+15	7	0.594	7	0	70	1	5.8	8.5	7.0	45.69		1.4
MRSI-Ie-35-SP4	10/10+15	7	0.594	7	0	70	1	6.0	8.5	7.0	43.45		1.8

CA= Calcium

PC= Phosphate Carbonate

Ini. pH= Initial pH

Fin. pH= Final pH

HAP= Hydroxyapatite

*HPO₄+HCO₃ denotes Na₂HPO₄+ NaHCO₃** 10/10+5 denotes 10 mmolal CaCl₂·2H₂O/10 mmolal Na₂HPO₄+ 5 mmolal NaHCO₃

Table 3.10. Oxygen isotope data and oxygen isotope fractionation factors between HAP and water at 10, 25, and 40 °C.

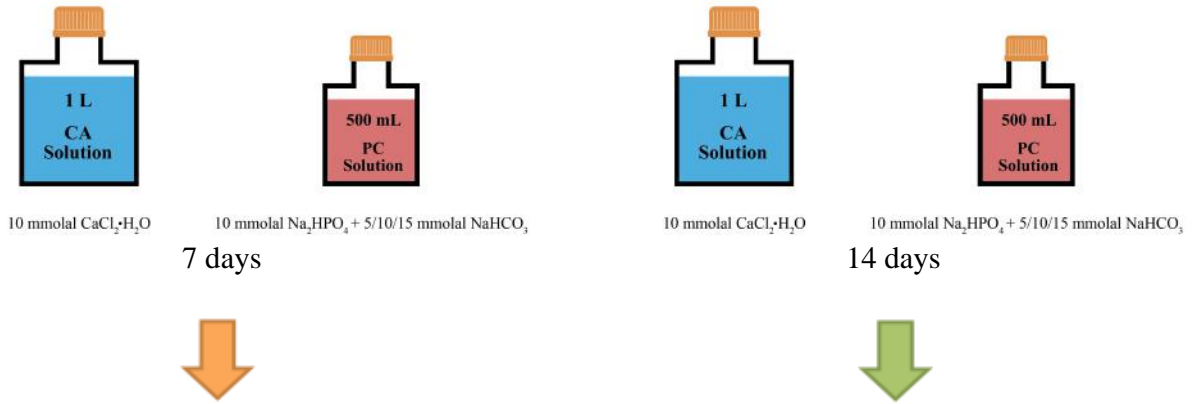
Sample #	T (°C)	$\delta^{18}\text{O}(\text{PO}_4)^n$ (‰ V-SMOW)	$\delta^{18}\text{O}(\text{H}_2\text{O})^n$ (‰ V-SMOW)	$\alpha_{\text{HAPBC-H}_2\text{O}}$	$1000\ln\alpha_{\text{HAPBC-H}_2\text{O}}$
MRSI-Ie- 25A2 r1	10	10.42	-6.63	1.01716	17.02
MRSI-Ie- 25A2 r2	10	10.84	-6.63	1.01759	17.44
MRSI-Ie- 25A2 r3	10	11.88	-6.63	1.01863	18.46
MRSI-Ie-25A2 r4	10	11.66	-6.63	1.01841	18.24
MRSI-Ie-25B2 r1	10	11.98	-6.63	1.01874	18.56
MRSI-Ie-25B2 r2	10	11.45	-6.63	1.01820	18.04
MRSI-Ie-17B r2	25	12.03	-6.64	1.01879	18.62
MRSI-Ie-17A r1	25	12.59	-6.70	1.01942	19.23
MRSI-Ie-17A r2	25	12.38	-6.70	1.01920	19.02
MRSI-Ie-17A r3	25	12.32	-6.70	1.01915	18.97
MRSI-Ie-1TS r1	25	11.15	-6.46	1.01772	17.57
MRSI-Ie-1TS r2	25	12.04	-6.46	1.01862	18.45
MRSI-Ie-1TS r3	25	12.02	-6.46	1.01860	18.43
MRSI-Ie- 8TS r1	25	10.99	-6.46	1.01756	17.41
MRSI-Ie- 8TS r2	25	11.71	-6.46	1.01829	18.12
MRSI-Ie- 8TS r3	25	11.51	-6.46	1.01809	17.93
MRSI-Ie-28SP r1	25	12.30	-6.54	1.01896	18.79
MRSI-Ie-28SP r2	25	12.07	-6.54	1.01873	18.56
MRSI-Ie-30 SP r1	25	11.30	-6.54	1.01796	17.80
MRSI-Ie-30 SP r2	25	10.85	-6.54	1.01751	17.36
MRSI-Ie-34SP r1	25	11.99	-6.60	1.01871	18.54
MRSI-Ie 34SP r2	25	11.90	-6.60	1.01862	18.45
MRSI-Ie-35SP r1	25	10.44	-6.64	1.01719	17.05
MRSI-Ie-35SP r2	25	11.61	-6.64	1.01837	18.20
MRSI-35SP2 r1	25	12.46	-6.64	1.01923	19.05
MRSI-35SP2 r2	25	11.62	-6.64	1.01838	18.21
MRSI-Ie-22 B2 r1	40	10.82	-6.50	1.01744	17.29
MRSI-Ie-22 B2 r2	40	9.96	-6.50	1.01657	16.44
MRSI-Ie-22 B2 r3	40	11.78	-6.50	1.01840	18.23
MRSI-Ie-23A r1	40	10.73	-6.70	1.01755	17.40
MRSI-Ie-23A r2	40	12.71	-6.70	1.01954	19.35
MRSI-Ie-23A r3	40	10.27	-6.70	1.01708	16.94
MRSI-Ie-23B r1	40	11.43	-6.70	1.01825	18.09
MRSI-Ie-23B r2	40	10.95	-6.70	1.01777	17.61
MRSI-Ie-23B r3	40	12.02	-6.70	1.01885	18.67
MRSI-Ie-17B r1	40	11.44	-6.64	1.01820	18.04

T= Temperature

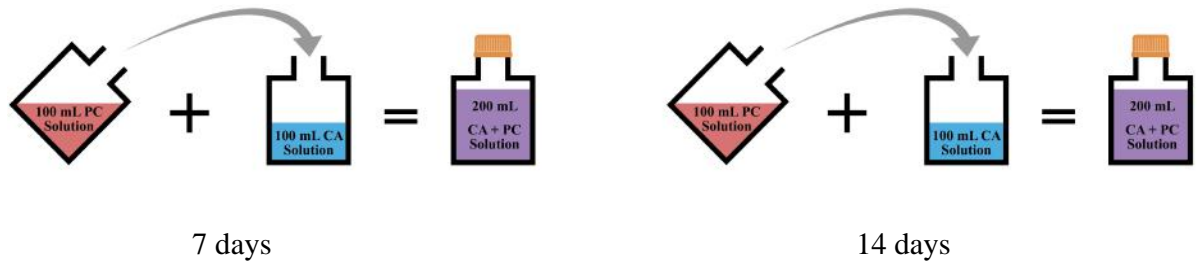
n= Each HAP samples has been duplicated for the $\delta^{18}\text{O}$ analysis

The Instantaneous Mixing Method: 10, 25, and 40 °C

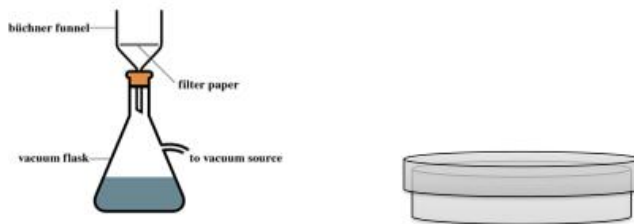
Stage I: Preparation and maturation of CA + PC solutions before instantaneous mixing



Stage II: Instantaneous mixing solutions and maturations of the mixed solutions



Stage III: Filtration and drying

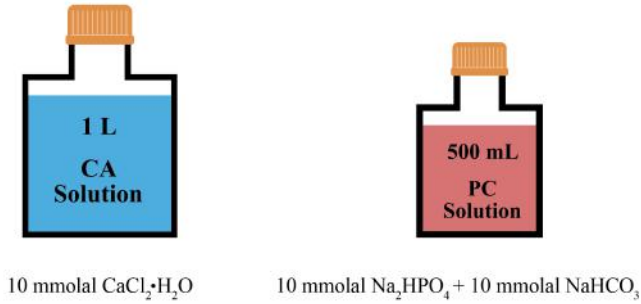


Vacuum filter, rinse with DI water and methanol. Stored in 70 °C over for 1 day

Figure 3.1. Schematic illustration demonstrating the instantaneous mixing method used in this study to synthesize HAP and HAP-bound carbonate at 10, 25, and 40 °C.

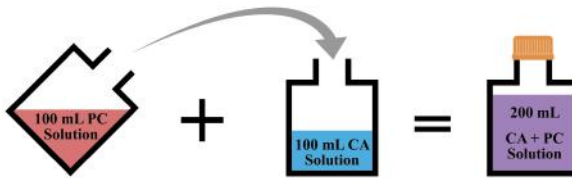
The Instantaneous Mixing Method: Time-Series at 25 °C

Stage I: Maturation of CA+PC solutions before mixing (2, 4, 6, 12, 24, 48, 120, and 168 hours)

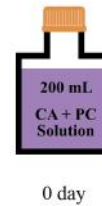


Stage II: Instantaneous mixing and 0 day maturation

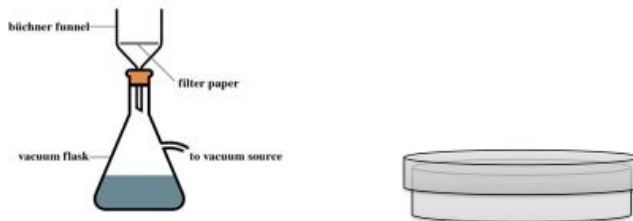
I. Mixing



II. Maturation



Stage III: Filtration and drying

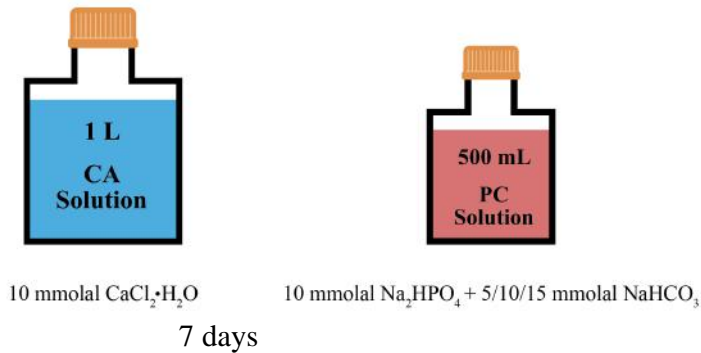


Vacuum filter, rinse with DI water and methanol. Stored in 70 °C over for 1 day

Figure 3.2. Schematic illustration demonstrating the time-series experiments used in this study to synthesize HAP and HAP-bound carbonate at 25 °C.

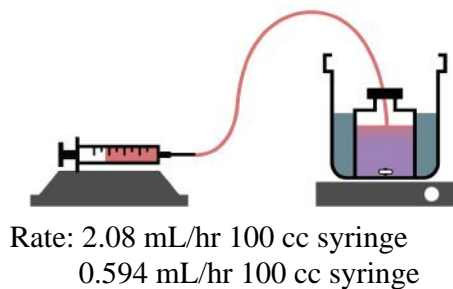
The Slow Mixing Method: 25 °C

Stage I: Preparation and maturation of CA and PC solutions for 7 days before slow mixing

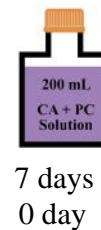


Stage II: Mixing solutions and maturations

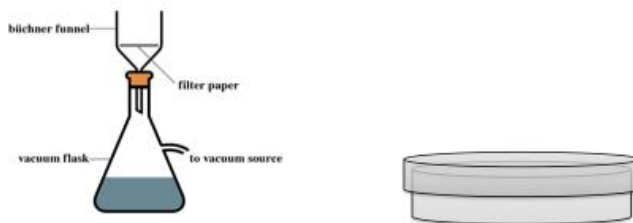
I. Injection PC to CA



II. Maturations



Stage III: Filtration and drying



Vacuum filter, rinse with DI water and methanol. Stored in 70 °C over for 1 day

Figure 3.3. Schematic illustration demonstrating the slow mixing method used in this study to synthesize HAP and HAP-bound carbonate at 25 °C.

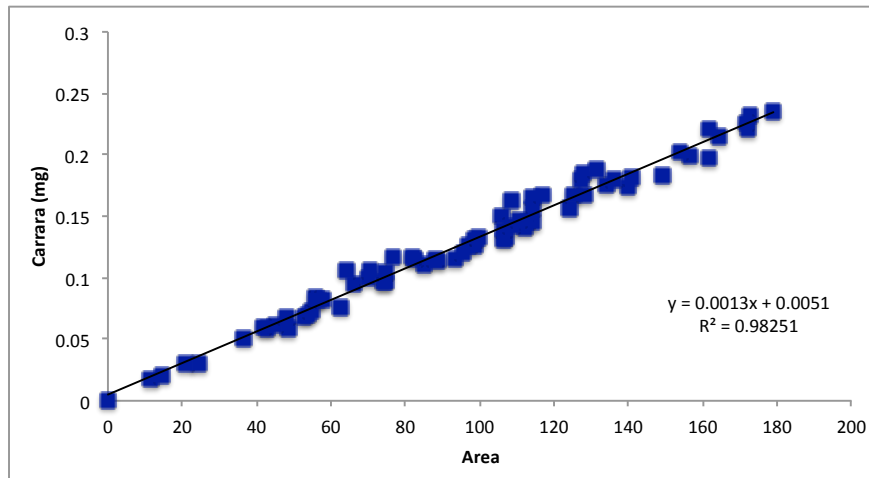


Figure 3.4. The calibration of mass 44 peaks area based on different weights of Carrara laboratory standards.

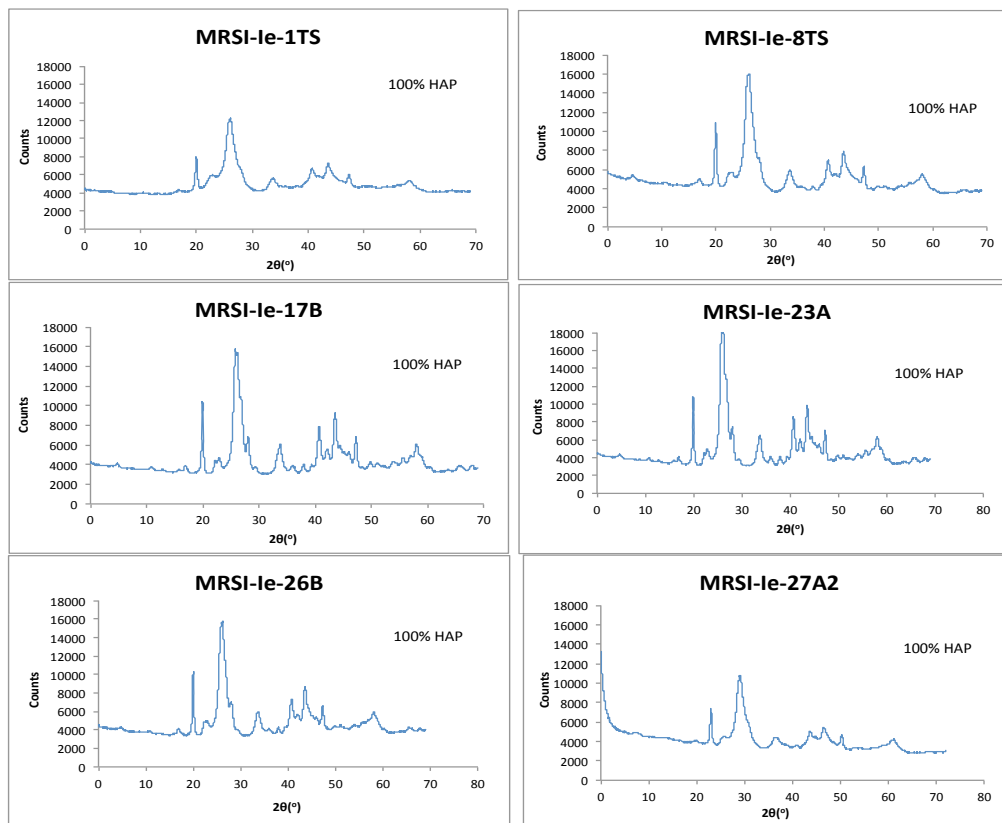


Figure 3.5. XRD results from the instantaneous mixing rate experiments that demonstrated pure HAP.

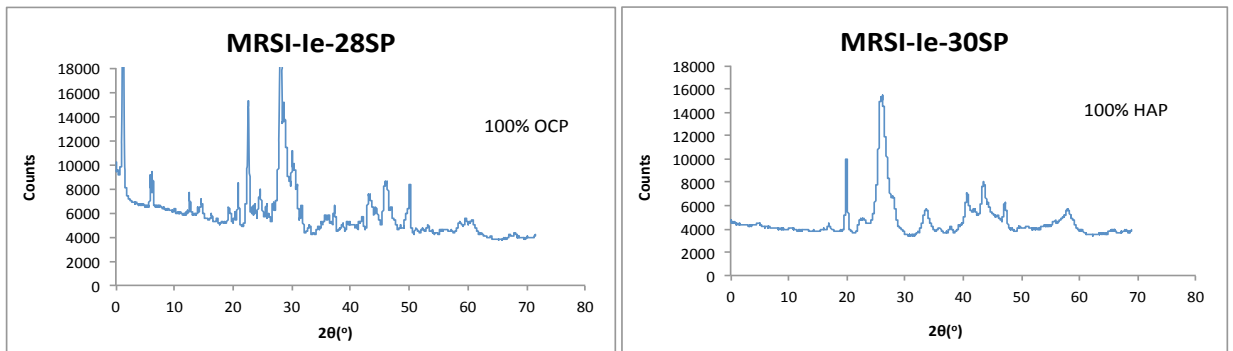


Figure 3.6. XRD results that demonstrated of pure OCP (left) and pure HAP (right) under slow mixing of 2.08 mL/hr (2 days).

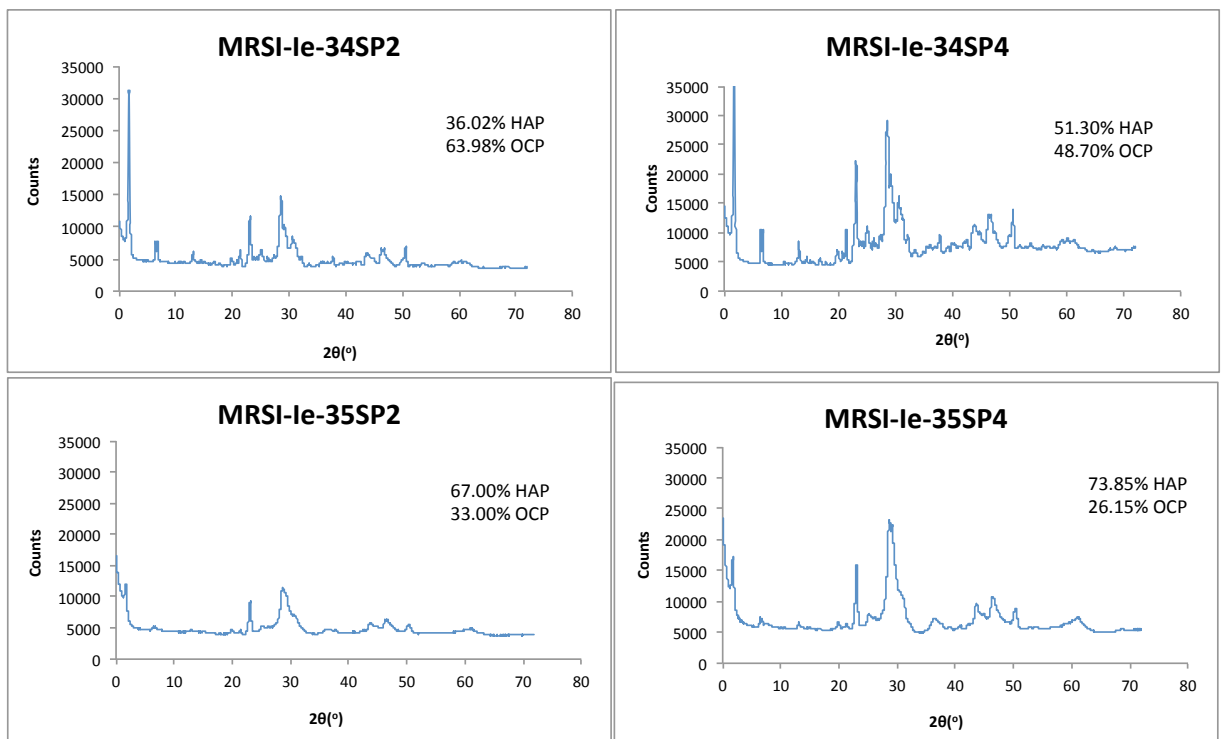


Figure 3.7. XRD results from slow mixing of 0.594 mL/hr (7 days) that demonstrated mixtures of OCP and HAP crystal.

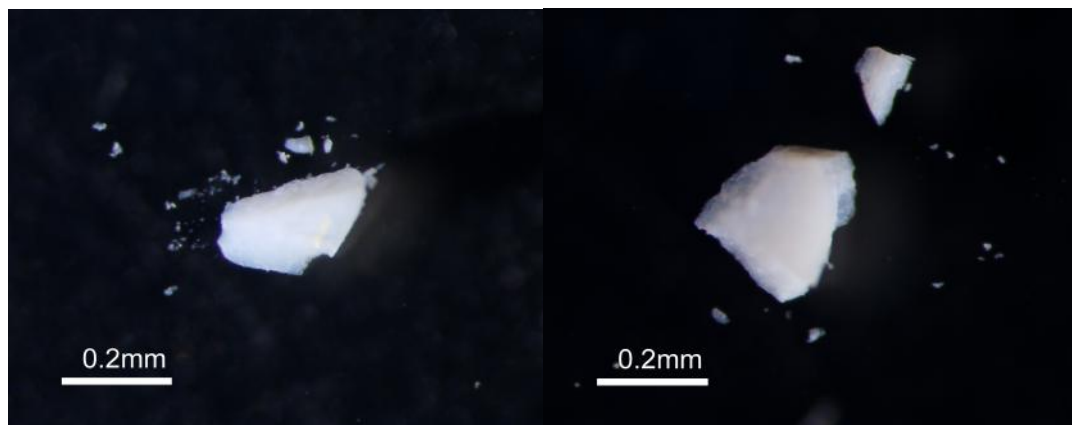


Figure 3.8. Pure HAP crystals from the instantaneous mixing experiments.

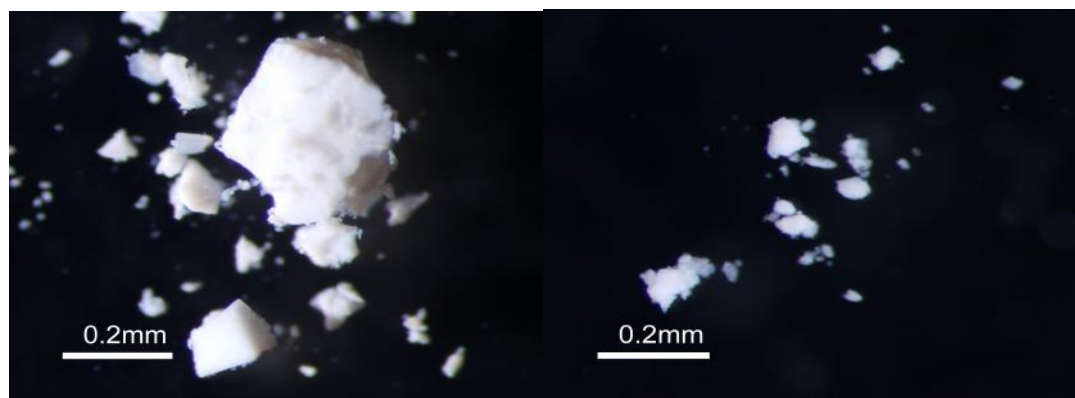


Figure 3.9. All of the heterogeneous HAP crystals under microscope from time-series instantaneous mixing experiments: MRSI-Ie-1FP (left) and MRSI-Ie-8FP (right).

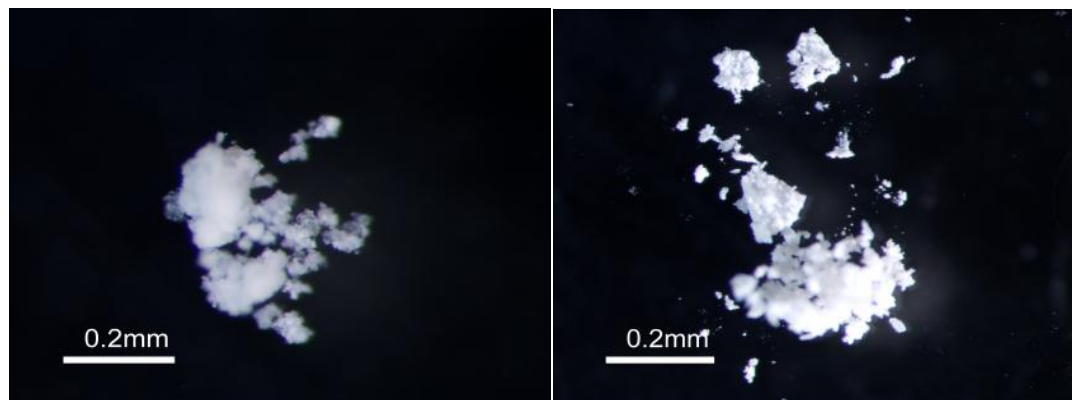


Figure 3.10. Mixtures of HAP and OCP under microscope: MRSI- Ie-34SP (left) and MRSI-Ie-35SP (right).



Figure 3.11. Pure OCP crystals from slow mixing experiment (MRSI-Ie-28SP).

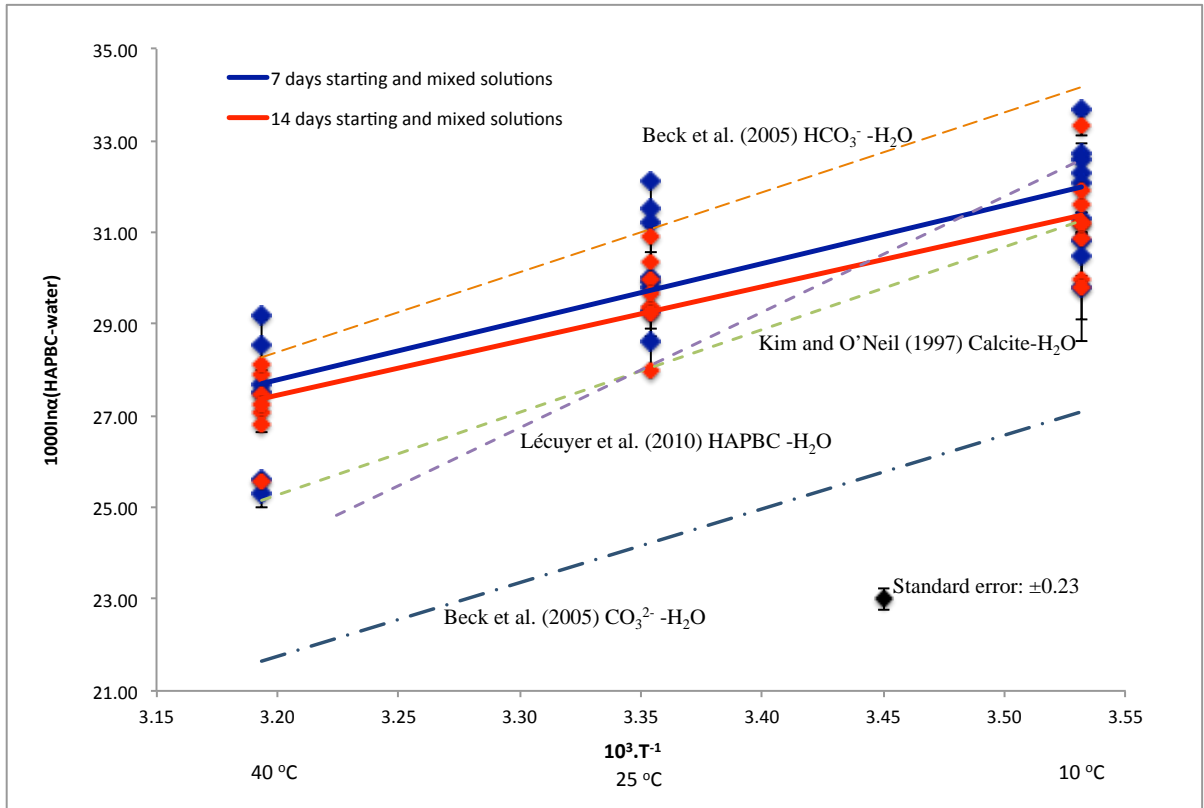


Figure 3.12. Oxygen isotope fractionation between inorganic carbonate-bearing HAP and water from the instantaneous mixing method compared to the inorganic calcite and water (Kim and O'Neil, 1997), carbonic acid system and water (Beck et al., 2005), and inorganic carbonate-bearing HAP and water (Lécuyer et al., 2010).

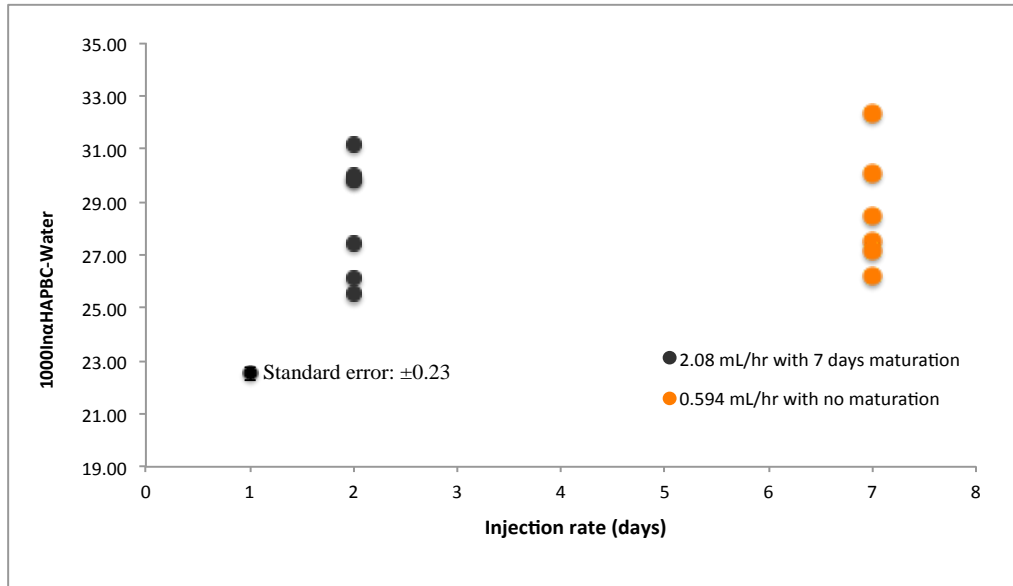


Figure 3.13. Oxygen isotope fractionation between non-pure inorganic carbonate-bearing HAP and water from the slow mixing method maturations at 25 °C

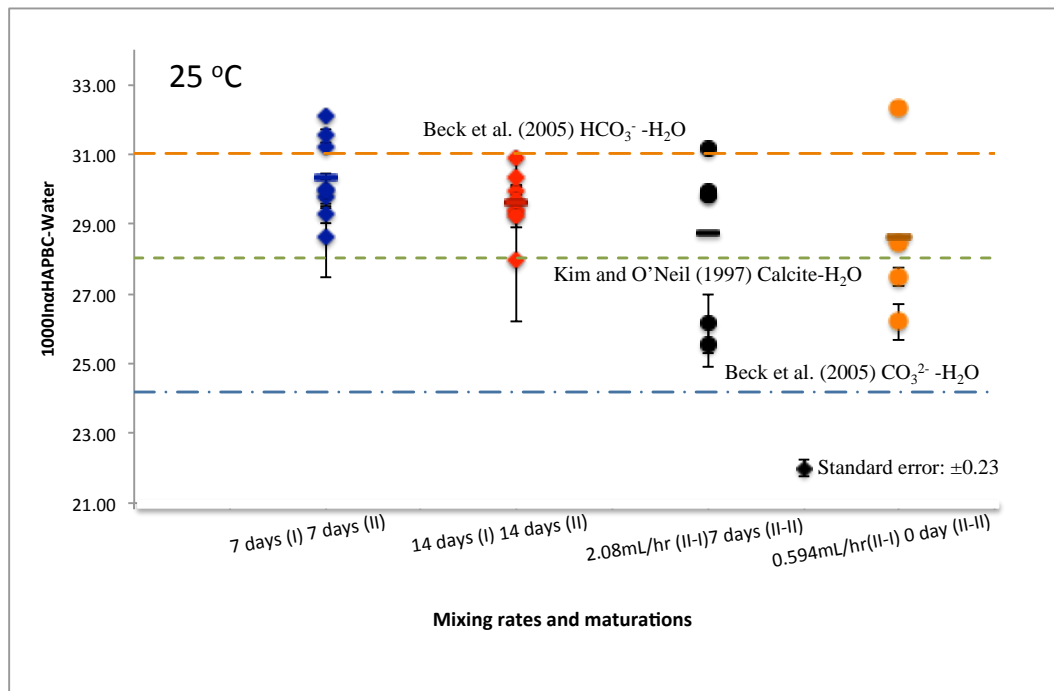


Figure 3.14. Oxygen isotope fractionation between non-pure inorganic HAP-bound carbonate and water from the slow mixing method at 25 °C vs. pure inorganic HAP-bound carbonate and water from the instantaneous mixing method.

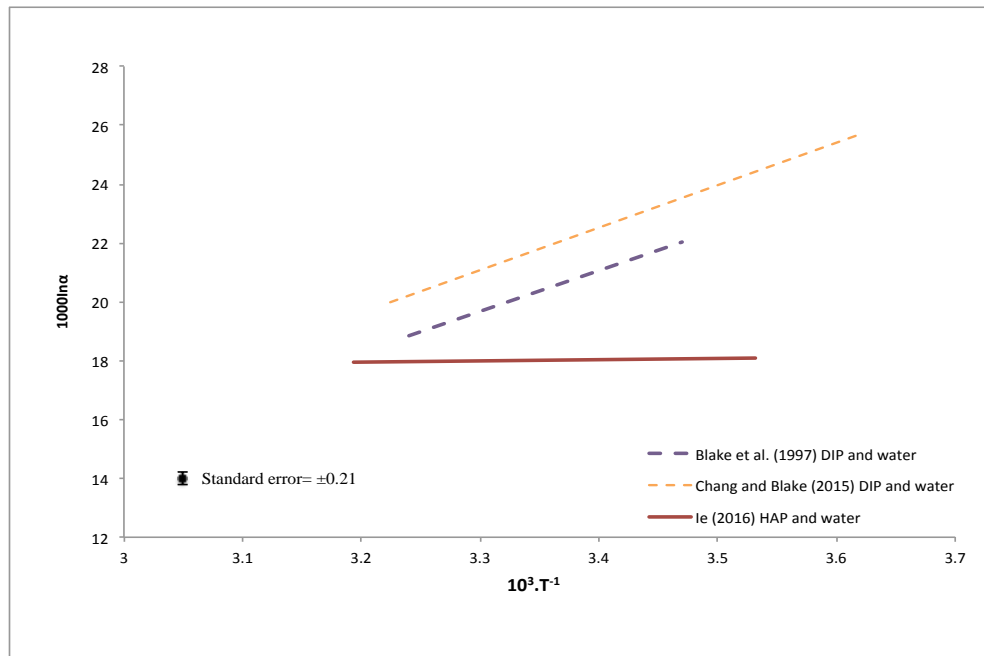


Figure 3.15. Oxygen isotope fractionation between inorganic HAP and water compared to the dissolved inorganic phosphate and water equation (Blake et al., 1997; Chang and Blake, 2015).

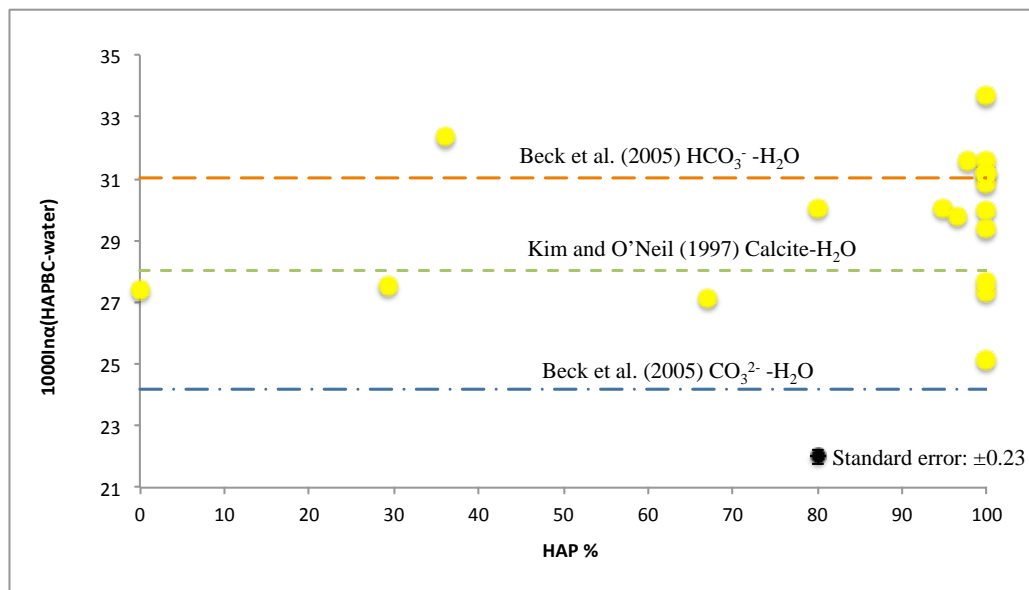


Figure 3.16. Oxygen isotope fractionation between inorganic HAP and water trends with yield HAP (%) based on XRD analysis.

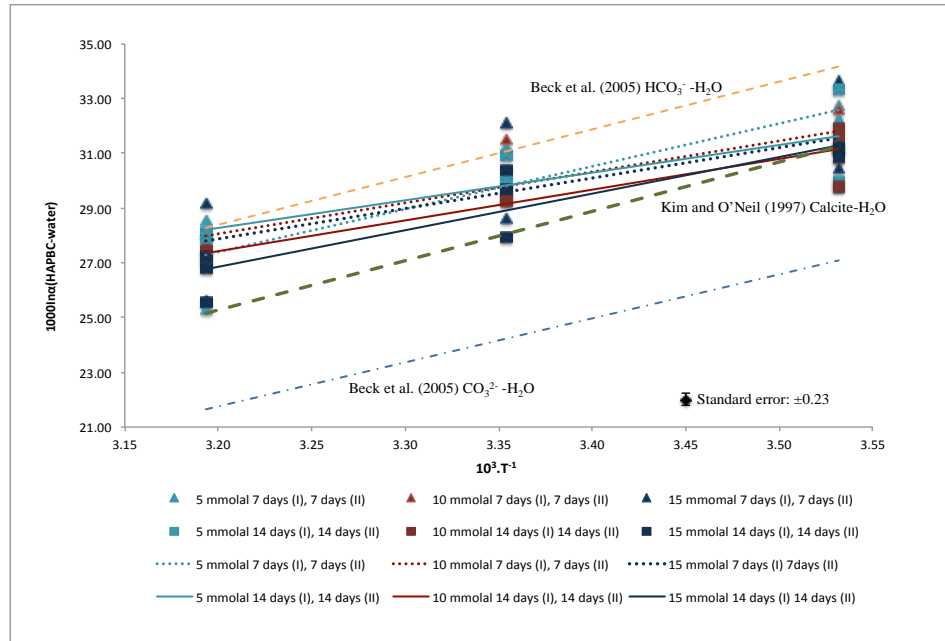


Figure 3.17. Oxygen isotope fractionation between HAP-bound carbonate and water trends with temperature as a function of initial concentrations of NaHCO_3 in the PC solutions.

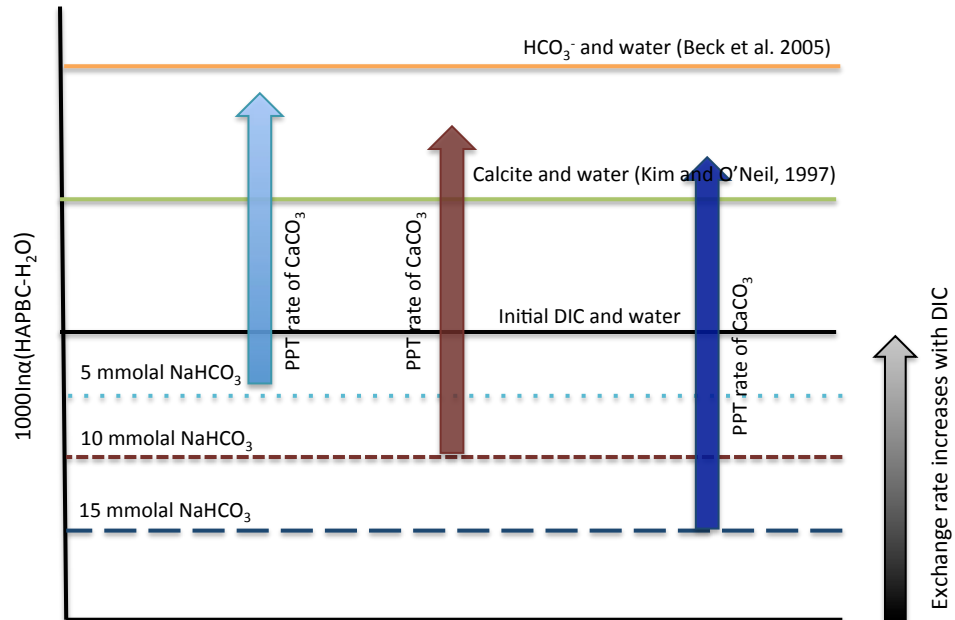


Figure 3.18. A schematic illustration of the effect of initial concentrations of NaHCO_3 in the HAP-bound carbonate and water system at low temperatures.

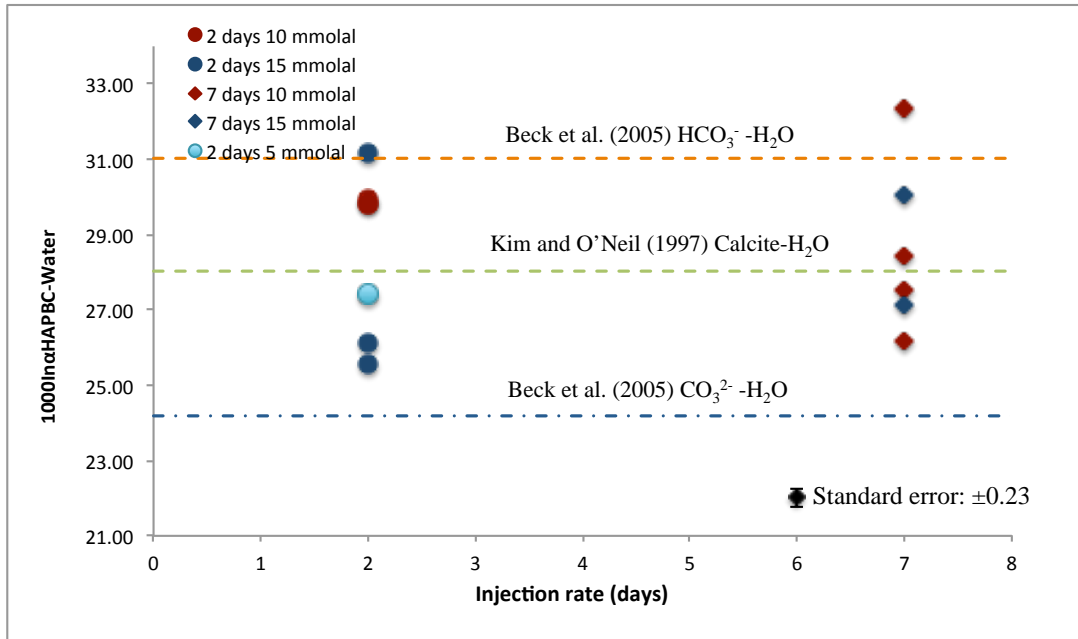


Figure 3.19. Oxygen isotope fractionation between HAP-bound carbonate and water under slow mixing experiments at 25 °C.

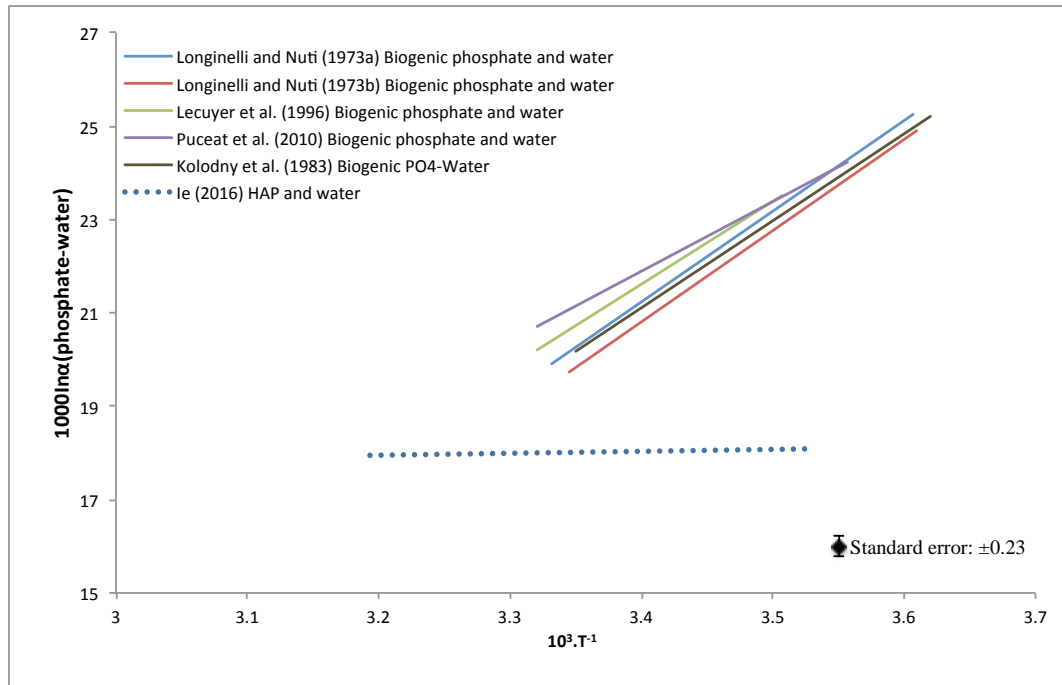


Figure 3.20. Oxygen isotope fractionation equation between HAP and water (this study) compared to the oxygen isotope fractionation between biogenic phosphate and water (Longinelli et al., 1973a; 1973b; Lécuyer et al., 1996; Puceat et al., 2010).

CHAPTER 4:

Conclusions and research contributions

4.1 Research summary

This dissertation refined the synthesis method for HAP-bound carbonate at low temperatures which was proposed by Lécuyer et al. (2010). Our results have revealed that brushite and octacalcium phosphate (OCP) were precursor to hydroxyapatite (HAP). Therefore, the conditions under which pure HAP formed were identified and overall this dissertation elucidated a good example for highlighting the importance to achieve the desire mineralogy of HAP crystals and HAP-bound carbonate.

The purpose of this dissertation was to developed and refined the synthesis method for carbonate-bearing HAP that was proposed by Lécuyer et al. (2010), and also to evaluate the oxygen isotope systematics between HAP-bound carbonate and water at low temperatures. The synthesis of inorganic HAP crystals and HAP-bound carbonate in this study were studied under two mixing techniques (instantaneous and slow). In addition, crystalline HAP were prepared over various pH values of the mixed solutions (5.5 to 7.4) at 25 °C under a variety of experimental conditions (rates of mixing and maturation of the starting and mixed solutions, and concentrations of NaHCO₃). Based upon X-Ray diffraction (XRD) analyses, a pH above 6.7 under the instantaneous mixing experiment was found to produced a single phase of pure HAP. However, a mixture of brushite, OCP, and HAP was obtained at a pH between 5.5 and 6.4. Under the slow mixing experiments, XRD patterns indicated the presence of a secondary mineral phase, OCP when the pH value was above 6.7. Furthermore, NaHCO₃ concentration of the starting solution influenced the amount of structural carbonates (CO₃²⁻) in the HAP. All of the samples prepared from the instantaneous mixing method yielded pure HAP crystals

regardless of the initial NaHCO_3 concentration used in this study. In contrast, an initial concentration of 5 mmolal NaHCO_3 in the starting solution produced only pure OCP crystals when the slow mixing experiment was employed. Nevertheless, all of the samples appeared to be a mixture of OCP and HAP crystals when the initial NaHCO_3 concentration was above 10 mmolal. In addition, our findings showed no relationship between initial concentration of NaHCO_3 and the amount of structural CO_3^{2-} in HAP under the instantaneous mixing method. However, under the slow mixing method, the amount of structural CO_3^{2-} in HAP increased as the NaHCO_3 concentration of the starting solution increases. From the characterization of the crystals produced in this study, it was concluded that the mixing rates and the final pH of the mixed solutions, as well as the NaHCO_3 concentrations in the starting solution were critical for the synthesis of pure HAP and HAP-bound carbonate, and its crystallographic characteristics.

On the basis of the information obtained from our synthesis experiments, the produced HAP and HAP-bound carbonate minerals were analyzed for their oxygen isotope compositions using a stable isotope ratio mass spectrometer. Because HAP and HAP-bound carbonate can be synthesized at different temperatures, a temperature-dependent relationship of oxygen isotope fractionation between HAP-bound carbonate and water were investigated. Although many research had been done for the determination of the oxygen isotope fractionation between biogenic apatites (bioapatites) and water at all temperatures; however, very little had been investigated on the oxygen isotope fractionation between carbonate-bearing apatite and water. This thesis specifically determined the oxygen isotope fractionation between HAP-bound carbonate and water at

10, 25 and 40 °C. It is important to understand the oxygen isotope systematics in the HAP-bound carbonate-water system since this knowledge allows us to understand the formation temperature of biogenic HAP samples, such as teeth enamel from marine and terrestrial environments. Several physicochemical conditions (mixing rates and maturations of the starting as well as the mixed solutions, and initial concentrations of NaHCO_3) were examined to determine the oxygen isotope fractionation between HAP-bound carbonate and water. It was observed that the maturation of the starting solutions and the initial concentrations of NaHCO_3 were the most likely cause the non-equilibrium oxygen isotope effect on the oxygen isotope fractionation between HAP-bound carbonate and water in this study. The oxygen isotope fractionation obtained from the experiments with a longer maturation period (14 days) of the starting solutions and a lower concentration (5 mmolal) of NaHCO_3 was closer to the oxygen isotope fractionation proposed by Kim and O'Neil (1997). In contrast, the oxygen isotope fractionation between HAP-bound carbonate and water with a shorter maturation period (7 days) and a higher initial NaHCO_3 concentration (15 mmolal) were larger than those from Kim and O'Neil (1997).

Chapter 1 provided an introduction to the fundamentals of phosphate minerals and their applications in stable isotope geochemistry. It also discussed previous studies on the oxygen isotope fractionation between phosphate and water, DIP and water, as well as apatite-bound carbonate and water. Chapter 2 examined the synthesis method for inorganic HAP-bound carbonate that was first described by Lécuyer et al. (2010). Various physicochemical conditions, such as temperatures, solution pH, and initial

solution concentrations of NaHCO_3 , were tested in order to obtain pure HAP crystals and carbonate-bearing HAP, as well as to better determine the oxygen isotope fractionation between HAP-bound carbonate and water. Chapter 3 evaluated the oxygen isotope fractionation between HAP-bound carbonate and water at low temperatures with different maturations and three distinct initial concentrations of NaHCO_3 (5, 10, or 15 mmolal). These characteristics are crucial for the establishment of the oxygen isotope equilibrium between the HAP-bound carbonate and water, as well as between HAP and water. Lastly, Chapter 4 briefly summarized the major hypotheses, findings, and purposes from Chapters 2 and 3. This chapter also includes the candidate's contributions to the research, and identifies future areas of research for the oxygen isotope fractionation between HAP-bound carbonate and water.

4.2 Candidate's contributions to collaborative research

4.2.1 Ch. 2: Synthesis of hydroxyapatite-bound carbonate at 25 °C

This collaborative study was a continuation of Julianne Bagg's undergraduate thesis (2013) on the synthesis of HAP at 25 °C. Therefore, the candidate refined the experimental protocols initially developed by Julianne Bagg and Dr. Sang-Tae Kim and applies these protocols to different temperatures for the synthesis of HAP bound carbonate. The candidate prepared a manuscript for publication by incorporating feedback from two co-authors (Julianne Bagg and Dr. Sang-Tae Kim).

4.2.2. Ch. 3: Oxygen isotope fractionation between HAP-bound carbonate and water at low temperatures.

In this collaborative work with the candidate's supervisor, my contributions included: assisting in the development of the initial experimental conditions, the preparation of the starting solutions, subsequent stable isotope analyses of the solution and solid samples, and XRD analyses. The candidate wrote a manuscript with feedback from the supervisor.

4.3 Future investigation in stable isotope geochemistry

Although the results of this study elucidate the oxygen isotope systematics regarding the apatite-bound carbonate-water system, but several amendments need to be addressed. In order to gain a better understanding of the mineralogy of the carbonate and phosphate precipitates, Scanning Electron Microscopy (SEM) and Infrared Spectroscopy is necessary to be conducted. These results will identify the presence of HAP structure and the degree of crystallization of inorganic HAP that is synthesized in the carbonate lattice. Moreover, the impact of pH on the synthesis of HAP, specifically under the slow mixing experiment, should be investigated in order to obtain pure HAP crystals. An additional consideration to be investigated includes the influence of mixing rates of the mixed solution on the amount of structural CO_3^{2-} in HAP. At a slower mixing, a higher concentration of NaHCO_3 would lead to a larger amount of structural CO_3^{2-} in HAP, reaching the value that is similar to the natural carbonate yield from bioapatites.

Assessing the temperature dependence of the oxygen isotope fractionation between inorganic HAP-bound carbonate and water has yielded promising results, consistent with the results from Kim and O'Neil et al. (1997) and Beck et al. (2005). However, some of our experimentally determined oxygen isotope fractionation are larger than the oxygen isotope fractionation between HCO_3^- and water that was determined by Beck et al. (2005). Therefore, several conditions (i.e., heterogeneity of the HAP samples) must be carefully considered to improve the precisions between the two replicate analyses in order to avoid this discrepancy in the oxygen isotope systematic between HAP-bound carbonate and water. In addition, in the phosphate-water system, the P-O bonds are covalently strong which influence the rate of isotopic exchange between HAP-bound carbonate and water particularly at low temperatures. Thus, a longer maturation period of the starting and the mixed solutions, as discussed in Chapter 3, may be necessary in order for the DIC to be isotopically equilibrated with water, and/or for the DIC to move closer towards to that proposed by Kim and O'Neil. (1997).

Unfortunately, our study could not demonstrate the temperature dependence of the oxygen isotope fractionation between inorganic HAP and water as a function of a mixing rate and a maturation period of the starting and mixed solutions, as well as the initial NaHCO_3 concentration. The isotopic difference between HAP and water, compared to that between bioapatite/dissolved inorganic phosphate and water, are quite large. As a result, further research on the temperature dependence of oxygen isotope fractionation between HAP and water is required. Moreover, in order to avoid and resolve considerable inconsistencies among different standard calibrations and analytical techniques, much

attention has to be made on the geochemical procedures of the calibrations between HAP and water compared to other laboratories standard reference materials. Several permutations for this finding have yet to undergo experimentation to fill in the remaining gaps.

References

- Beck, W. C., Grossman, E. L. and Morse, J. W. (2005) Experimental studies of oxygen isotope fractionation in the carbonic acid system at 15 °, 25 °, and 40 °C. *Geochimica et Cosmochimica Acta* 69, 3493-3503.
- Kim S-T. and O'Neil J. R. (1997) Equilibrium and nonequilibrium oxygen isotope effects in synthetic carbonates. *Geochimica et Cosmochimica Acta* 61, 3461-3475.
- Lécuyer C., Balter V., Martineau F., Fourel F., Bernard A., Amiot R., Gardien V., Otero O., Legendre S., Panczer G., Simon L. and Martini R. (2010) Oxygen isotopes fractionation between apatite-bound carbonate and water determined from controlled experiments with synthetic apatites precipitated at 10-37 °C. *Geochimica et Cosmochimica Acta* 74, 2072-2081.